ALEXANDRIA UNIVERSITY

"FLOW IN A SPIRAL CASING"

Thesis submitted for the Ph.D. (Eng.) degree

by

A. Abdel Halim,
D.I.C. ; B.Sc.(Eng.).

October 1954

ACKNOWLEDGEMENT

The author wishes to express his sincerest gratitude to Professor C. M. White, D.SC.,Ph.D. , Professor of Fluid Mechanics and Hydraulic Engineering at the City and Guilds College, for his guidance and supervision.

The author is also very grateful to Alexandria University for the scolarship which enabled him to proceed with his study at the Imperial College, and to Professor H. El-Dib who supervised the completion of the thesis.

CONTENTS

INTRODUCTION

Investigations of the vortex motion, and in particular the free vortex motion, were carried out on a simplified model of a logarithmic spiral casing designed to give free vortex flow. The experimental results were remarkably close to that of a free vortex, although the vortex centre did not coincide with the centre of the casing. The effect of viscosity on the pattern of free vortex motion was examined theoretically and the results were found to agree with the experimental conclusions.

The distribution of energy inside the casing is described and the existance of a region in which the total head tube recorded a total energy higher than the inlet energy of the flow, was confirmed. This paradoxical phenomenon was confirmed visually, by chemical smoke, and recorded by photography. After examining several possible causes, this apparent excess energy was found to be due to the rotation of the vortex axis.

CHAPTER I

VORTEX MOTION

Helmholtz was the first to investigate the subject of vortex motion in a paper in 1858 " On the Integrals of the Hydrodynamical Equations Corresponding to Vortex Motions". He demonstrated several laws concerning their behaviour. These laws are as follows:

I. A vortex is of constant strength along its length and cannot terminate at a point within the fluid except at a boundary.

2. The vorticity, $\xi = \frac{\partial v}{\partial x} - \frac{\partial u}{\partial y}$ of a particle of a frictionless fluid does not change with time. Consequently, the vorticity is constant along the stream lines of such a fluid in steady motion.

These laws are applicable to ideal vortices.

Considering the free vortex motion for ideal fluids, the equation $v = \frac{c}{r}$, would imply that the velocity becomes infinitly large as the radius is decreased to zero. Obviously this is an impossible condition. In real fluids, viscous effects which were neglected in deriving the equation $v = \frac{c}{r}$, are expected to cause a portion of the fluid in the region near the vortex centre to rotate like a solid body. Outside this central core is the free vortex region. There must of course be a gradual transition between the two regions, rather than a sharp devision.

In this chapter, the effect of viscosity on the two dimensional free vortex flow, is examined theoretically. Considering a simple spiral vortex, the equations of motion for the two dimensional steady flow in cylindrical polar coordinates are:

$$u\frac{\partial u}{\partial r}+\frac{v}{r}\frac{\partial u}{\partial \theta}-\frac{v^2}{r}=-\frac{1}{\rho}\frac{\partial p}{\partial r}+\nu\left[\nabla^2 u-\frac{u}{r^2}-\frac{2}{r^2}\frac{\partial v}{\partial \theta}\right] \quad \text{----(I)}$$

$$u\frac{\partial v}{\partial r}+\frac{v}{r}\frac{\partial v}{\partial \theta}+\frac{uv}{r}=-\frac{1}{\rho}\frac{1}{r}\frac{\partial p}{\partial \theta}+\nu\left[\nabla^2 v+\frac{2}{r^2}\frac{\partial u}{\partial \theta}-\frac{v}{r^2}\right] \quad \text{---(2)}$$

where $\nabla^2 \equiv \frac{\partial^2}{\partial r^2}+\frac{1}{r}\frac{\partial}{\partial r}+\frac{1}{r^2}\frac{\partial^2}{\partial \theta^2}$.

Equation of continuity

$$\frac{u}{r}+\frac{\partial u}{\partial r}+\frac{1}{r}\frac{\partial v}{\partial \theta}=0 \quad \text{---(3)}$$

where
u is the radial velocity,
v is the tangential velocity,
ρ is the density,
ν is the kinematic viscosity.

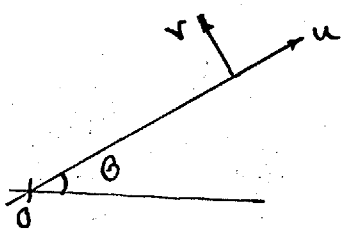

For motion symmetrical about the axis, so that $\frac{\partial}{\partial\theta}=0$, the equations become:

$$u\frac{du}{dr} - \frac{v^2}{r} = -\frac{1}{\rho}\frac{dp}{dr} + \nu\left[\frac{d^2u}{dr^2} + \frac{1}{r}\frac{du}{dr} - \frac{u}{r^2}\right] \qquad \text{------}(4)$$

$$u\frac{dv}{dr} + \frac{uv}{r} = \nu\left[\frac{d^2v}{dr^2} + \frac{1}{r}\frac{dv}{dr} - \frac{v}{r^2}\right] \qquad \text{------}(5)$$

and the equation of continuity gives $u=\frac{q}{r}$, where

$$q = \frac{\text{flow per unit width}}{2\pi}$$

Equation (4) gives $\frac{dp}{dr} = \rho\left(\frac{u^2+v^2}{r}\right)+\mu\times 0$ ------(6)

We are interested in the spiral vortex in which the motion is nearly $vr = c$. Thus the solution is conveniently written as $v = c/r + f(r)$, where $f(r)$ is that small deviation from $vr \doteq$ constant, which occurs due to viscous stress.

$$\therefore v = \frac{c}{r} + v' \quad , \quad \frac{dv}{dr} = -\frac{c}{r^2} + \frac{dv'}{dr}$$

$$\text{and} \quad \frac{d^2v}{dr^2} = \frac{2c}{r^3} + \frac{d^2v'}{dr^2}$$

Substituting in equation (5) ,

$$\therefore \frac{q}{r}\left(-\frac{c}{r^2} + \frac{dv'}{dr}\right) + \frac{1}{r}\,\frac{q}{r}\left(\frac{c}{r} + v'\right)$$
$$- \nu\left[\left(\frac{2c}{r^3} + \frac{d^2v'}{dr^2}\right) + \frac{1}{r}\left(-\frac{c}{r^2} + \frac{dv'}{dr}\right) - \frac{1}{r^2}\left(\frac{c}{r} + v'\right)\right] = 0 .$$

i.e. $$\frac{d^2v'}{dr^2}(-\nu) + \frac{dv'}{dr}\left(\frac{q}{r} - \frac{\nu}{r}\right) + v'\left(\frac{q}{r^2} + \frac{\nu}{r^2}\right)$$
$$- \frac{qc}{r^3} + \frac{qc}{r^3} - \frac{2\nu c}{r^3} + \frac{\nu c}{r^3} + \frac{\nu c}{r^3} = 0 .$$

Let $A = \frac{c}{\nu}$

and multiply the previous equation by $\left(-\frac{r^2}{\nu}\right)$;

$$\therefore \quad r^2 \frac{d^2v}{dr^2} + (I-A)r\frac{dv}{dr} - (I+A)v = 0 .$$

Let $r = e^t$, $\frac{dr}{dt} = e^t = r$.

$$\frac{d}{dt} = \frac{d}{dr}\cdot\frac{dr}{dt} = r\frac{d}{dr}$$

let $\quad \mathcal{J} = \frac{d}{dt} = r\frac{d}{dr}$

Also $\quad \frac{d^2}{dt^2} = \frac{d}{dt}\left(\frac{d}{dt}\right) = \frac{d}{dt}\left(r\frac{d}{dr}\right)$

$$= \frac{d}{dr}\left(r\frac{d}{dr}\right)\cdot\frac{dr}{dt}$$

$$= \frac{dr}{dt}\cdot\left(r\frac{d^2}{dr^2} + \frac{d}{dr}\right)$$

$$= r^2\frac{d^2}{dr^2} + r\frac{d}{dr}$$

$$\therefore \quad \mathcal{J}^2 = r^2\frac{d^2}{dr^2} + \mathcal{J}$$

or $\quad r^2\frac{d^2}{dr^2} = \mathcal{J}^2 - \mathcal{J}$

Substituting in the equation, $\therefore$

$$\left[(\mathcal{J}^2 - \mathcal{J}) + (I-A)\mathcal{J} - (I+A)\right]v = 0$$

or $\quad \left[\mathcal{J}^2 - A\mathcal{J} - (A+1)\right]v = 0$

$$\therefore \quad \left[(\vartheta+1)(\vartheta-(A+1))\right] v = 0 .$$

This gives

$$v = \alpha_1 r^{-I} + \alpha_2 r^{A+I} \qquad \text{------}(7)$$

The first term is the free vortex, while the second term gives the deviation due to viscosity. This means that viscosity changes the pattern of the free vortex. The amount of deviation increases as $A = q/\nu$ decreases. For large values of A, i.e., for small kinematic viscosities, the effect of viscous stresses on the free vortex pattern is negligible, and the function of the second term would be to bring the velocity down to zero at a finite distance from the centre, instead from at infinity, figure(I).

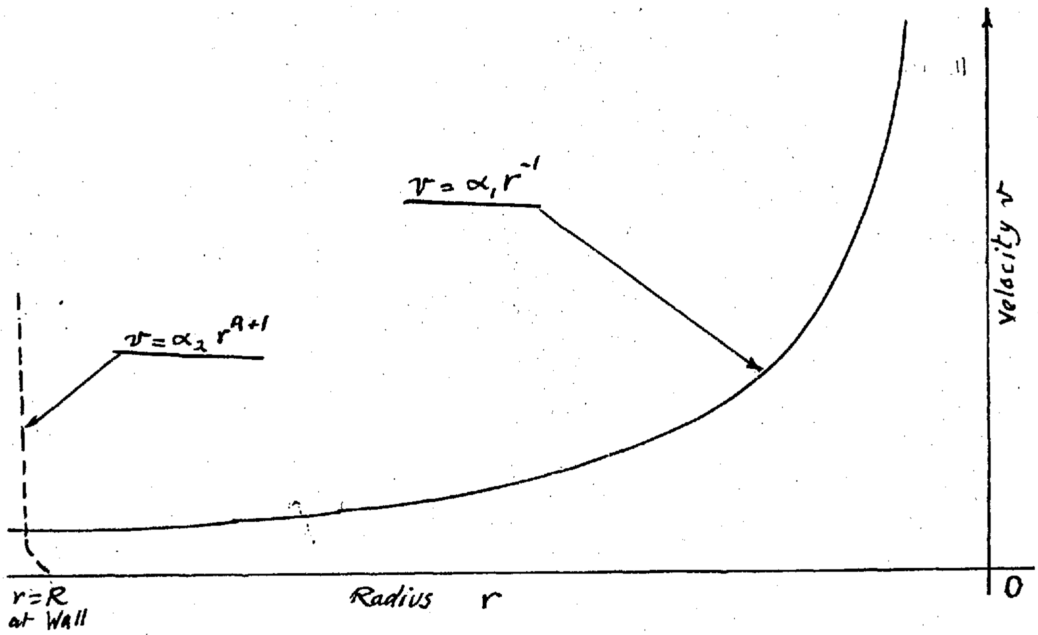

Figure (1)

This agrees with the experimental results discussed later, where A was -1.397×10^4 which is quite large, and the effect of the viscosity on the pattern of flow was negligible.

Experimental Procedure

Apparatus: A simplified spiral casing with rectangular cross section, shown in figure (2), was used. It is three inches wide and its side wall is a logarithmic spiral of 80° spiral angle, $R = 6\, e^{\theta \cot 80^{\circ}}$. The throat is $5\frac{3}{8}$ inches diameter. Air was drawn through the casing, then through a diverging pipe, by a I2 inches diameter fan. The amount of flow was regulated by varying the fan speed.

The front and side of the casing are made of perspex. The back is made of wood and painted black to enable visual observation of the stream lines by using smoke. The measuring points, 2 inches apart, are on movable slides to enable taking measurements at any point on ten radial sections. There is also one measuring point at a radius of four inches and 360° with inlet. Measuring points not in use were sealed with flush fitting brass plugs. Readings were only taken at radii of four inches or more, where the flow could be safely assumed to be two dimensional.

Preliminary tests gave velocity distributions far from that of a free vortex. This was much improved by placing a fine mesh wire gauze cylinder, $5\frac{1}{4}$ inches diameter, in the centre of the casing. With this gauze, reasonably uniform velocity distributions along axial lines were obtained. (Velocity distributions were uniform within about 2%.)

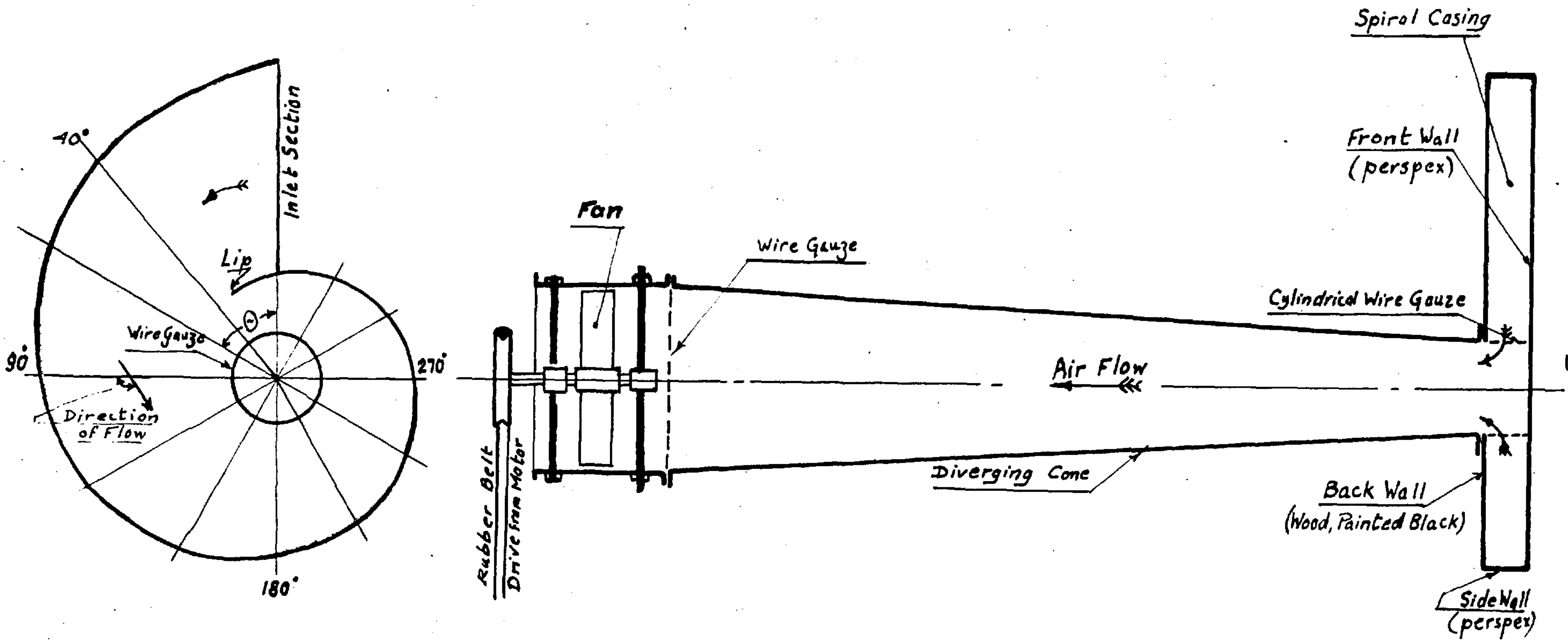

Figure (2)a. Diagram of Apparatus

(1 cm → 4 inches)

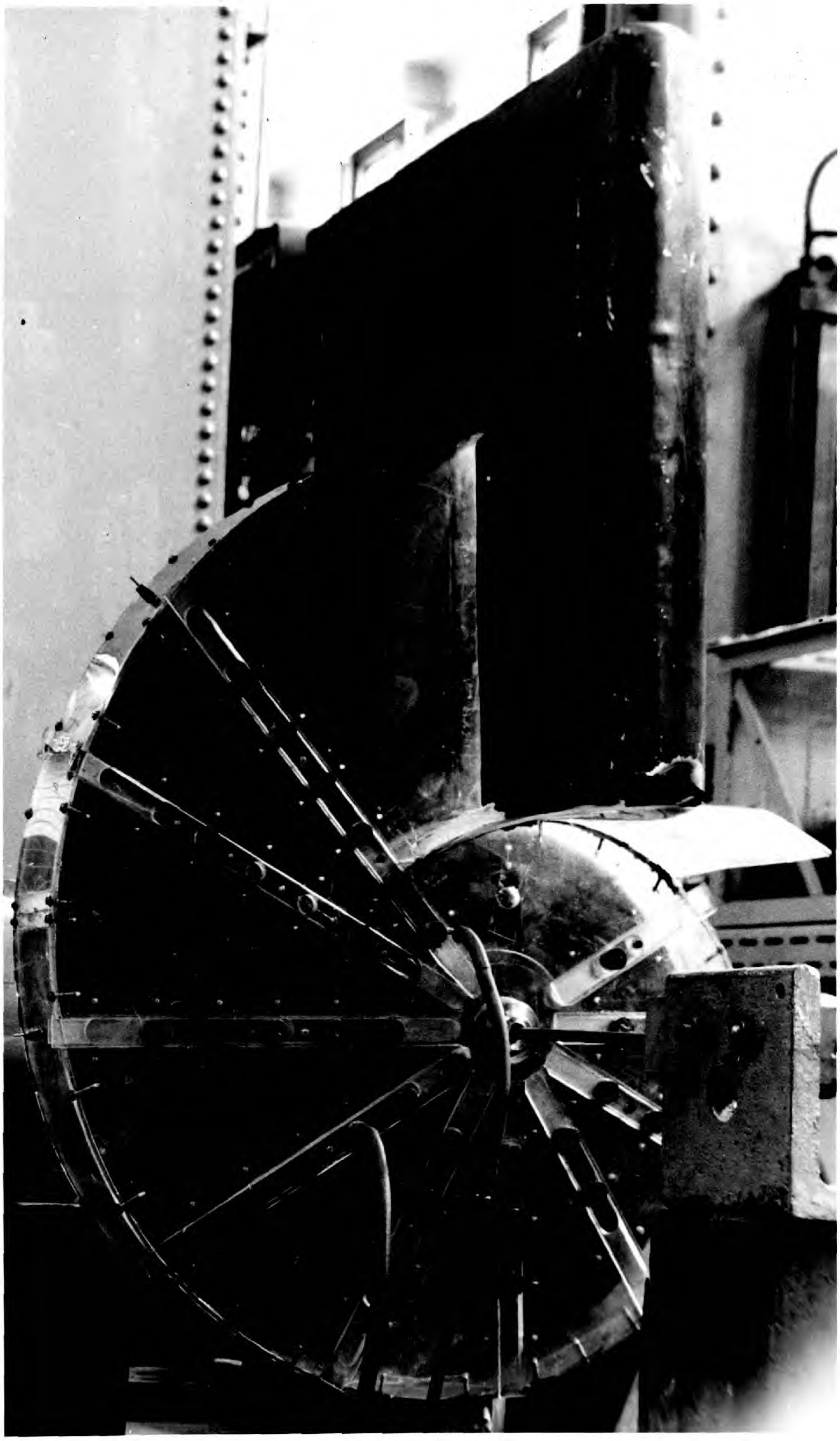

Figure (2b)- Spiral Casing.

An alchol sloping tube manometer connected to an arrow-head yawmeter, a total head tube,or a disc static tube, was used for measuring the direction of flow, the total head,or the static head inside the casing. For measuring the static heads at the front wall, the manometer was connected to a I/32 inch hole in one of the brass plugs.

The static pressure at the front wall at a radius of 6 inches and I20° with the inlet, was measured on another similar manometer and taken as an indication of the flow through the casing. This was kept constant throughout the investigation of the corresponding flow.

The amount of flow was calculated from the measured velocity distributions at the section making 40° with inlet, taking into account the small radial flow between the lip and that section, appendix (3).

Measuring instruments

I. Static Head: Owing to the stream lines being curved, it was thought that the usual pitot tube would not be suitable for measuring the static head, figure (3).

On the other hand, a thin straight tube

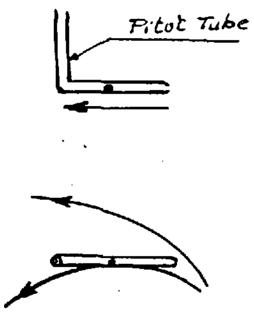

Figure (3)

inserted so that the opening at its end is in the plane of the stream lines, gives a misleading measurement due to the large amount of induction caused by the air flowing across the end of the tube, figure (4).

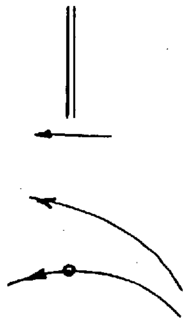

Figure(4)

Professor Unwin found that a plate placed across at the end of the tube prevents this inductive action, and subsequently Heenan and Gilbert used a disc static tube, figure (5), for measuring static heads. They found that it gave very correct results.

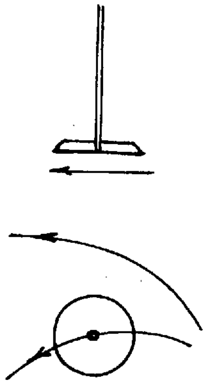

Figure(5)

The author used a tube similar to that used by Heenan and Gilbert, but with different dimensions, figure (6). It was calibrated against a pitot tube, for straight stream lines, and the readings were identical. The curves in figure (7),give the error in the measured head when

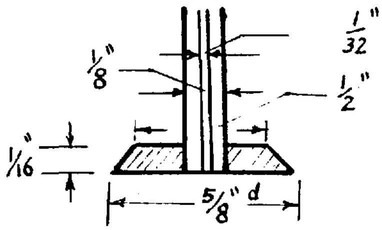

Disc Static Tube
Figure(6)

the disc is inclined to the plane of the stream lines. It shows that for a deviation of 2^{o} which is the maximum expected, the possible error is I% of the velocity head.

2. Direction of Flow: An arrow-head type of Yawmeter was used for measuring the air direction. Two I/I6 th. inch tubes are placed symmetrically with respect to the aerodynamic - centre line, as shown in figure (8). The pressures recorded by both these tubes will then be the same when the air direction and the aerodynamic centre line coincide. But if the direction of the flow is changed, a differential pressure will be recorded.

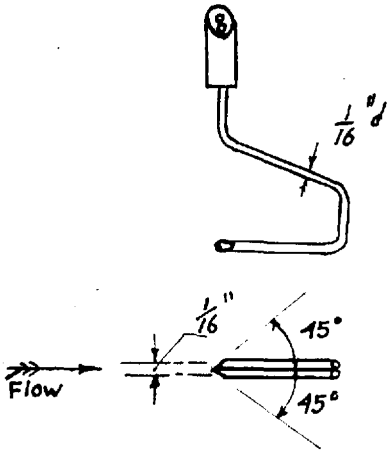

Arrow Head Yawmeter

Figure(8)

The author agrees with Carter, Andrews and Shaw, that this type of yawmeter is more suitable than the claw type, as it is more robust and therefore maintains its calibration.

To estimate the degree of accuracy of the direction measurement, the yawmeter centre line was deviated from the direction of the flow, and a curve was drawn for the differential head recorded by the manometer against the angle of deviation. It is clear from this curve, shown in figure (9), that a deviation of one degree causes an increase, or decrease, of one millimeter on the manometer, and a change of one third of a degree was readily detectable.

To measure the direction of flow and the total head with one instrument, a pitot cylinder was later used after being calibrated against the yawmeter for the direction measurement. They agreed within the limits of measurement, namely one third of a degree.

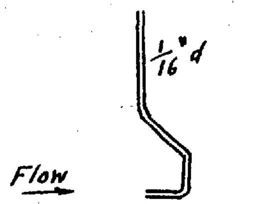

Total Head Tube

Figure (10)

3. Total Head: When the yawmeter was used for measuring the direction of flow, the total head was ~~meas~~ measured by a total head tube shown in figure(IO). For convenience, this was later replaced by a pitot cylinder which measured both the direction and total head. When compared, both instruments gave the same total head readings.

Visual Observation of Stream Lines

In "Modern Developments in Fluid Dynamics", it is stated that "the smoke produced by hygroscopic salts, like titanium tetrachloride, on exposure to air, contain a large percentage of small particles of water held in suspension, to which they mainly owe their obscuring powers. This presence of water makes them heavier than air."

The author, however, noticed that the smoke generated in still air did not sink under gravity. Titanium tetrachloride was therefore used, and was found to give very satisfactory results. A drop of the liquid was placed at the end of a glass rod which was held in the air stream. For studying the flow close to the wall, the drop was placed on the wall. The smoke produced was drawn into a thin trail which remained visible for a long distance downstream. The front perspex wall of the casing is devided by radial sections every 30°, and every section is marked every two inches. The back wall is painted black. This made it easy to map the stream lines.

There were some disadvantages for using this smoke. Besides its harmful effect on the person using it, the hydrochloric acid present in the smoke corrodes any metal it contacts. It also corrodes the rough edges of the perspex, and when passing through a narrow passage, the smoke leaves a deposit which blocks this passage. This was experienced while using the smoke to illustrate the presence of excess energy, when the total head tube was blocked several times.

Experimental Results

In these experiments where the flow was 3.53 cusecs., the value of 'A' in equation (8) page 7 was :

$$A = -\frac{q}{\gamma} = \frac{3.53}{1/4} \times \frac{1}{2\pi} / 0.161 \times 10^{-3}$$

i.e. $A = -1.397 \times 10^{4}$ which is quite large, and therefore according to that equation, the effect of viscosity on the free vortex pattern is negligible.

The observed contours of static head at the front wall of the casing are shown in figure(II). They are close to a circular shape, which indicates that the motion is very nearly symmetrical about the axis, as assumed in deriving equations (4) and (5) page 4. Near the side wall however, the spiral angle of IO degrees is sufficient to give quite large derivatives with θ , whereas equation (7) is for the case when $\frac{\partial}{\partial\theta} = 0$ only. Static pressures at the side wall did not agree with the pressures at the corresponding radii inside the casing. Also it was not possible to take measurements at $'r' < 4$ inches in this spiral casing as the flow in that region is three dimensional, and in any case the equation would be untenable there for that reason.

Vortex Centre;

It is suggested here that the motion observed was almost exactly a free vortex, which agrees with the theory, but the vortex centre O_1 , was rotating in a circle of radius 'b' round a point 'D'. This suggestion is supported by visual observations of water flowing from a tank through a vertical diverging cone. The axis of the central core, at the 3 inches diameter inlet to the cone, was seen to be rotating in a circle about ½ inch diameter. The centre of that circle was slightly displaced from the centre of the inlet. This explains the slight deviation from the free vortex for $r < 6$ inches in the casing as shown below.

If v_1 is the instantaneous tangential velocity at a point P inside the casing, figure (33), then the measured tangential velocity v is in fact the root mean square value.

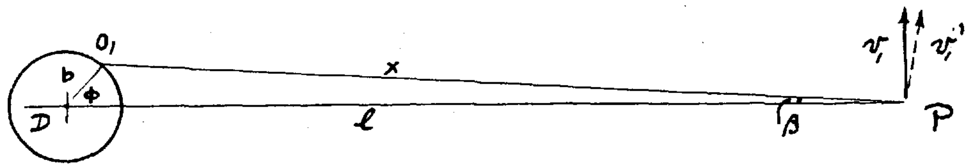

P	is the measuring point in the casing
v_1	is the instantaneous tangential velocity at P ($v_1 = v_1'$ as β is small)
O_1	is the vortex centre
D	is the centre of the circle described by O_1
b	$= DO_1$, $\ell = DP$, $\phi = O_1\hat{D}P$
x	$= O_1P$ is the vortex radius $= \sqrt{\ell^2 + b^2 - 2\ell b\cos\phi}$
v	is the measured tangential velocity at P

Figure (33)

i.e. $v^2 = \frac{1}{2\pi}\int_0^{2\pi} v_1^2 \, d\phi$ where $v_1 = \frac{c}{x}$ (free Vortex)

$$\therefore \quad v^2 = \frac{c^2}{2\pi}\int_0^{2\pi} \frac{d\phi}{\ell^2+b^2-2\ell b\cos\phi}$$

By integration, this finally gives;

$$v^2 = \frac{c^2}{2\pi} \times \frac{2}{\ell^2-b^2}\left[\tan^{-1}\left\{\left(\frac{\ell+b}{\ell-b}\right)\tan\frac{\phi}{2}\right\}\right]_{\phi=0}^{\phi=2\pi}$$

$$\therefore \quad v = \frac{c}{\sqrt{\ell^2-b^2}} \qquad \text{or} \qquad v\ell\left[1-\left(\frac{b}{\ell}\right)^2\right]^{\frac{1}{2}} = c$$

i.e. $v\ell\left[1-\frac{1}{2}\left(\frac{b}{\ell}\right)^2-\frac{1}{8}\left(\frac{b}{\ell}\right)^4-\frac{1}{16}\left(\frac{b}{\ell}\right)^6-\cdots\right] = c$

Since $\frac{b}{\ell}$ is small, we can take $v = \dfrac{c}{\ell\left[1-\frac{1}{2}\left(\frac{b}{\ell}\right)^2\right]}$

For large values of ℓ , $v = \frac{c}{\ell}$

The mean tangential velocities v , figure(34), were obtained from the observed velocities figures (I2-3I). A larger scale of figure (34) showed that D which is the centre of the circular velocity contours, is at ($\Theta = 90^\circ$, r = 0.065 inches). Hence the values of $\ell = \overline{DP}$ for the different measuring points were measured.

The values of c(the vortex strength = vr) = I3.43 ft.^{2}/ sec. , and b = 0.52 inches gave remarkably close results to the observed velocities as shown in figure (34).

CHAPTER 2

SECONDARY FLOW AND ENERGY DISTRIBUTIONS

EXCESS ENERGY

SECONDARY FLOW

It was noted from the measured flow directions, and also visually, by using smoke, that there are three different streams in the casing. The front and back ones, i.e., near the boundaries, tend to flow radially. The central stream tends to flow tangentially, as shown in diagram (35). This confirms the motions described by I.A. Winter. There must be a secondary flow from the centre to the boundaries

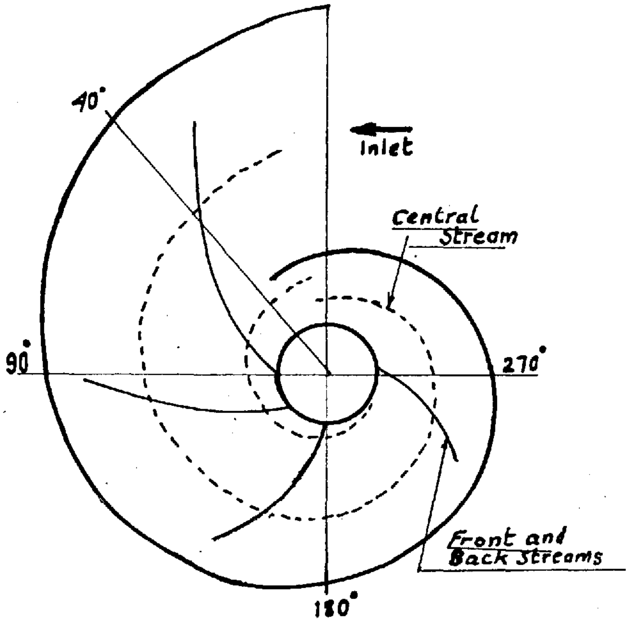

Different Streams in Casing
Diagram (35)

to replace the radial flow which passes through the wire gauze. This secondary flow was detected by the disc tube when measuring the static pressure along a line parallel to the axis. It indicated a static head higher in the front half and lower in the back half than the mean head, diagrams (36). The difference however was only about two percent.

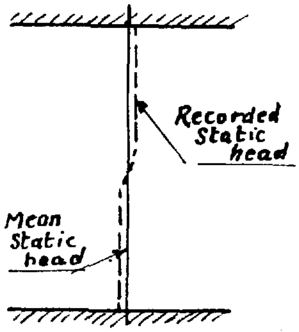

Diagram(36) a

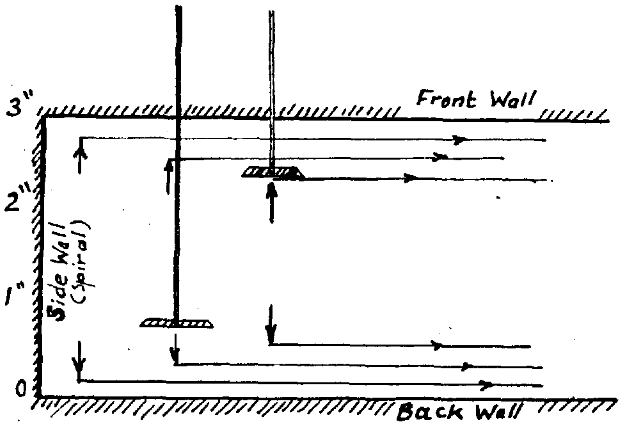

Diagram (36) b

The secondary flow is more powerfull at the 270° section, where the radial component near the boundaries is much larger than that at the 90° section, and considerably larger than that at the 180° section, figures (29), (19) and (25). Also by comparing the static pressure distribution at (90°, R=14 inches), figure (49), (180°, R=10 inches), figure (53), and (270°, R=6 inches), figure (56), the difference of head between front and back halves increases towards the small end of the casing.

<u>Radial Velocity</u>

The change in mean radial velocity with θ, i.e., angle with inlet, is shown in figure (37). For a flow of 3.53 cusecs., the area under the curve gives the flow as 3.4 cusecs., i.e., with an error of 3.7 %.

Pressure Distribution Inside The Casing

Graphs in figures (38) - (56), show the total and static head distributions at different points in the casing. For different depths from the back of casing, $\frac{1}{8}$, $\frac{1}{2}$, I, I$\frac{1}{2}$, and 2 inches, the total head curves along radial sections are drawn in figures (58) - (62). The inlet total energy is atmospheric, i.e., zero.

The Wake

The total head curves give an indication of the wake extending from the lip of the casing. The front and back parts of the wake, being near the boundaries, move more rapidly towards the axis than the central part, and leaves the casing as a low grade fluid, figure (58). Some of the central wake passes to the boundaries and so it diminishes gradually. The rest disappears a little before I80^{o} by mixing with the fluid with excess energy nearby.

EXCESS ENERGY

Measurement of the total head indicated that there is a region in which the total energy is more than the total inlet energy. This occured in the central stream at the 40^{o}, 90^{o}, 270^{o} and 360^{o} sections, figures (6I) and (62). There is no question of an error in the measuring instrument, as these were checked and rechecked, and by using chemical smoke, this excess energy was illustrated and the result photographed.

Excess energy was first mentioned by Mr. Firth in his M.Sc. thesis. While investigating the form of wake behind the lip in a similar casing, he noticed that the total head tube gave a reading greater than the inlet head. In the following part, this interesting phenomenon is investigated.

Visual Observation of Excess Energy

To illustrate visually the excess energy recorded by the total head tube at several points inside the casing, titanium tetrachloride was used. The total head tube was set at a point of 4 inches radius, making an angle of 400° with the inlet, and its axial distance from the back wall was 2 inches, figure (63). The total head tube was [illegible] disconnected from the manometer and connected to a short glass tube open to the atmosphere, figure (64). When a drop of titanium tetrachloride was placed inside this glass tube, the smoke produced was blown out in the atmosphere, which indicates that the total energy measured by the total head tube at that point was higher than the atmospheric pressure, i.e., higher than the inlet energy which is atmospheric, figures (65) and (66).

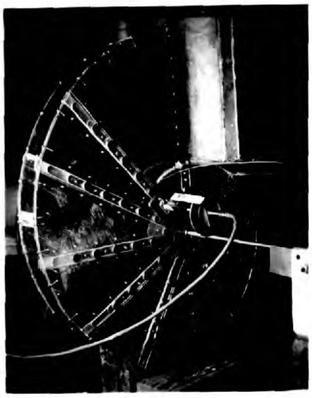

Figure (63)

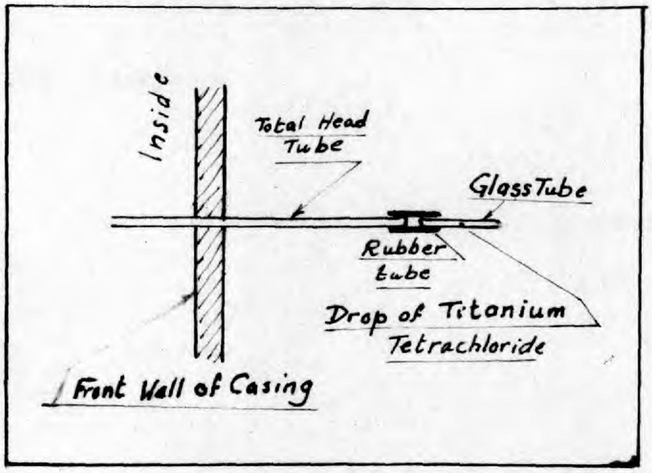

Figure (64)

For comparison, Figure (67) shows the smoke produced by the titanium tetrachloride when there was no flow through the casing,and the pressure inside was also atmospheric. It is noted that in this case the smoke flows freely, quite distinct from the two previous cases in figures (65-b) and (66-b), where the smoke is blown out of the tube.

Figure (65-a)

Total head tube connected to a short glass tube open to the atmosphere.

Figure (65-b)

(Flow = 3.53 cusecs.) Drop of titanium tetrachloride placed inside the glass tube.

Total head tube at

θ = 400°, R = 4 inches, Z = 2 inches from back wall.

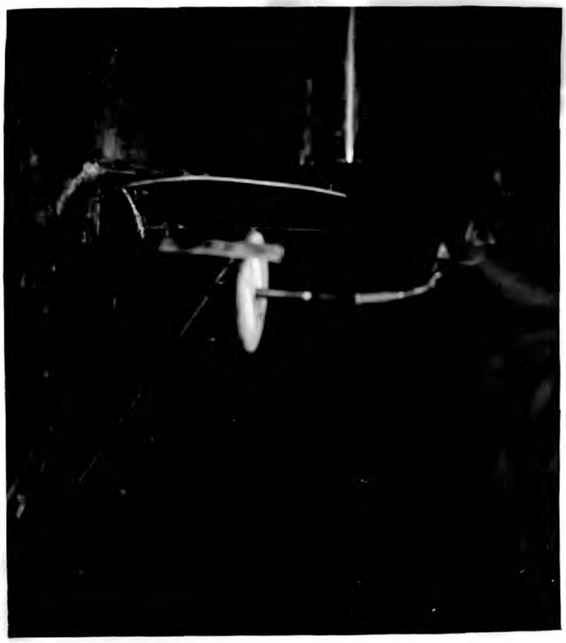

Figure (66-a)

(Flow = 3.2 cusecs.)
Before introducing titanium tetrachloride.

θ = 400°, R = 4 inches, Z = 2 inches from back wall.

Figure (66-b)

(Flow = 3.2 cusecs.)
A drop of titanium tetrachloride is placed inside the glass tube.

θ = 400°, R = 4 inches, Z = 2 inches from back.

Figure (67)

No flow through the casing.

Smoke flows freely on its own.

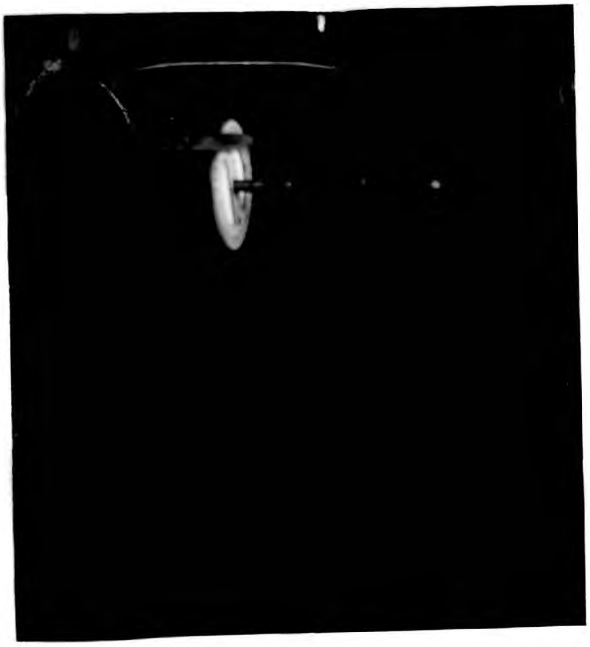

INLET CONDITIONS

To study the effect of inlet conditions on the flow in the casing, and in particular on the excess energy, a disturbance was introduced at the inlet. This was acheived by allowing a paper fan, 4 inches diameter and I inch wide, to rotate in the inlet air stream, diagram (68).

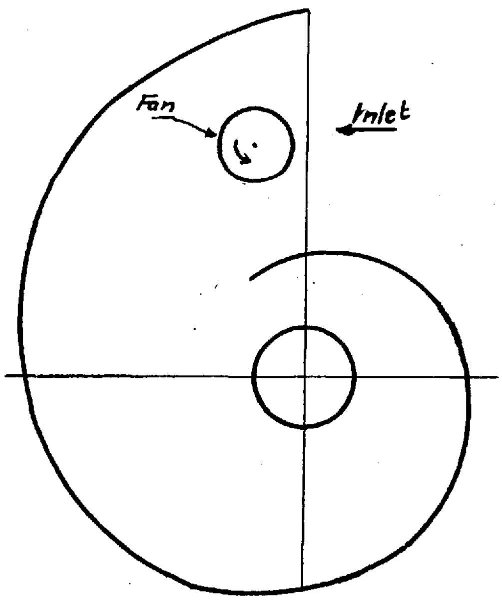

Fan Rotating at Inlet

Diagram (68)

Except for the energy consumed by the paper fan, both the contours of static head, figure (69), and the curves of total head, figures (70) to (75), have the same shape as before. The same region of excess energy again appears, though for this to be seen it is now necessary to base the energies not on the atmospheric pressure but rather upon the actually observed total energy in the region of the inlet, down stream of the paper fan, figures (74) and (75).

This indicates that disturbances at the inlet in themselves do not substantially affect the flow pattern inside the casing.

SHORT FLEXIBLE EXTENSION TO THE LIP

A thin rubber 2.2 inches long was fixed to the lip and allowed to flutter in the air stream, diagram (76), which it did at a frequency of about ten vibrations per second. Its effect on the flow pattern was to shift the centre of the vortex downwards, but the contours of static head remained closely circular, figure (77). The cheif effect of this extension was greatly to augment the losses as seen in figures (78.80). Any possible regions of excess energy are here completely masked.

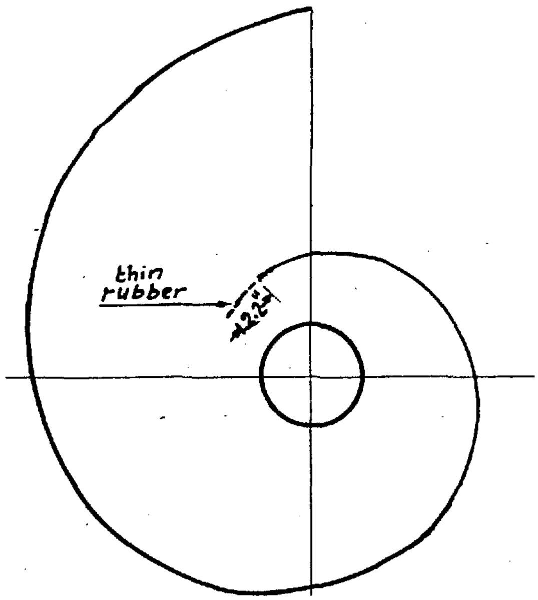

Rubber Extension

Diagram (76)

LONG EXTENSION TO THE LIP

The total head curves mentioned before, figures (6I) & (62), suggests that the excess energy only begins after the wake disappears. In the course of investigating the origin of this excess energy, a long extension to the lip was used; on the one hand to prevent the formation of the wake, and on the other hand to seperate the flow in the region (B) from the direct action of the flow at (A). The lip thus forms a discontinuity in the pressure system which otherwise would link (A) and (B), diagram(8I).

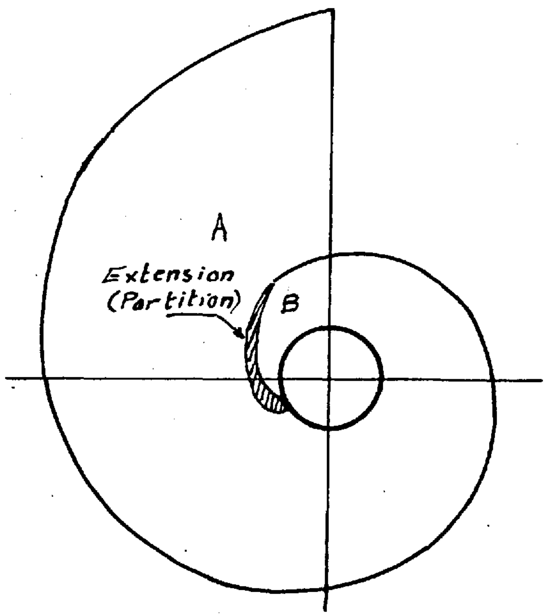

With Partition

Diagram (81)

The ideal extension would have been one with the same curvature as a stream line from the lip. Unfortunately the streams at different depths had different curvatures, and from a practical point of view the lip could only be curved one way. As seen from figure (82), it was made a little steeper than the original spiral.

With the long extension in position, the excess energy only appeared at ($\theta=270^\circ$, $R=4"$), figure (83). The presence of excess energy however, shows that it is not connected with the stresses between the flow at (A) and the flow at (B). It also eliminates the suggestion of a relation between the lip wake and excess energy. This is supported by the fact that the total head curves indicate that the excess energy originated a little before the 270° section, i.e., after the wake disappeared. The stream lines with excess energy at the 270° section kept it until after the (90° - 2π) section, where they mixed with the central wake as discussed on page (21).

It is interesting to note the effect of this partition on the pattern of flow in the casing. The contours of static head, figure (82), are assuming a spiral shape, rather than the circular one of the previous experiments.

CHAPTER 3

ROTATING GAUZE CYLINDER

Near the inlet of a diverging cone, supplied through a spiral casing as in figure (83), the velocities are as shown in figure (84), for which the author is indepted to Mr. A.Sinbel. Near the boundary there is a region of free vortex from A to B, while near the axis from C to O the motion is very nearly, though not exactly, a forced vortex. In that particular experiment, the forced vortex area was equal to 39% of the cross section, or "a", the core radius was equal to 0.623 of the whole radius.

This gives an idea of the kind of motion to be expected near the eye of the casing used in the

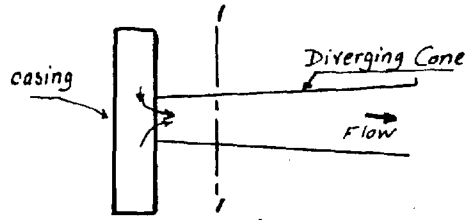

Figure (83)

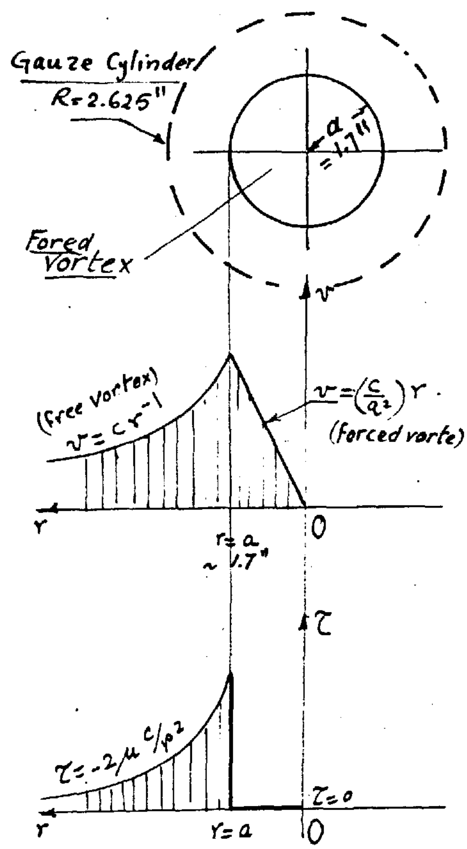

Figure (85)

present experiments, figure (85). Assuming that the inside core is a forced vortex, $v = \omega r$, and the outside a free vortex, $v = c/r$, then if 'a' is the radius where the two join, $\omega = c/a^2$. The shear stress $\tau = \mu\left(\frac{dv}{dr} - \frac{v}{r}\right)$

or $\tau = \mu \, r \frac{d}{dr}\left(\frac{v}{r}\right)$ *where μ is the viscosity*

$\therefore \quad \tau = 0 \qquad$ for $r < a$

and $\tau = -2\mu \frac{c}{r^2} \qquad$ for $r > a$.

Now in the previous investigation, excess energy was observed at r = 6 inches, and down to r = 4 inches which was the limit to which the measuring instrument would reach. While theoretically there is no reason to suggest any abnormal change in the energy distribution due to shear stress, an experiment was arranged to extend the area of forced vortex from $r \cong 1.7$ inches, i.e. 0.623 of eye radius, to r = 2.625 inches which is the gauze radius, particularly to see whether this would affect the excess energy.

This was done by rotating the gauze cylinder anti-clockwise, i.e. in the direction of the air, with a speed equal to that of the adjacent air. As described below, the result was negative, the pattern remained unchanged.

For this experiment, the stationary cylindrical wire gauze was replaced by another similar one, but fixed to a $\frac{5}{8}$ inch shaft. This shaft was rotated by a D.C. motor as shown in diagram, figure (86). It was possible to rotate the gauze either clockwise or anti-clockwise at different speeds which were measured by

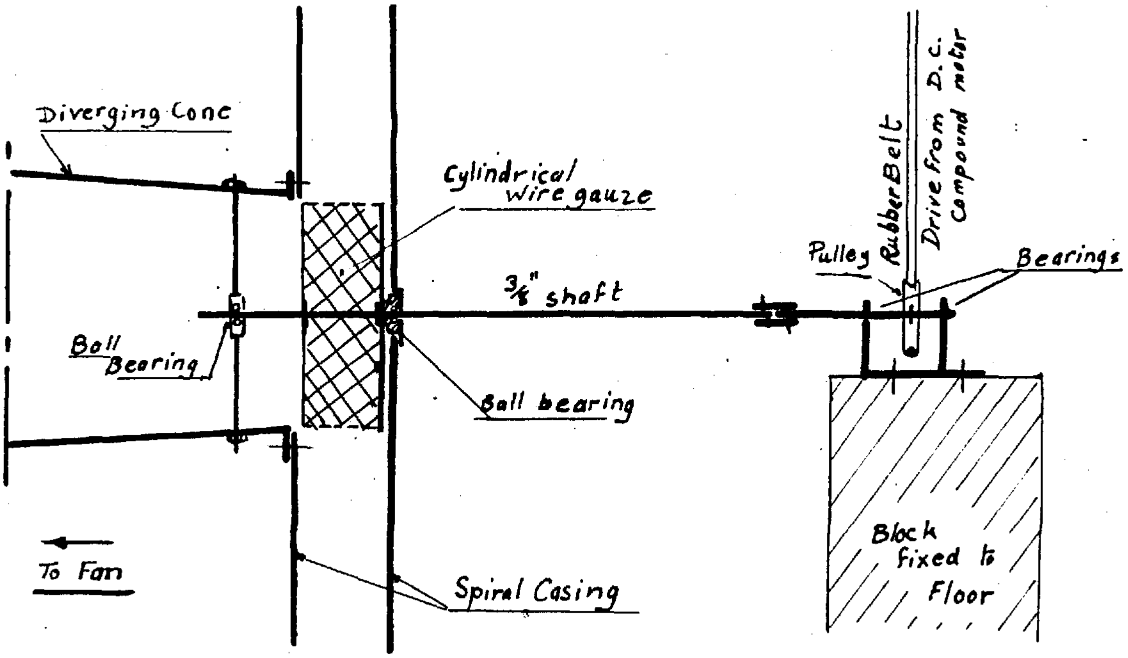

Figure(86). Diagram of arrangement for Rotating wire gauze a tacometer.

Incidentally the motion due to the gauze rotating alone without the fan can be inferred from figure (87) which shows the pressures at the front wall when the gauze was rotated anti-clockwise at a speed of 4300 r.p.m. The shape of the pressure curve at $\theta = 40$ agrees with the motions of smoke introduced near the inlet; it was sucked into the casing between r = 8 to 10 inches, but was blown out at r = 6 to 7 inches and also where $r > 12$ inches, as shown by the arrows.

To investigate the effect of the rotating gauze on the normal flow, the fan was run on its own and the air was driven through the casing as usual. When the gauze cylinder was rotated at 2100 r.p.m., anti-clockwise, i.e. with the direction of the stream, the flow was reduced and the fan speed had to be increased to keep the static pressure at ($\theta = 120^\circ$, r = 6 inches) = - 2.4 feet of air as before. The pressures for both cases are given in figure (88). According to this graph, there is an increase in the static pressures, but the contours of static pressure more or less keep their circular shape.

To make more detailed numerical comparisons, observations were restricted to $\theta = 90$ degrees, the static head at ($\theta = 90^\circ$, r = 8 inches) being kept constant at - 1.4 feet of air by adjusting the fan speed. The gauze was rotated at different speeds, the anti-clockwise rotation taken as positive. Figure (89) is a diagram of the results giving the r.p.m., the ratio of gauze peripheral velocity to the adjacent air velocity V_G/ V_A , and the change of static head at r = 4 inches. For $V_G / V_A > 0$, the static head decreases while it increases for $V_G / V_A < 0$. The experiment was repeated for several rates of flow and the results are shown in a graph of V_G / V_A against the change in static head at r = 4 inches, figure (90). It must be stressed however that the change in head is small and was very difficult to measure. For V_G / V_A from - 2 to + I , no change could be recorded.

Figure (9I) shows that the effect of rotating the gauze is to increase the velocity nearby, though only by 3% even when the gauze was driven at twice the air speed. Apparently the wire gauze is adding angular momentum to the flow long before it reaches it.

CONCLUSION

From the theoretical equations of the spiral motion, it was shown that viscosity changes the pattern of free vortex. The amount of deviation depends on the values of the flow and of the kinematic viscosity of the fluid. In the experiments carried out, where the ratio of the flow to the kinematic viscosity was large, it was shown that viscosity had no effect on the pattern, and the motion was almost exactly a free vortex, which agreed with the theory. The vortex centre however was rotating in a small circle round a point slightly displaced from the centre of the casing.

As shown, the rotation of the vortex centre causes a slight pulsation in the velocities and pressures at $R < 6$ inches. According to E. Ower, if we take the simple case where both the velocity v and the static pressure p vary according to a sine law, both having the same period, i.e.

$$v = v_0 \,(1 + \alpha \sin qt)$$

and

$$p = p_0 \,(1 + \beta \sin qt) ,$$

where v_0 and p_0 are respectively the average velocity and static pressure about which the fluctuations take place. Then the pressure acting at the mouth of the total head tube at any time t is

$$\tfrac{1}{2} \rho v_0^2 \,(1 + \quad \sin qt)^2 + p_0 (1 + \beta \sin qt) = P \text{ (say)}.$$

The periodic time is $2\pi/q$ and the average pressure at the mouth of the tube will be the average pressure over a cycle, i.e. $$\frac{q}{2\pi}\int_0^{2\pi/q} P\,dt$$

i.e. average pressure =

$$\frac{q}{2\pi}\left[\tfrac{1}{2}\rho v_0^2\int_0^{2\pi/q}(1+\alpha\sin qt)^2 + p_0\int_0^{2\pi/q}(1+\beta\sin qt)\right]$$

Integrating and introducing the limits we obtain,

average pressure $= p_0 + \tfrac{1}{2}\rho v_0^2(1+\alpha^2/2)$.

Hence the average pressure acting at the mouth of the total head tube exceeds that due to the sum of the static pressure and the velocity head corresponding to the average velocity.

It must be mentioned however, that in the previous experiments, these fluctuations and excess energy only occured at radii less than 6 inches, and therefore they do not affect the investigations of the vortex motion. In the region of R between 6 and 4 inches, the average excess energy is 0.01 of the velocity head. This gives $\alpha = 0.14$, i.e., velocity fluctuates by about 14 % of its mean value, whereas nearer to the centre of the casing the flow would be very unsteady.

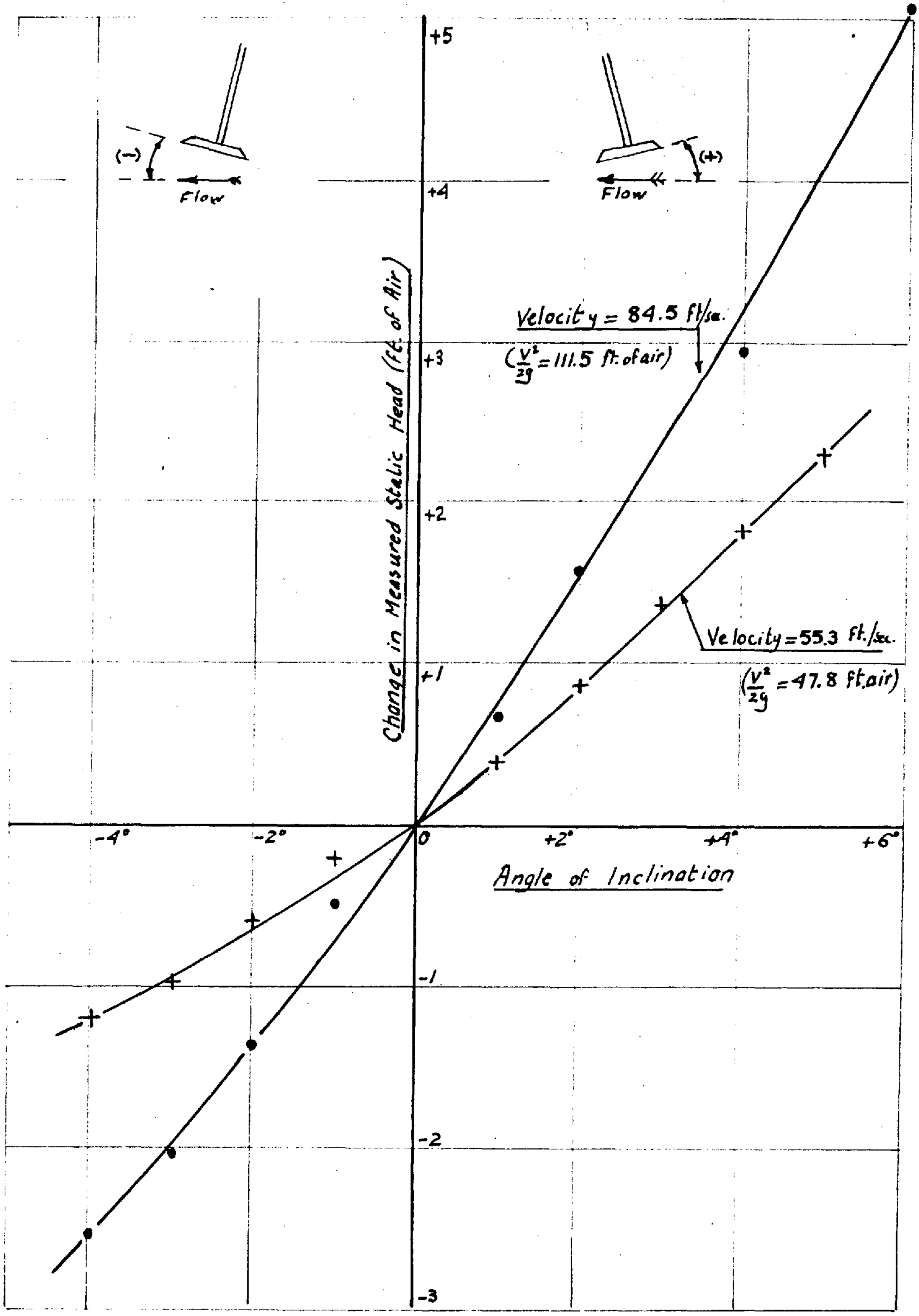

Figure (7). Disc Static Tube

Error in Measured Static Head due to inclination of Disc to the Flow.

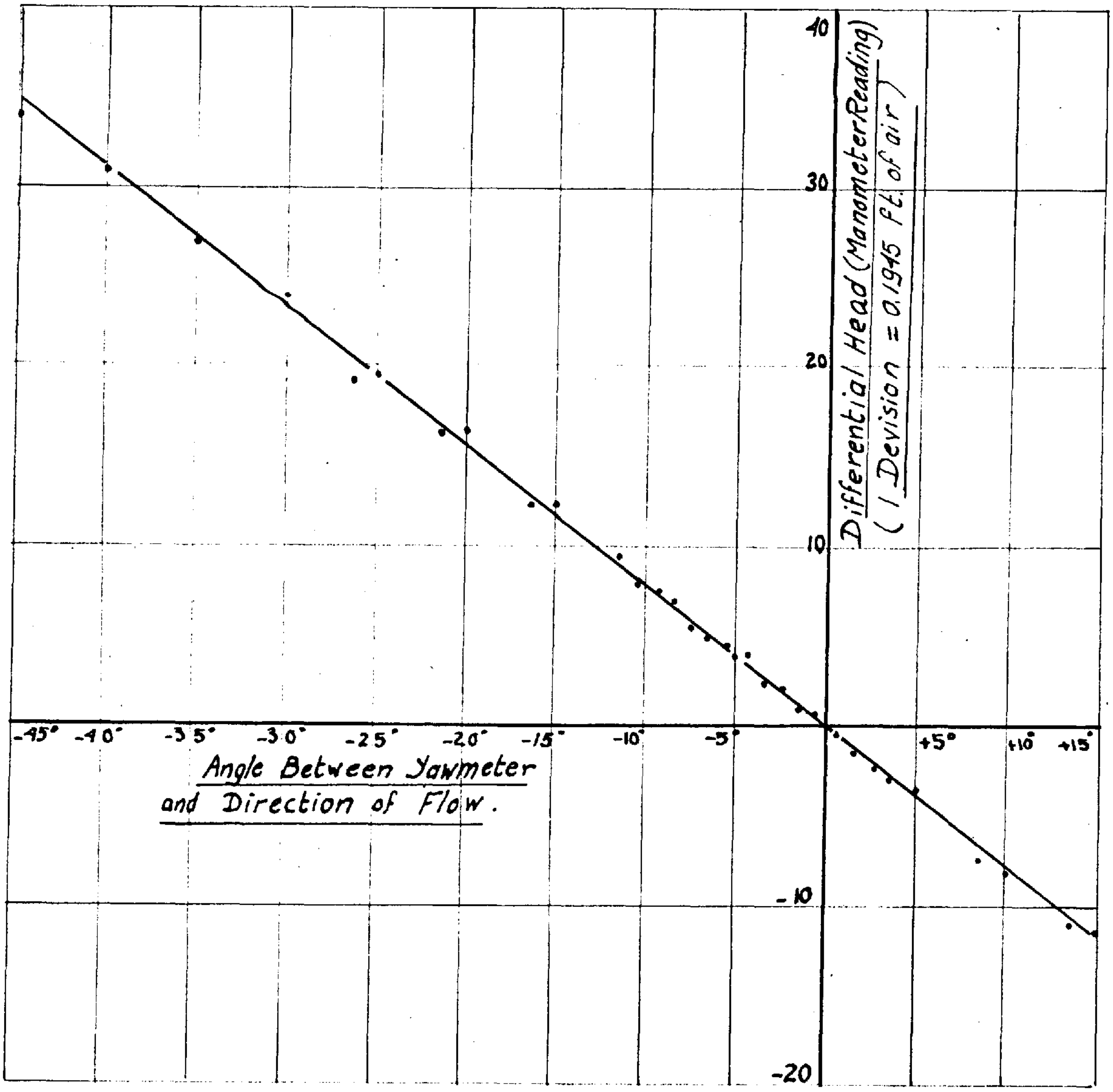

Figure (9) - Jawmeter (arrow-head type)

Differential Head - Angle between the centre line of the Jawmeter and the direction of air

(Velocity of air 9.5 ft/sec.)

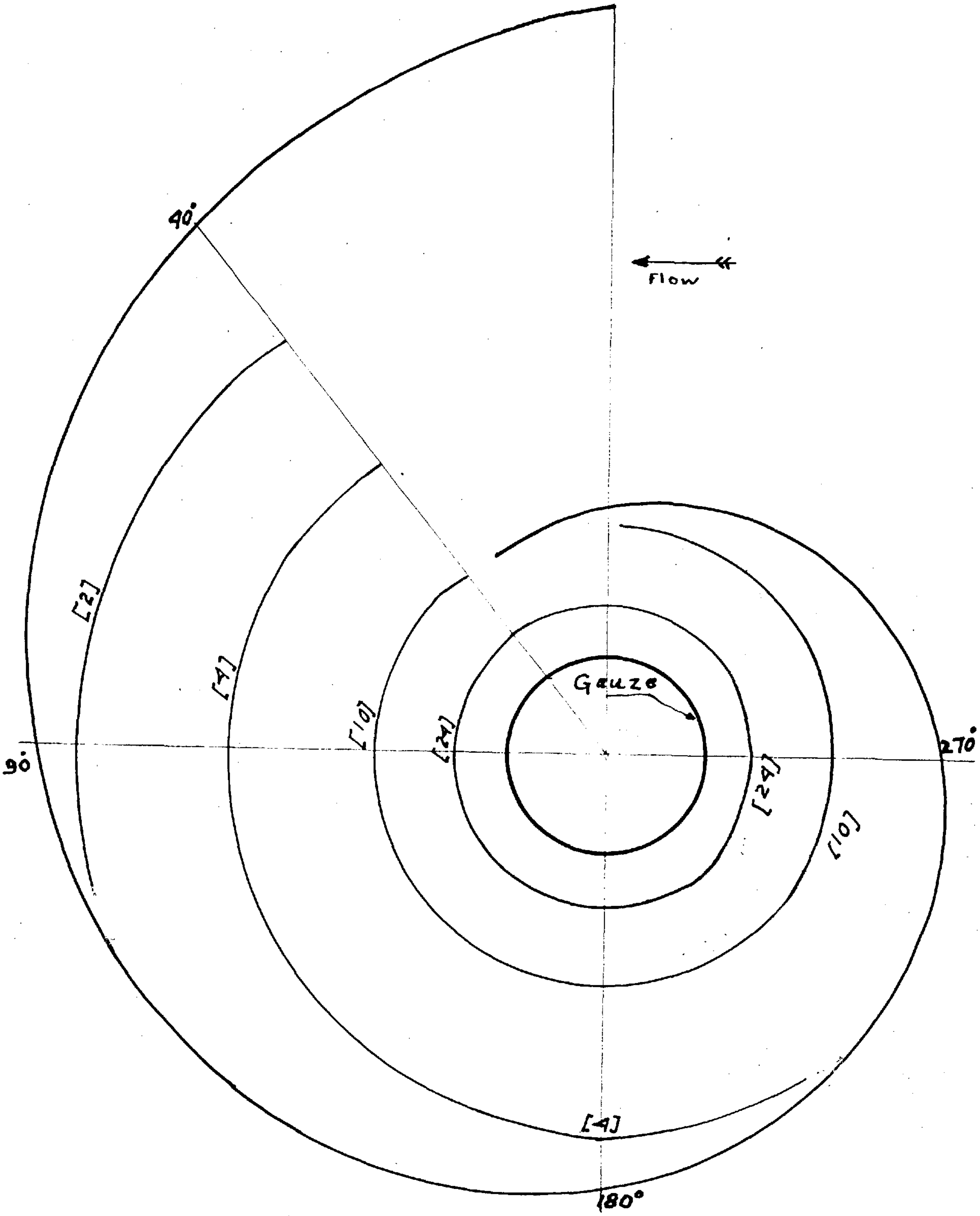

Figure (11) a. Contours of Static Head at Front Wall (ft. air)

(Flow = 3.53 cusecs.)

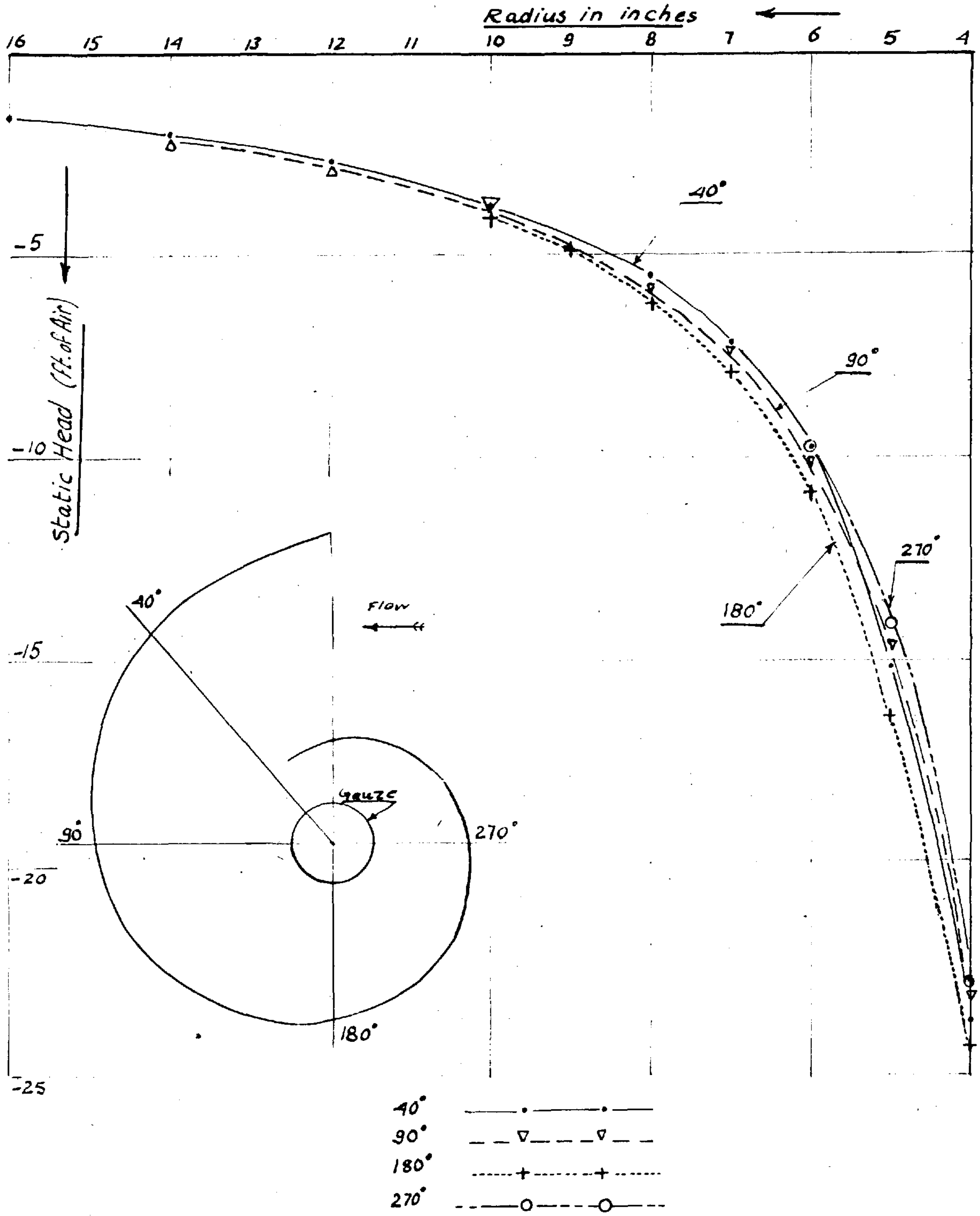

Figure (11)b. Static Head at Front Wall

(Flow = 3.53 cusecs.)

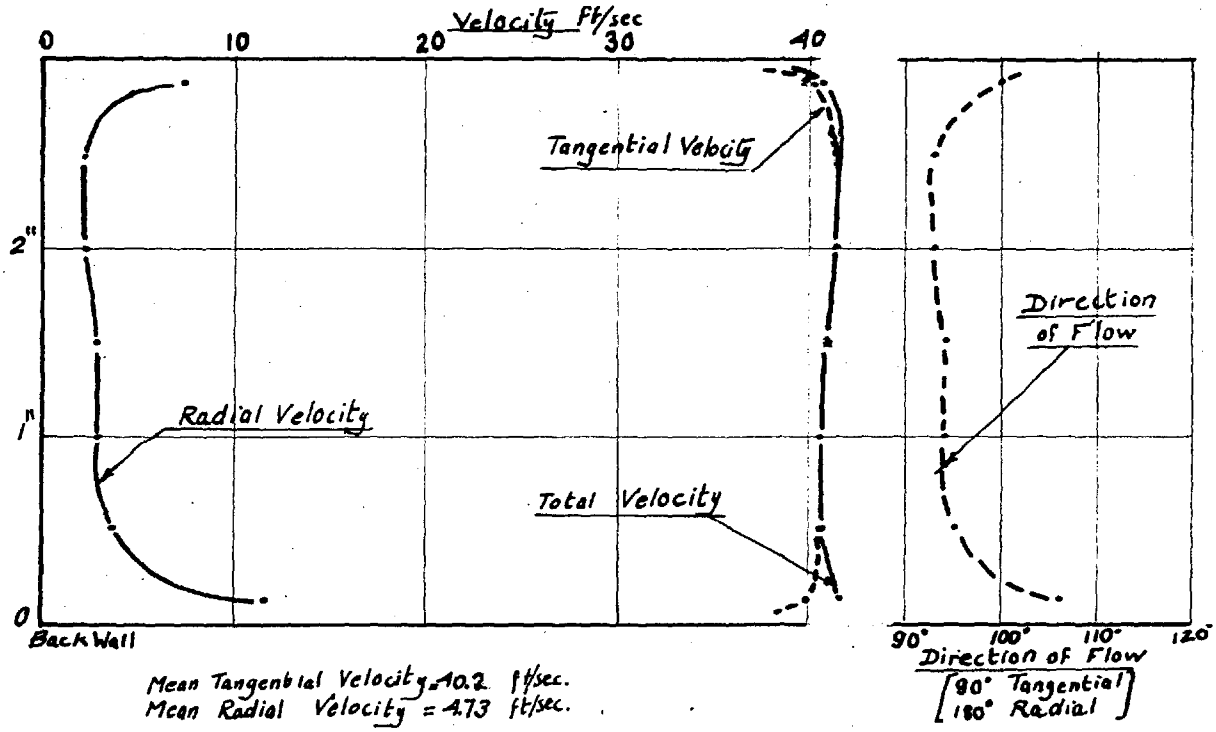

Mean Tangential Velocity = 40.2 ft/sec.
Mean Radial Velocity = 4.73 ft/sec.

Figure (12) - Velocities & Direction of Flow
At $\theta = 40°$, $R = 4$ inches (Flow = 3.53 cusecs.)

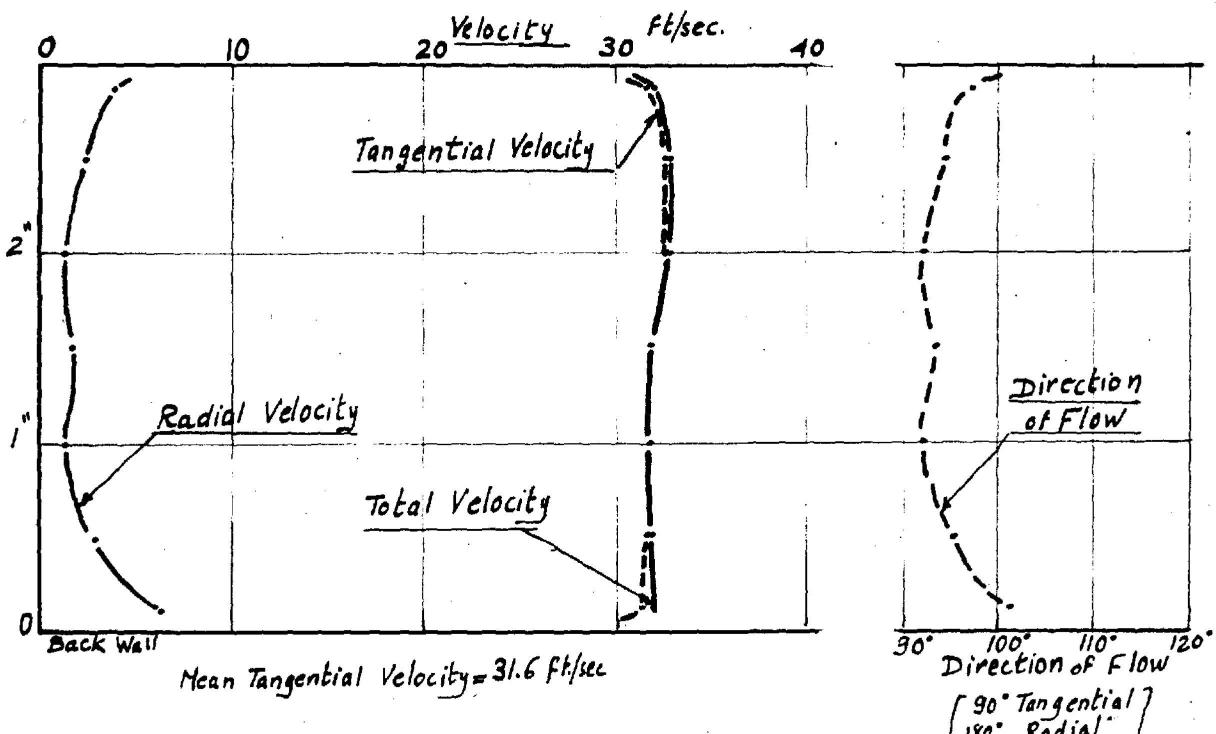

Mean Tangential Velocity = 31.6 ft/sec

Figure (13) . Velocities & Direction of Flow
At $\theta = 40°$, $R = 5$ inches (Flow = 3.53 cusecs.)

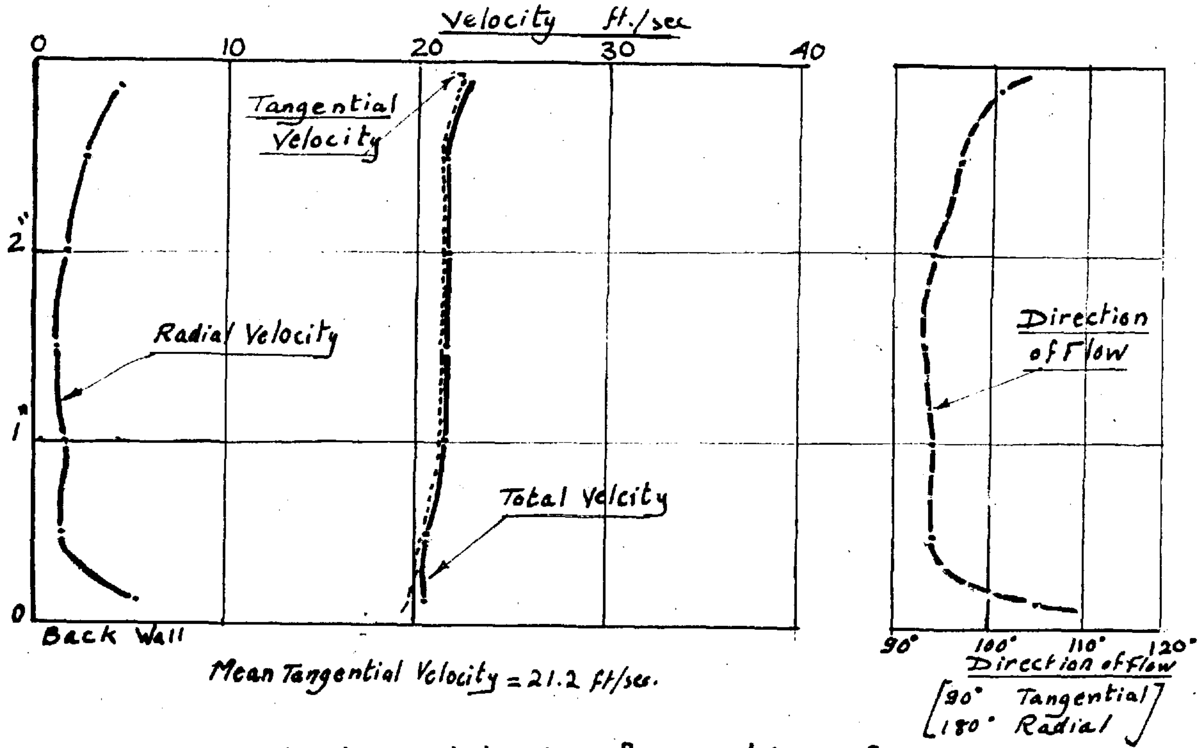

Figure (14). Velocities & Direction of Flow

At $\theta = 40°$, R = 6 inches (Flow = 3.53 cusecs.)

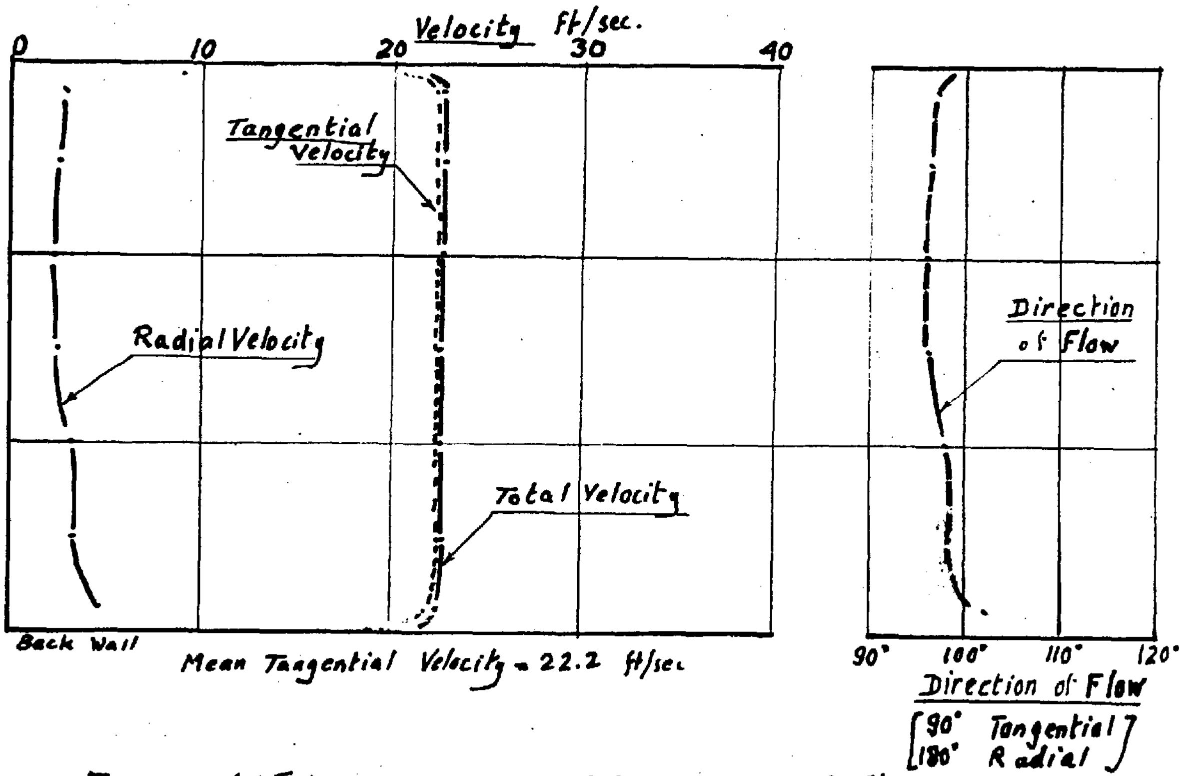

Figure (15) - Velocities & Direction of Flow

At $\Theta = 40°$, R = 7 inches (Flow = 3.53 cusecs.)

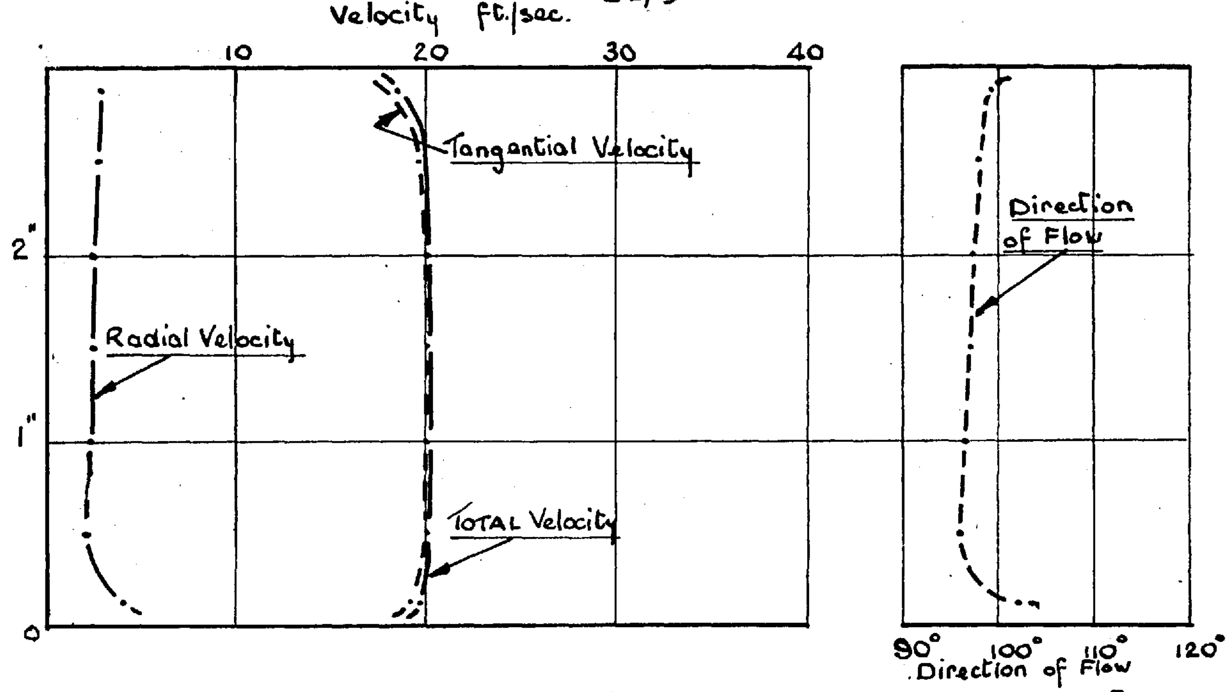

Direction of Flow
[90° Tangential
180° Radial]

Mean Tangential Velocity = 19·16 ft./sec.
Mean Radial Velocity = 2.80 "

FIGURE.(16) - VELOCITIES & DIRECTION OF FLOW
At $\Theta = 40°$ $R = 8"$ (Flow = 3·53 cusecs)

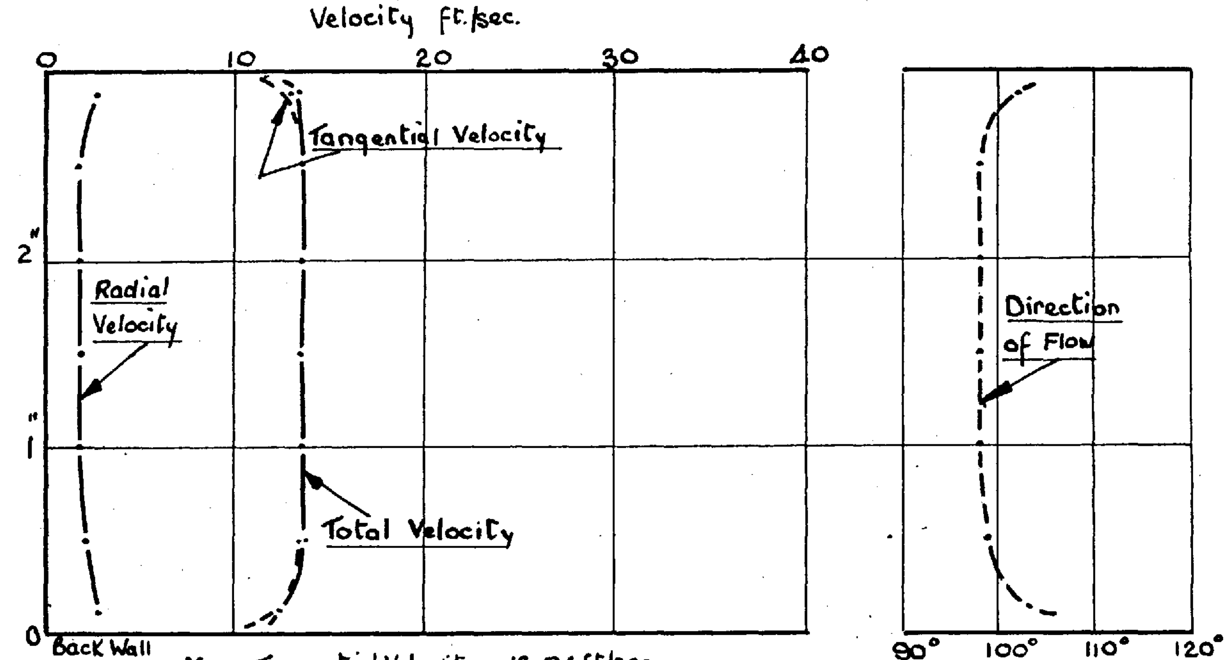

Mean Tangential Velocity = 13·04 ft./sec.

Direction of Flow
[90° Tangential
180° Radial]

FIGURE.(17) - VELOCITIES & DIRECTION OF FLOW
AT $\Theta = 40°$ $R = 12"$ (Flow = 3·53 cusecs)

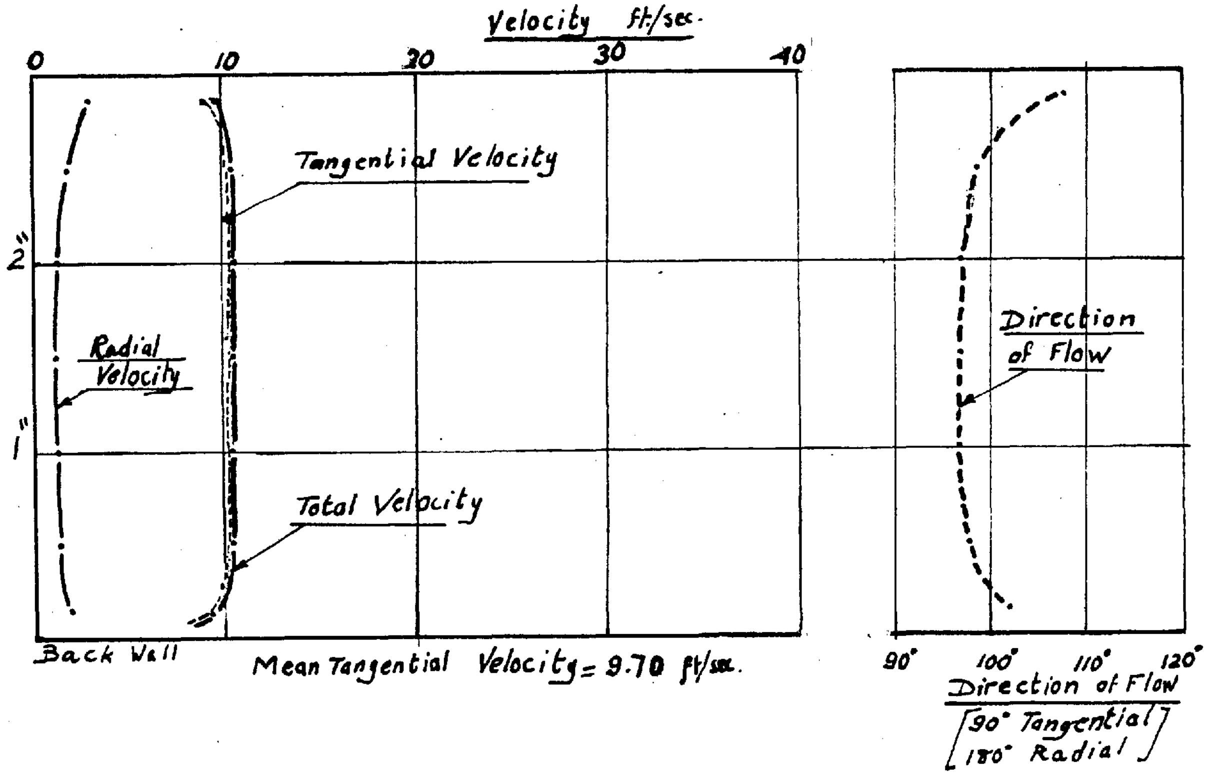

Figure (18). Velocities & Direction of Flow

At $\theta = 40^\circ$, R = 16 inches (Flow = 3.53 cusecs.)

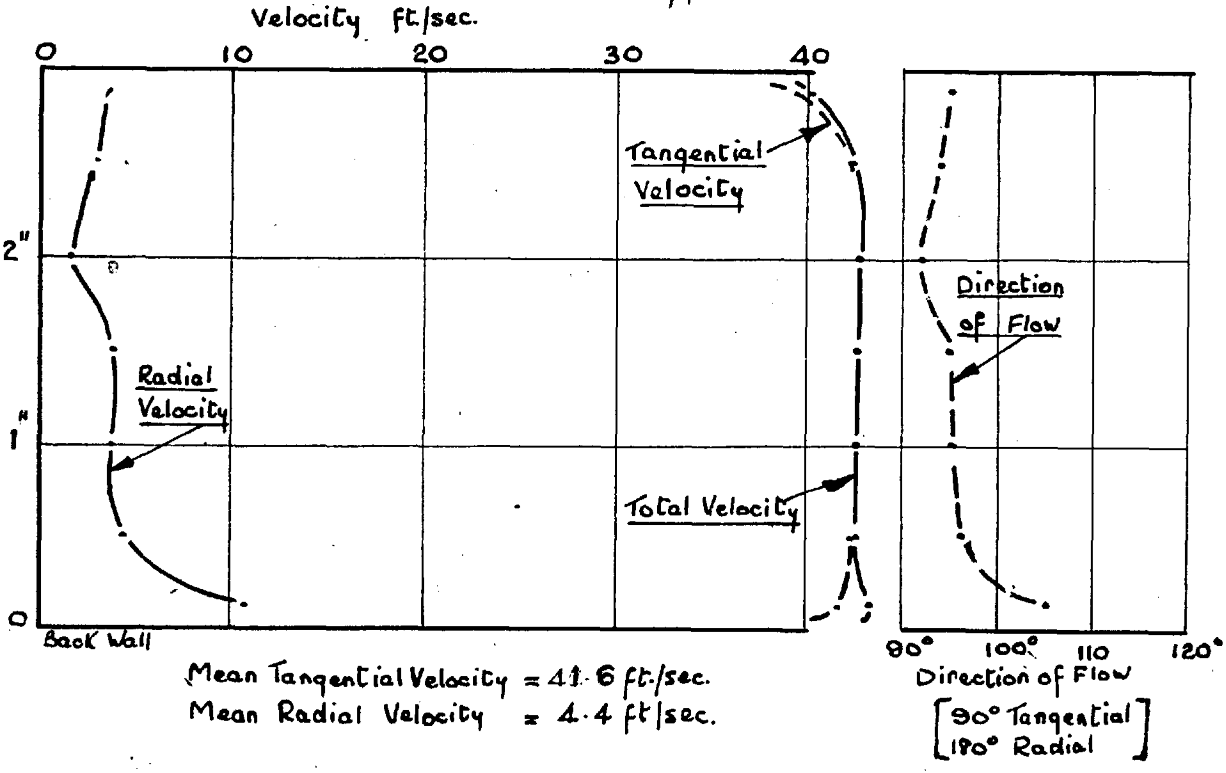

Mean Tangential Velocity = 41.6 ft./sec.
Mean Radial Velocity = 4.4 ft/sec.

FIGURE (19). VELOCITIES AND DIRECTION OF FLOW AT $\Theta = 90°$ $R = 4"$ (Flow = 3.53 cusecs)

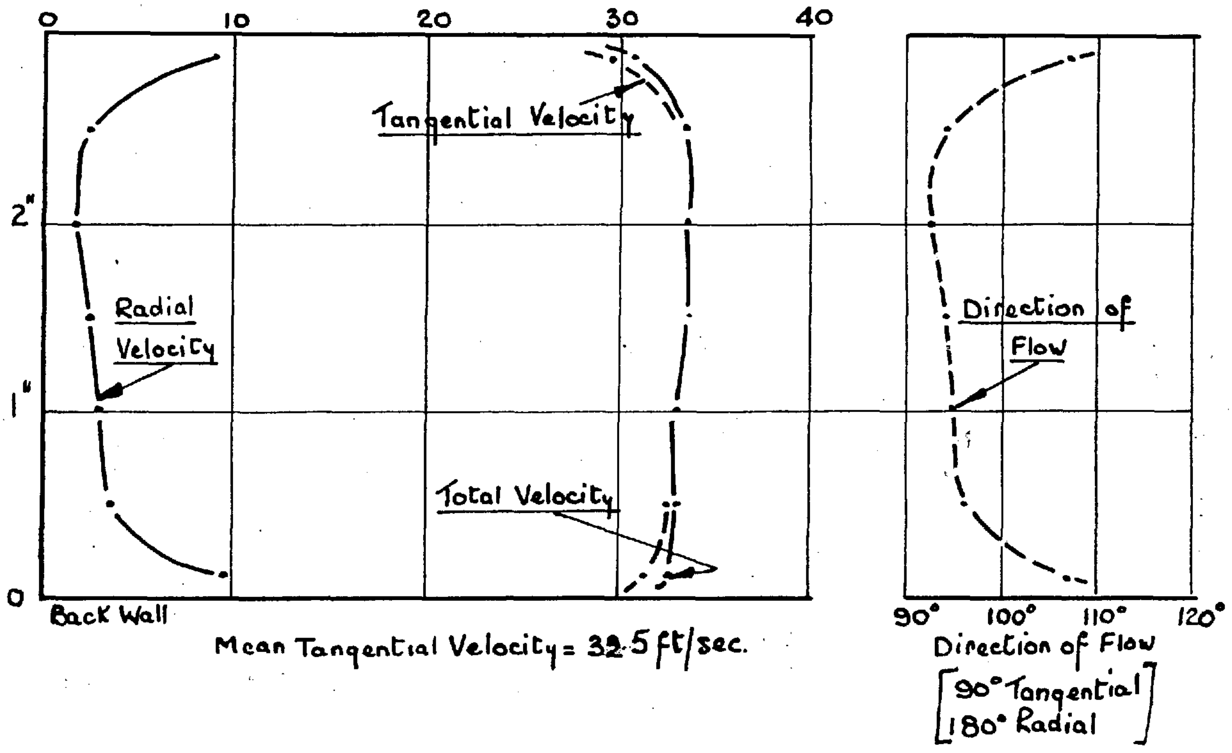

Mean Tangential Velocity = 32.5 ft/sec.

FIGURE (20)_VELOCITIES & DIRECTION OF FLOW AT $\Theta = 90°$, $R = 5"$ (Flow = 3.53 cusecs)

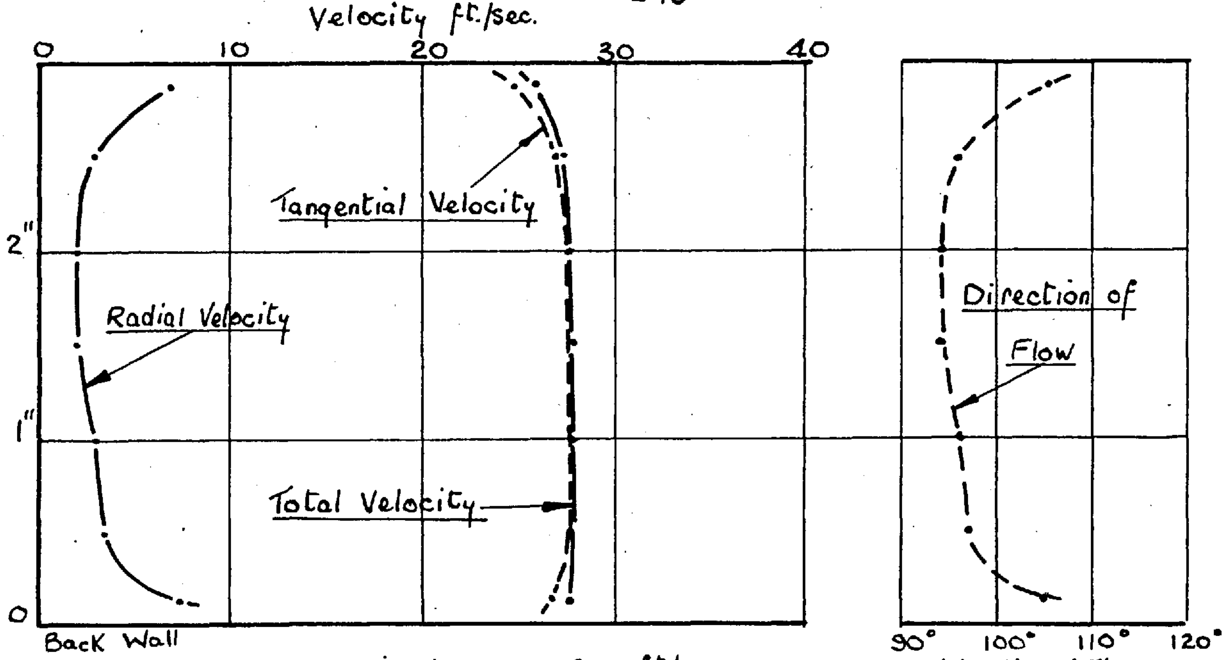

Mean Tangential Velocity = 27.0 ft./sec
Mean Radial Velocity = 3.75 ft./sec.

Direction of Flow
[90° Tangential
180° Radial]

FIGURE (21) - VELOCITIES & DIRECTION of FLOW
AT θ = 90° R = 6" (Flow = 3.53 cusecs)

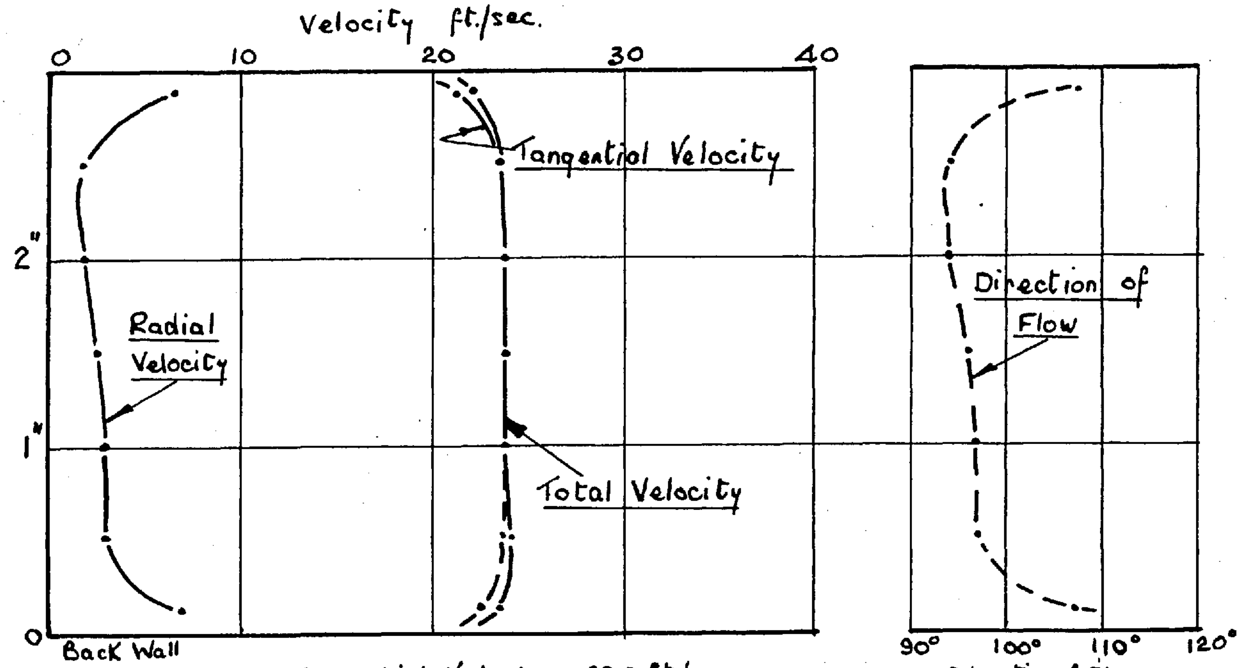

Mean Tangential Velocity = 23.0 ft./sec.

Direction of Flow
[90° Tangential
180° Radial]

FIGURE (22) VELOCITIES & DIRECTION of FLOW
AT θ = 90° R = 7" (Flow = 3.53 cusecs)

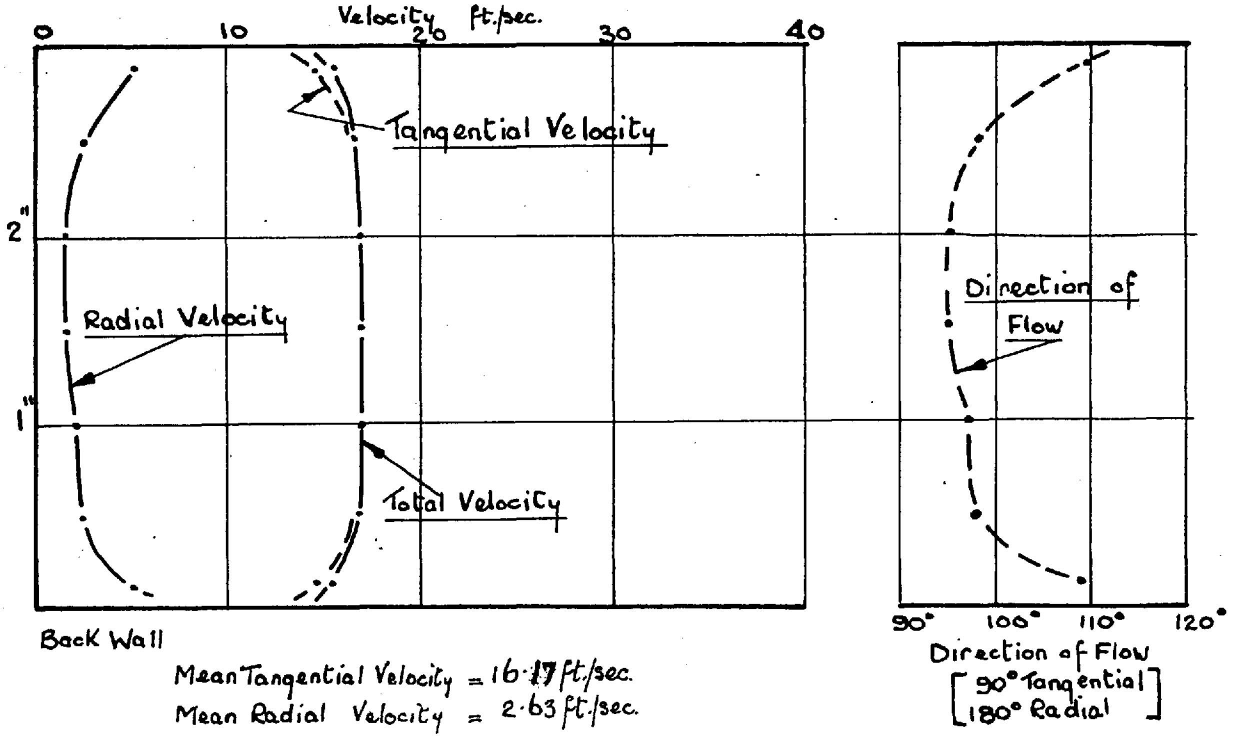

FIGURE (23) - VELOCITIES & DIRECTION of FLOW

AT Θ = 90° R = 10" (Flow = 3·53 cusecs)

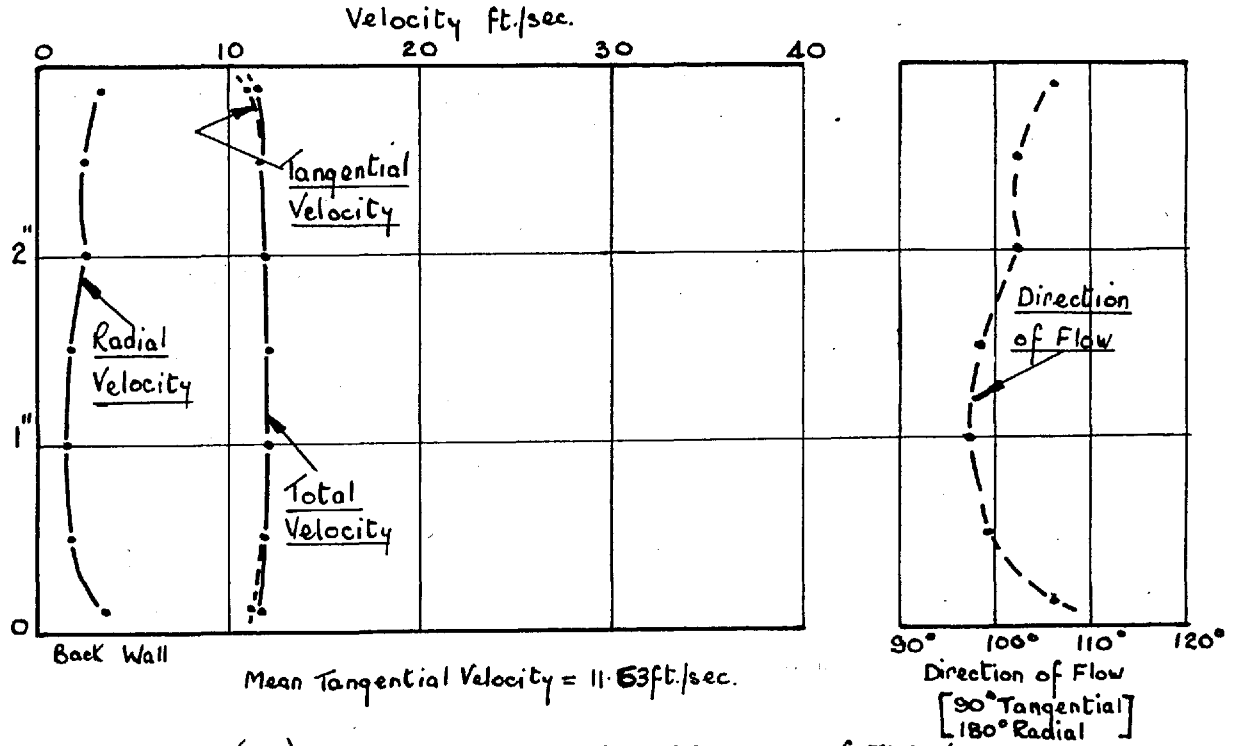

FIGURE (24) - VELOCITIES & DIRECTION of FLOW

AT Θ = 90° R = 14" (Flow = 3·53 cusecs)

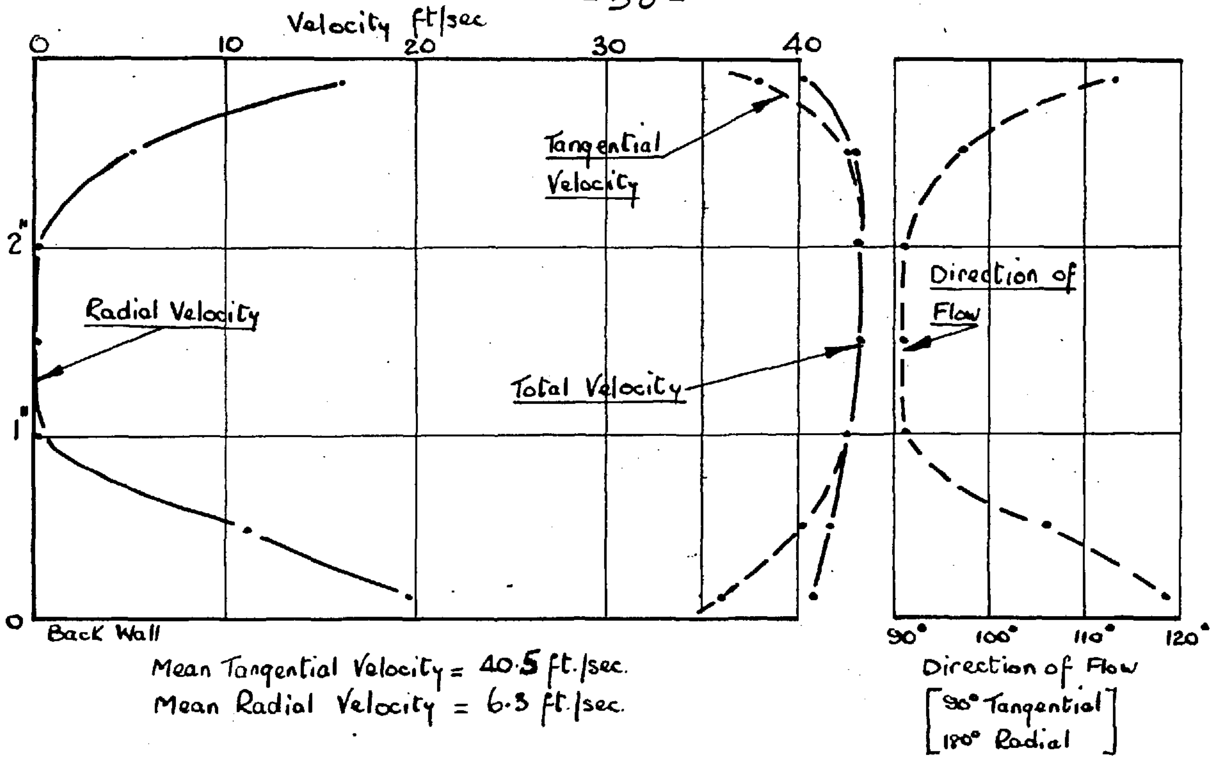

FIGURE(25)_VELOCITIES AND DIRECTION OF FLOW
AT $\Theta = 180°$, $R = 4"$ (FLOW = 3·53 cusecs)

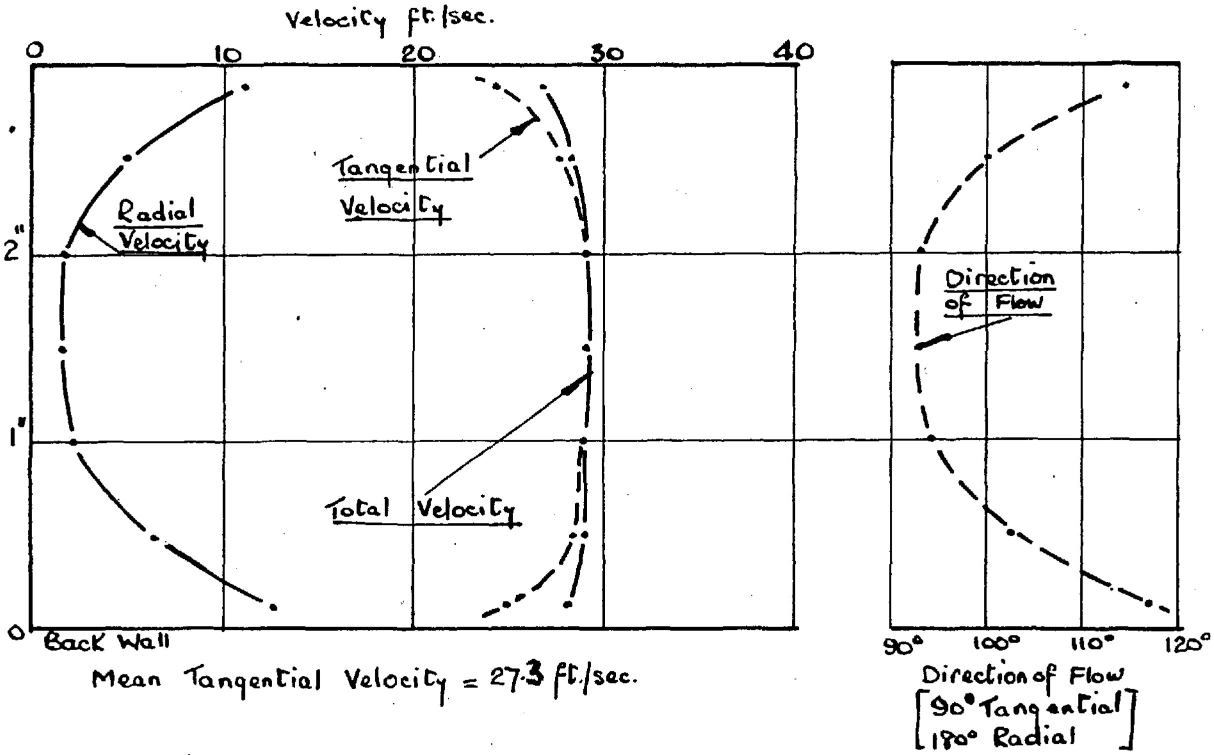

FIGURE (26)_VELOCITIES AND DIRECTION OF FLOW
AT $\Theta = 180°$, $R = 6"$ (FLOW = 3·53 cusecs)

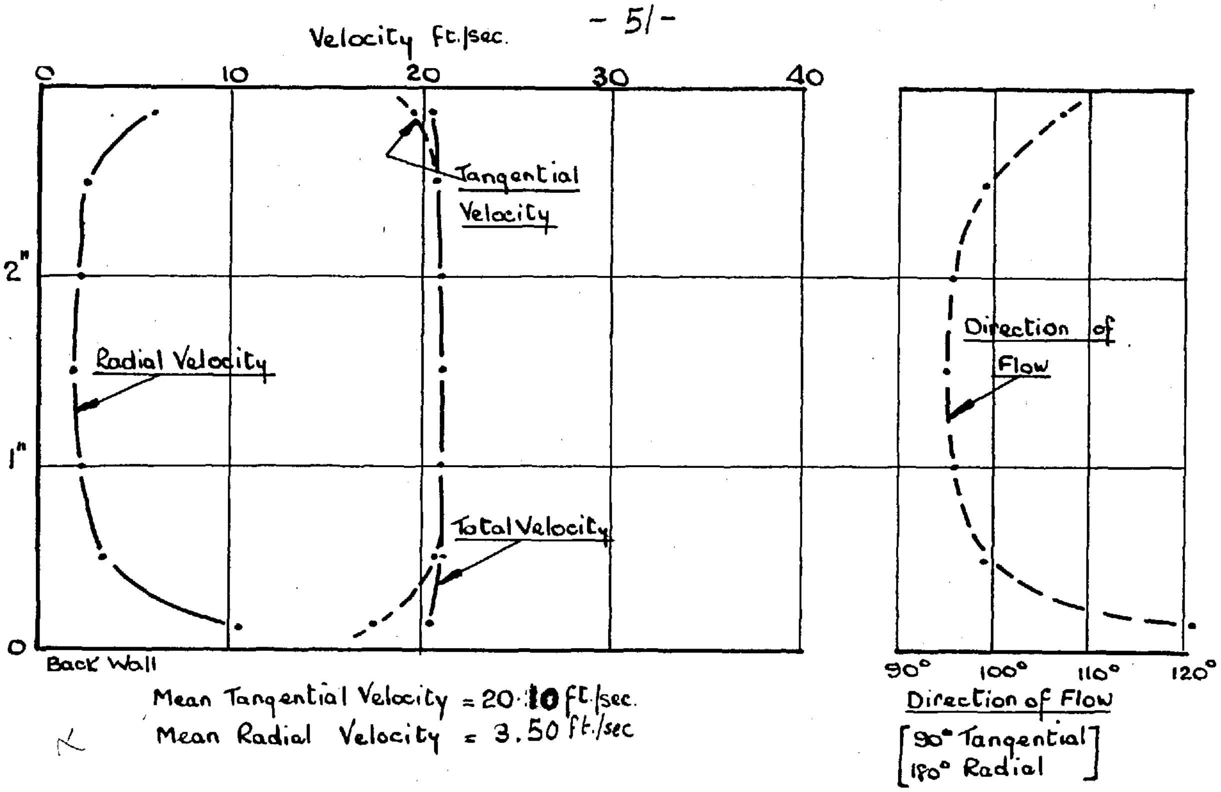

FIGURE (27) - VELOCITIES & DIRECTION OF FLOW

AT $\Theta = 180°$, $R = 8"$ (FLOW = 3·53 cusecs)

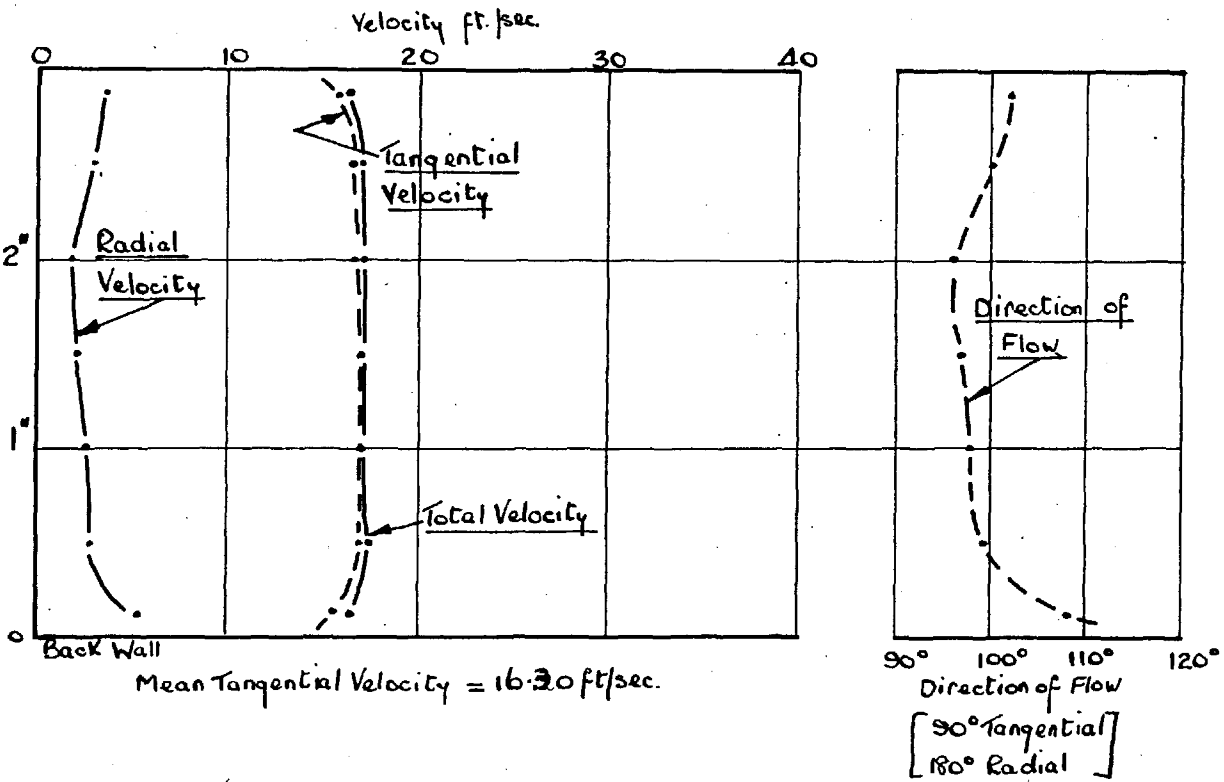

FIGURE (28) - VELOCITIES & DIRECTION OF FLOW

AT $\Theta = 180°$ $R = 10"$ (FLOW = 3·53 cusecs)

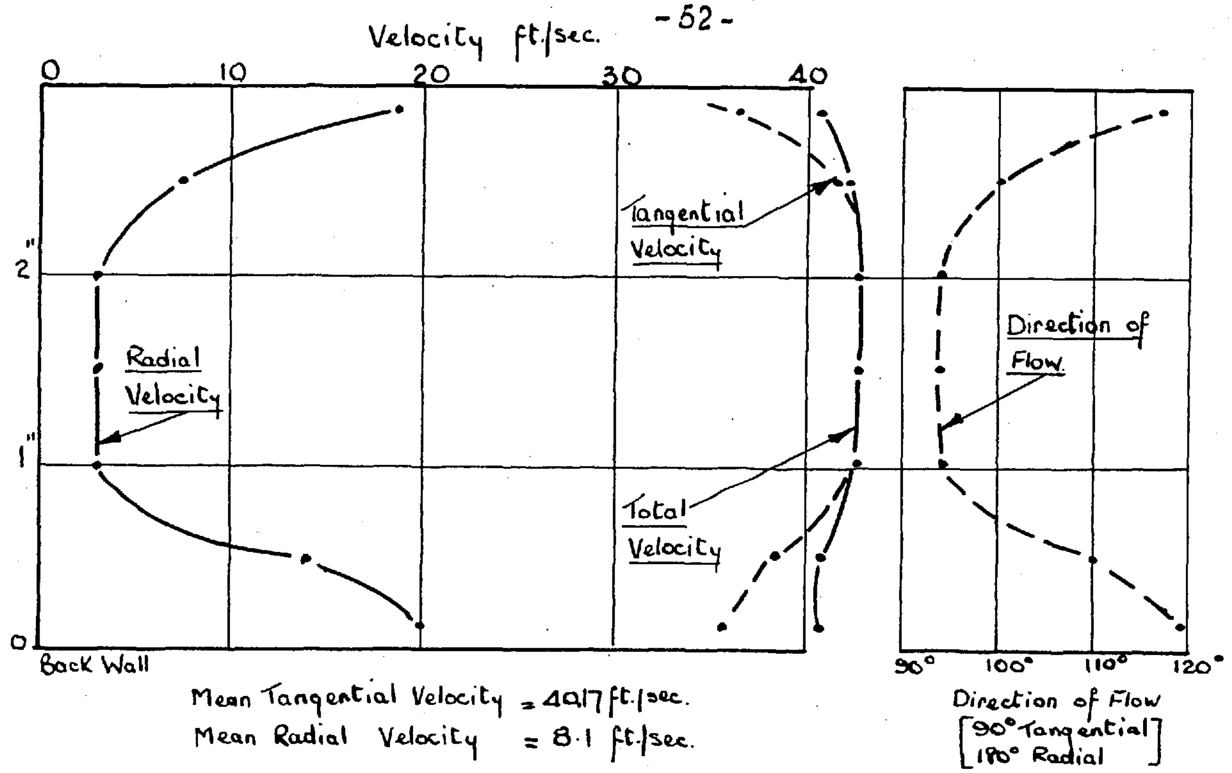

Mean Tangential Velocity = 40.17 ft./sec.
Mean Radial Velocity = 8.1 ft./sec.

FIGURE (29) - VELOCITIES & DIRECTION OF FLOW AT $\Theta = 270°$, $R = 4"$ (Flow = 3.53 cusecs)

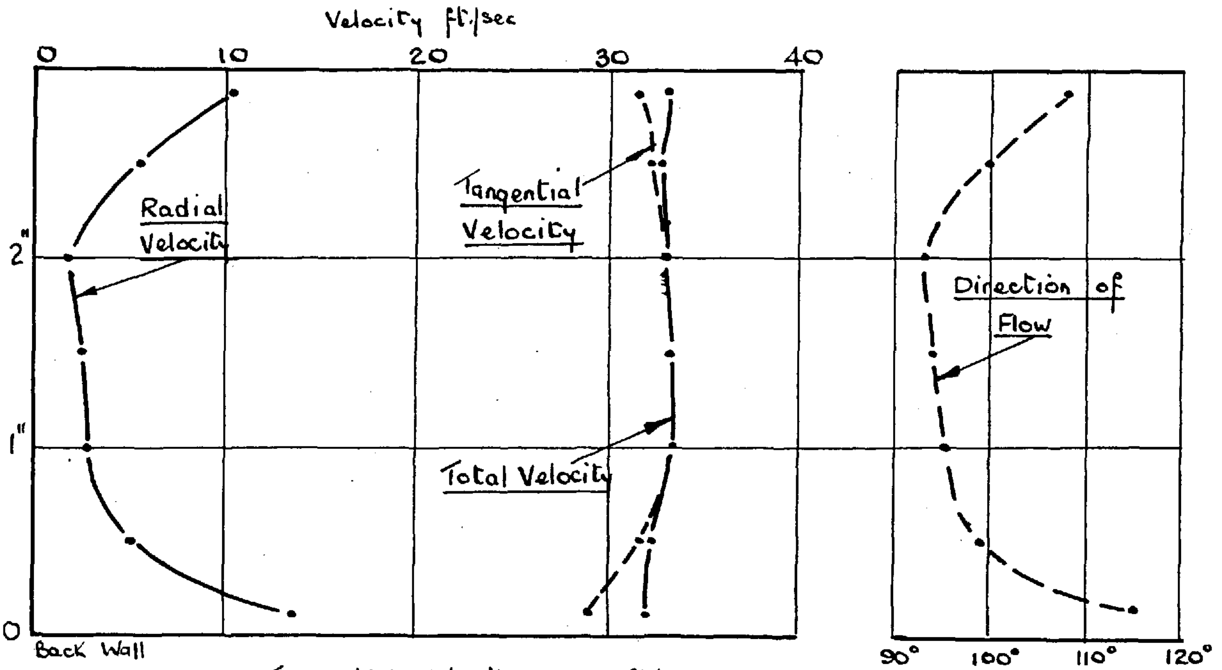

Mean Tangential Velocity = 32.0 ft./sec.

FIGURE (30) - VELOCITIES & DIRECTION OF FLOW AT $\Theta = 270°$, $R = 5"$ (Flow = 3.53 cusecs)

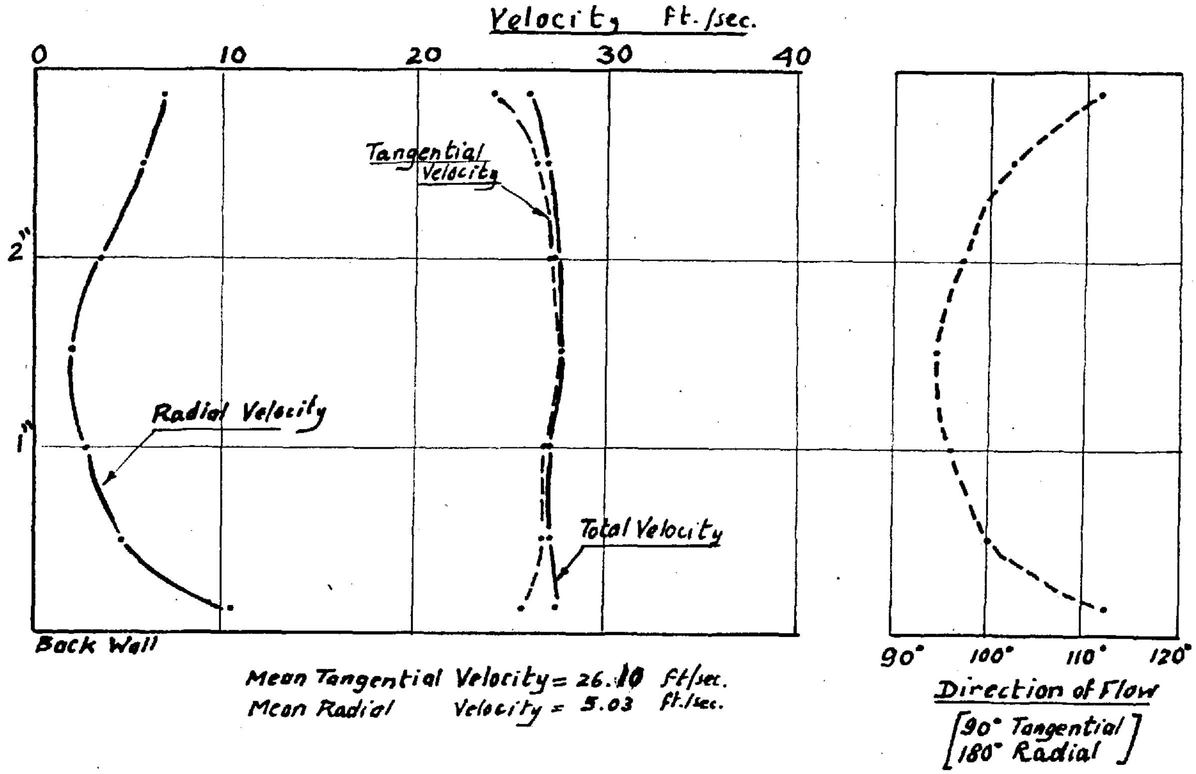

Figure (31). Velocities & Direction of Flow

At $\theta = 270°$, $R = 6$ inches.(Flow = 3.53 cusecs.)

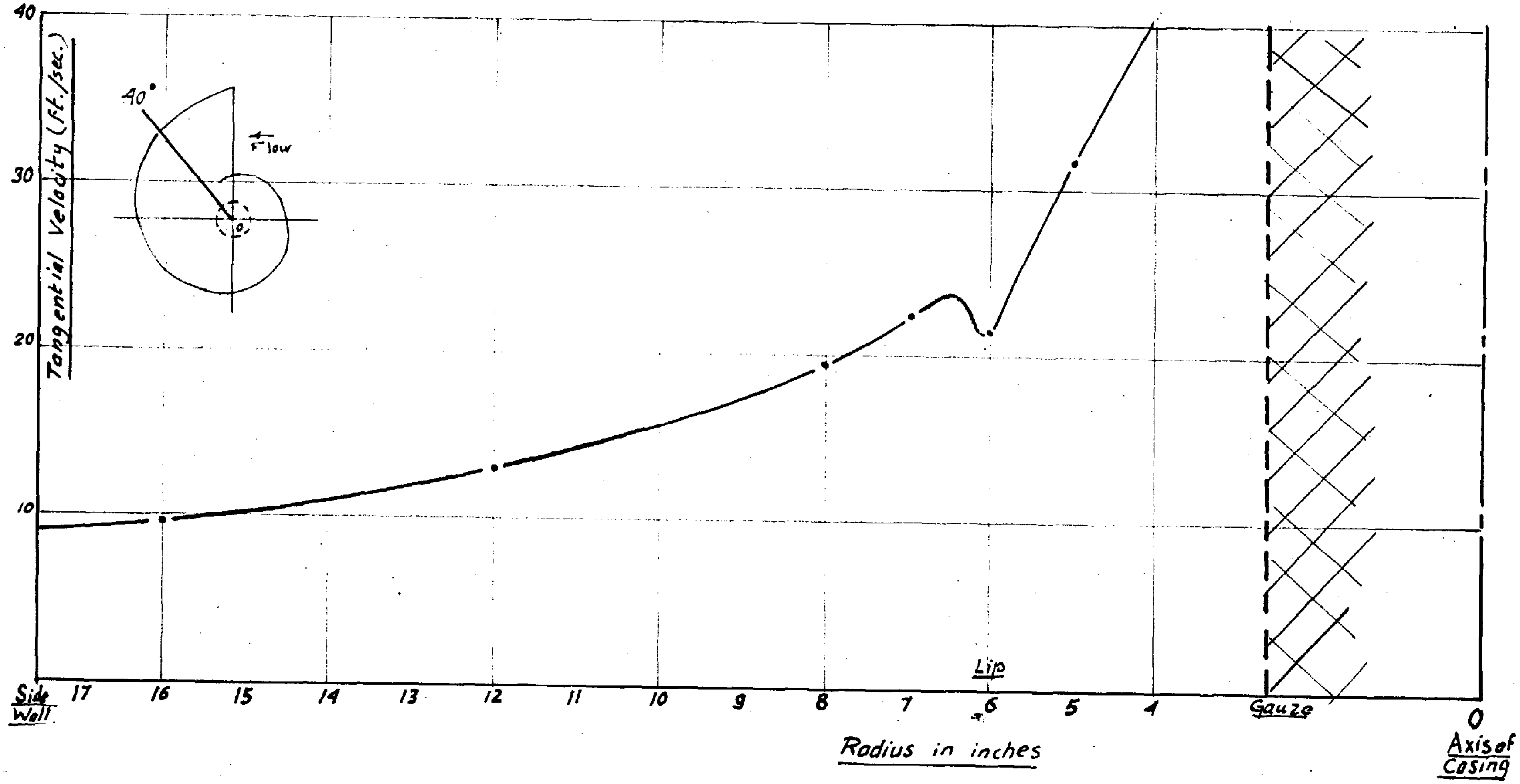

Figure (32) - Observed Mean Tangential Velocity at 40° with Inlet

This gives total Flow = 3.53 cusecs. (see appendix 3)

Static Head at ($\theta = 120°$, $r = 6"$) = 10.37 ft. air.

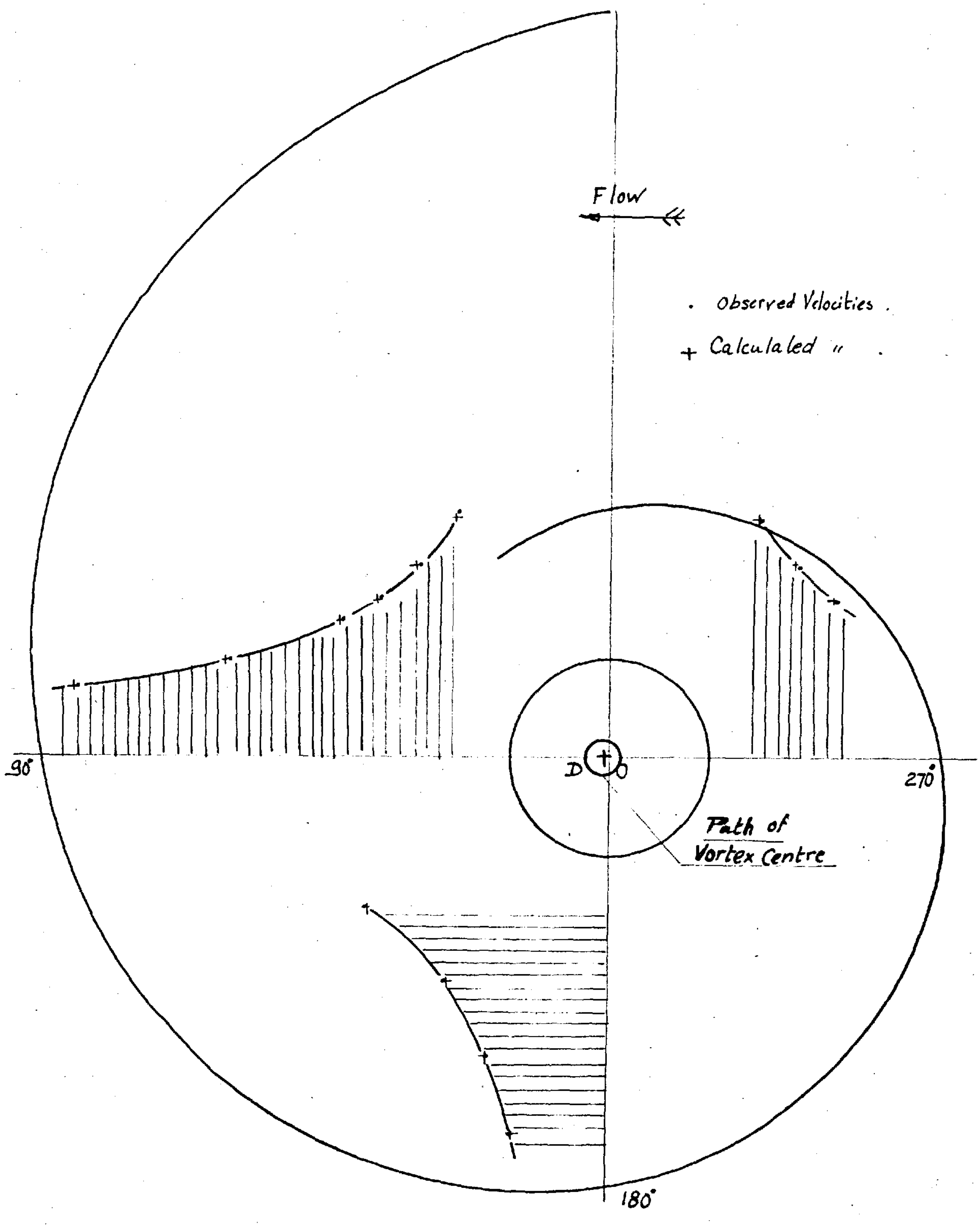

Figure (34) Mean tangential Velocities

[Flow = 3.53 cusecs]   1 cm → 10 ft/sec.

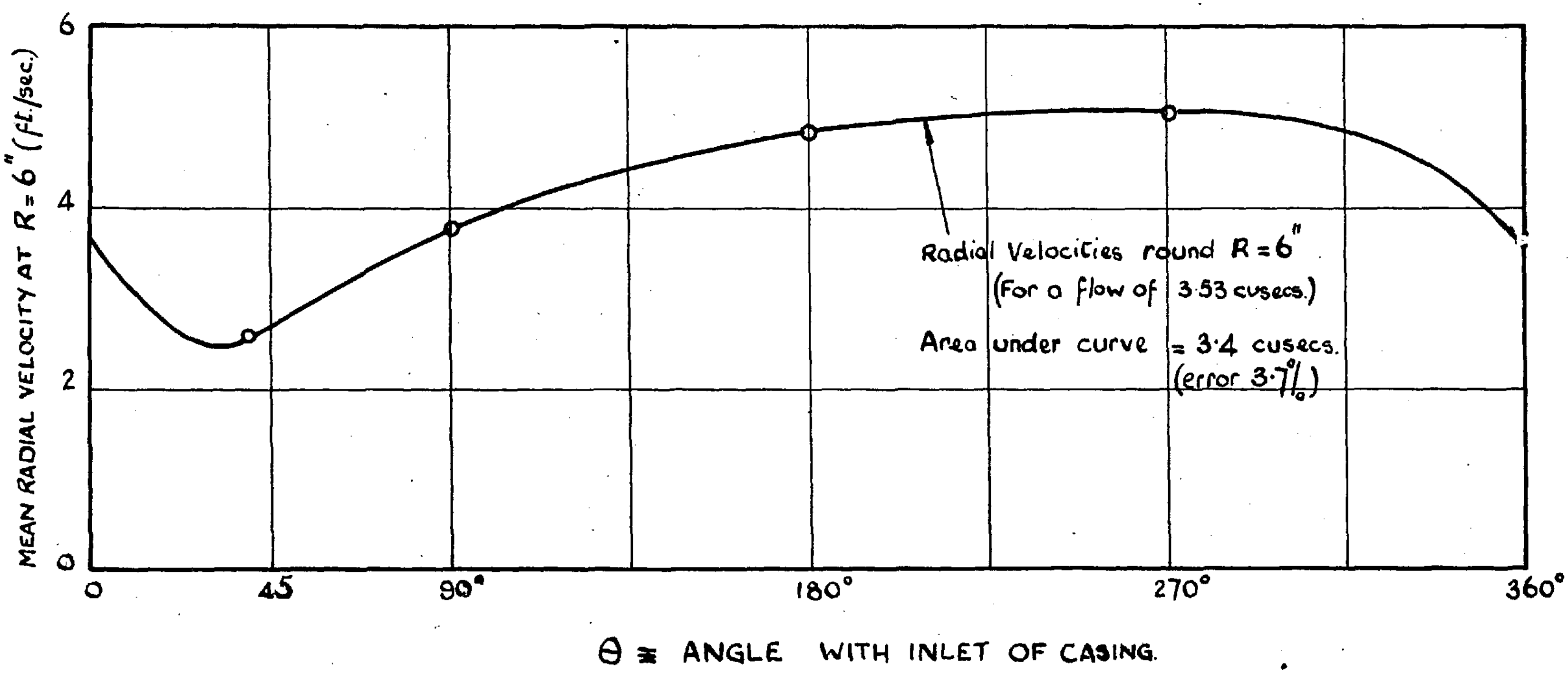

FIGURE (37) _ MEAN RADIAL VELOCITY DISTRIBUTIONS AT R = 6"

FLOW = 3.53 cusecs.

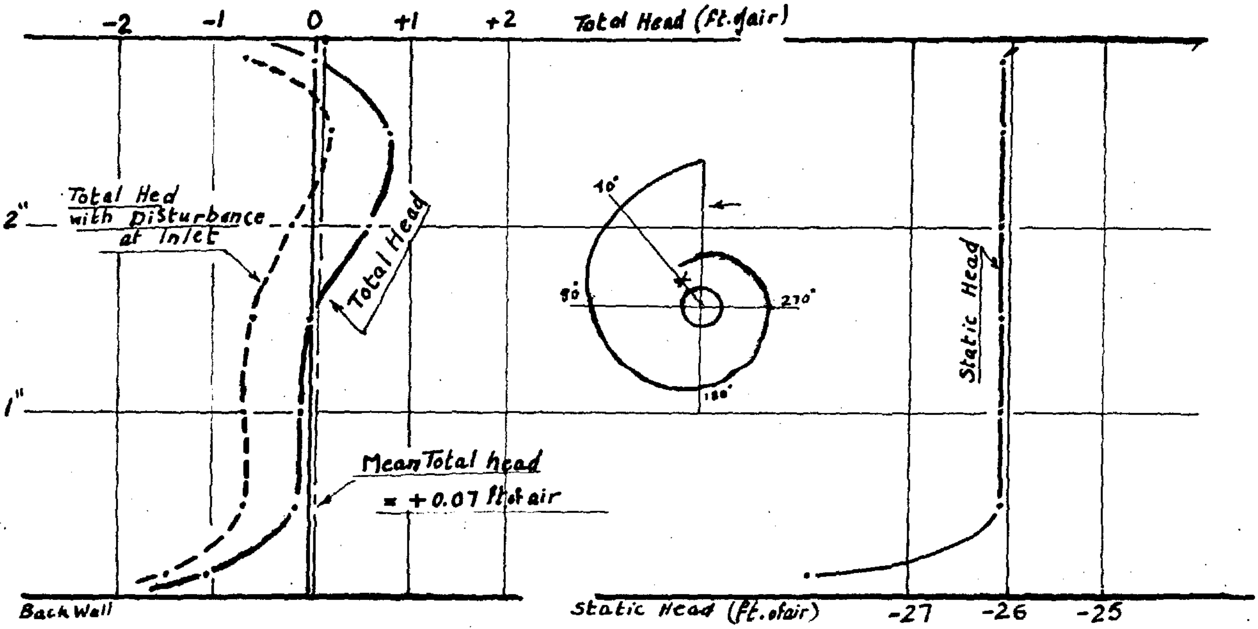

Figure (38) . Total & Static Head Distributions
At Θ = 40°, R = 4 inches (Flow = 3.53 cusecs.)

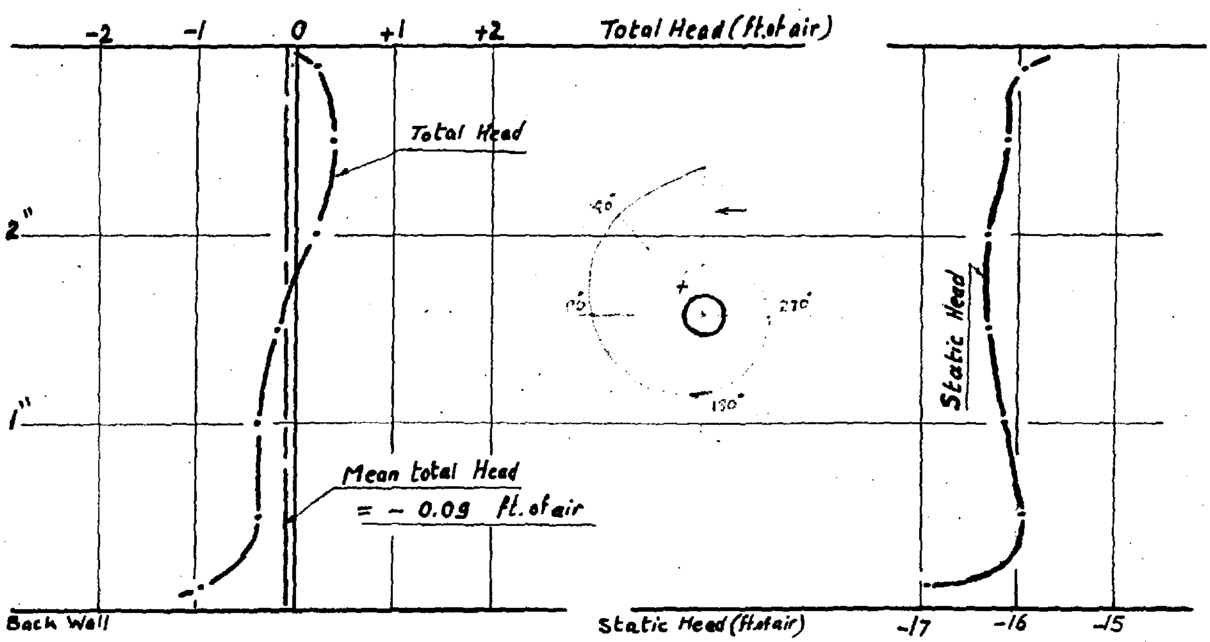

Figure (39) . Total & Static Head Distributions
At Θ = 40°, R = 5 inches (Flow = 3.53 cusecs.)

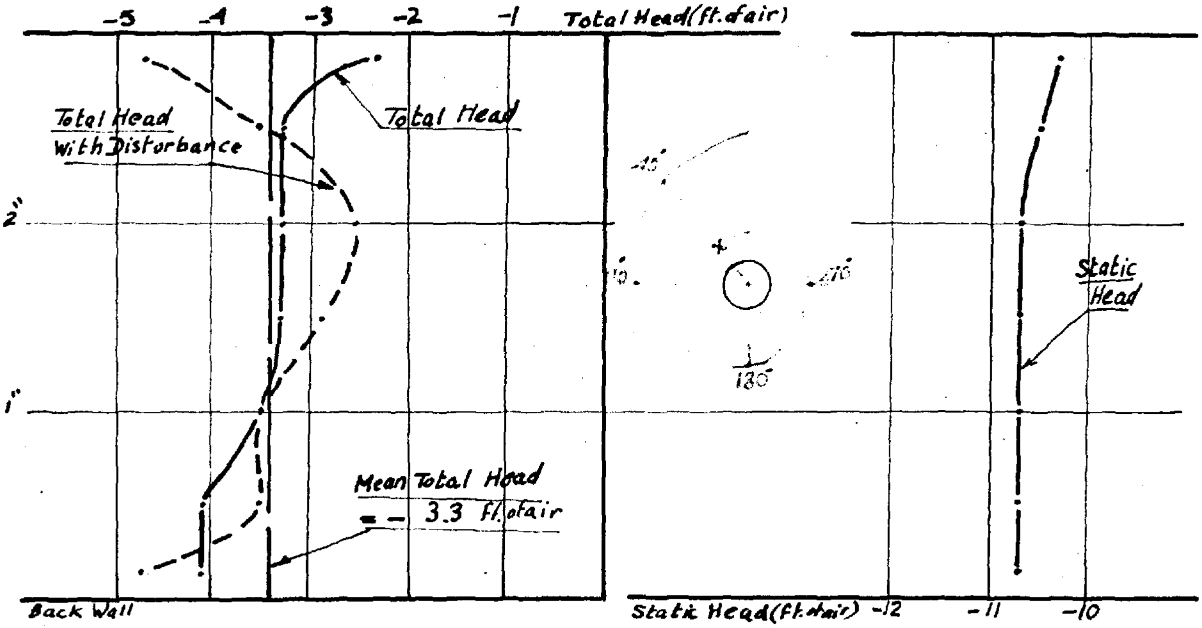

Figure (40) - Total & Static Head Distributions
At $\theta = 40^\circ$, $R = 6$ inches (Flow = 3.53 cusecs.)

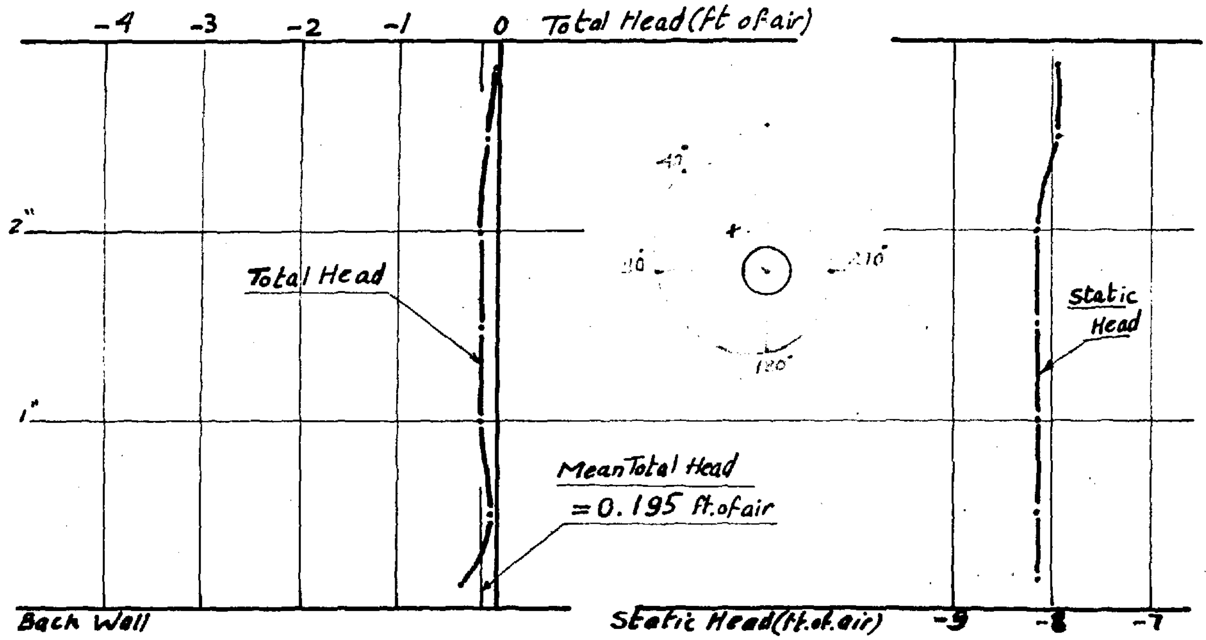

Figure (41) - Total & Static Head Distributions
At $\theta = 40^\circ$, $R = 7$ inches (Flow = 3.53 cusecs.)

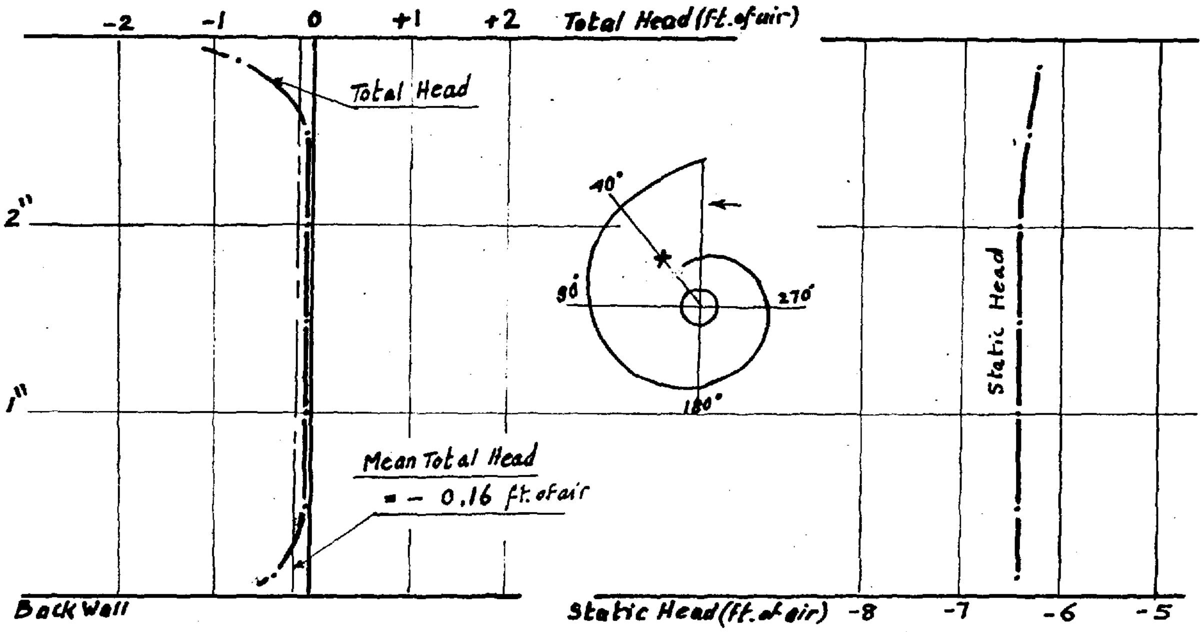

Figure (42) - Total & Static Head Distributions
At θ=40° , R=8 inches (Flow=3.53 cusecs)

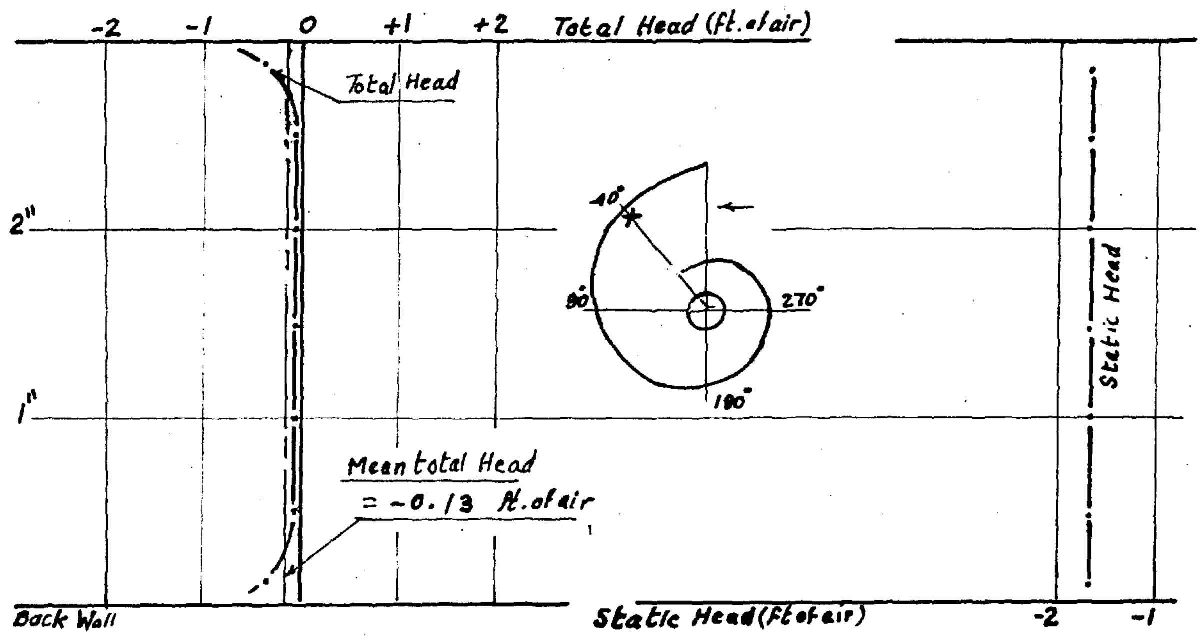

Figure (43) - Total & Static Head Distributions
At θ=40° , R=16 inches (Flow=3.53 cusecs.)

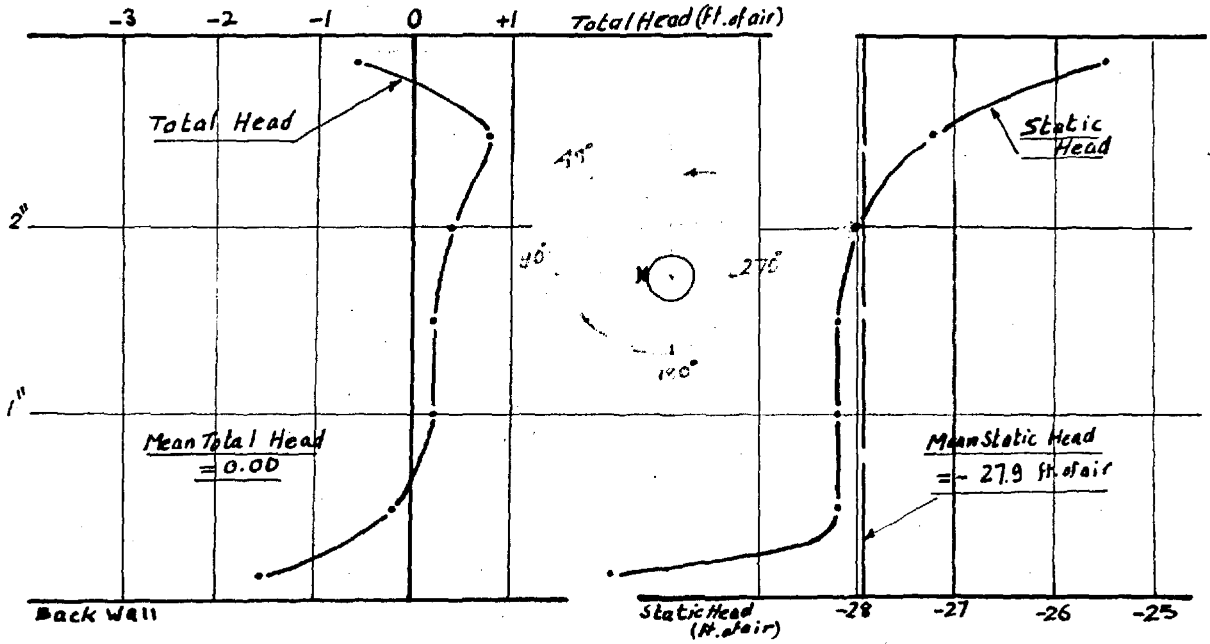

Figure (44) - Total & Static Head Distributions
At θ = 90°, R = 4 inches (Flow = 3.53 cusecs.)

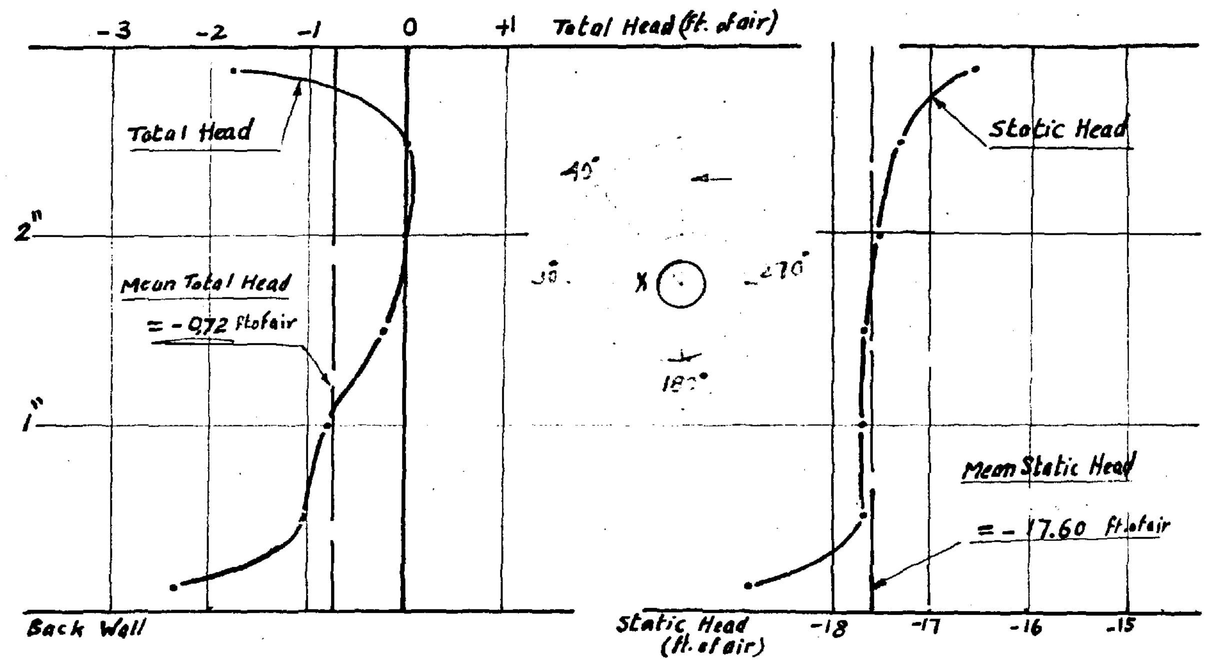

Figure (45) - Total & Static Head Distributions
At θ = 90°, R = 5 inches (Flow = 3.53 cusecs.)

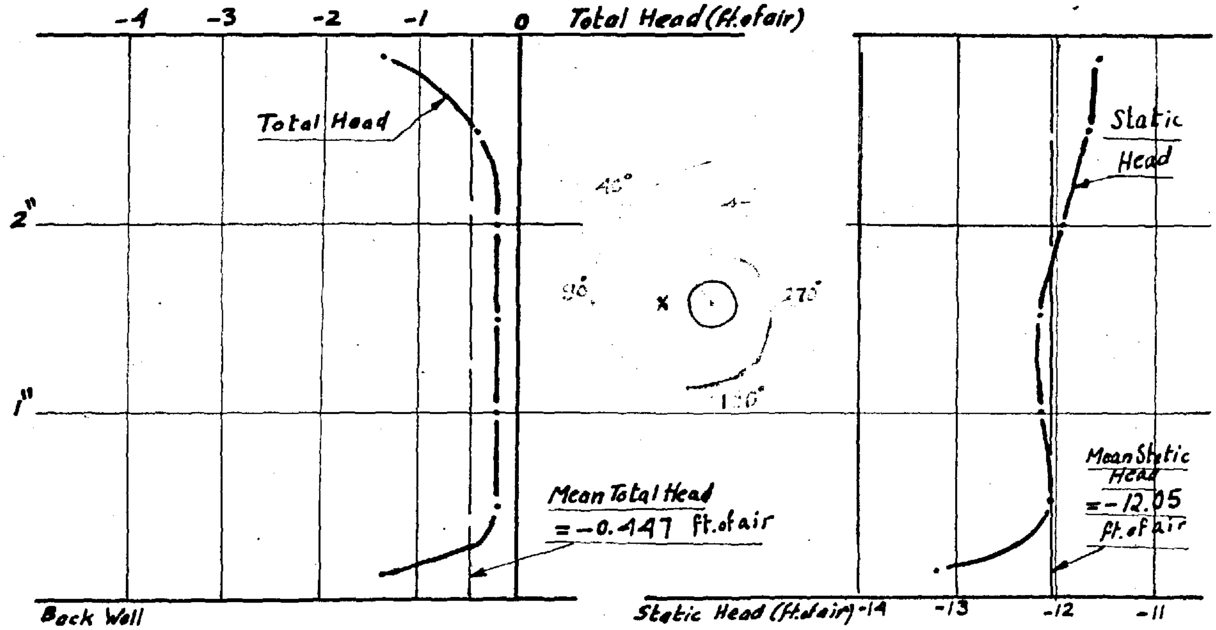

Figure (46) - Total & Static Head Distributions
At $\theta = 90°$, R = 6 inches (Flow = 3.53 cusecs.)

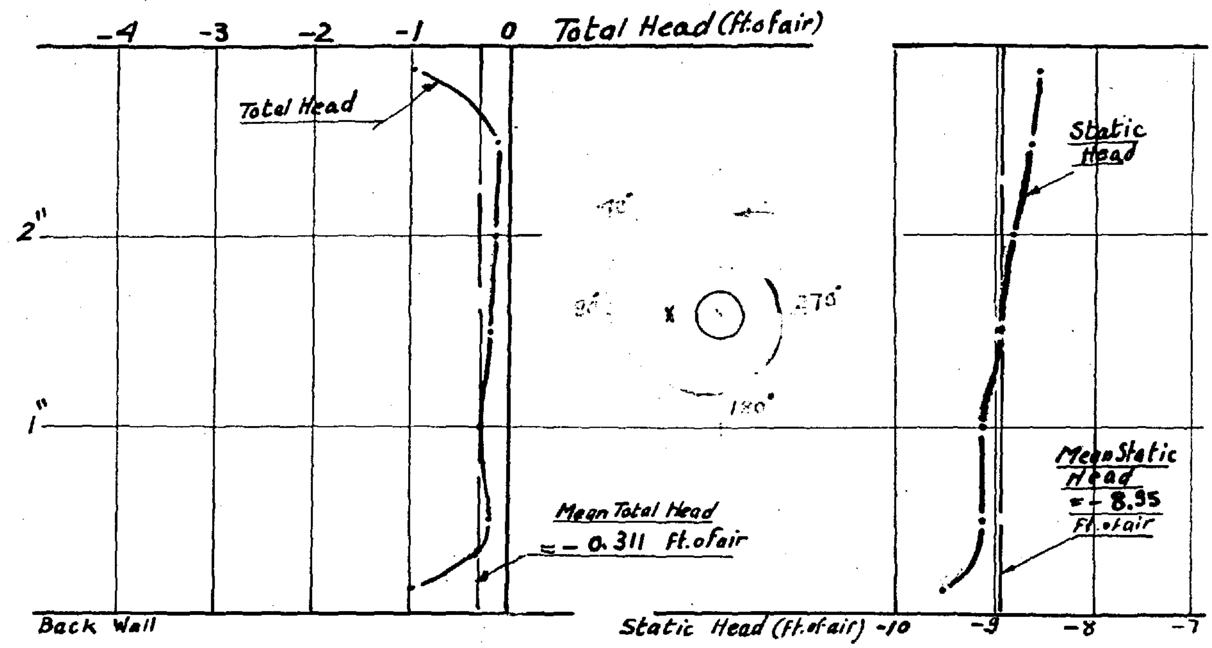

Figure (47) - Total & Static Head Distributions
At $\theta = 90°$, R = 7 inches (Flow = 3.53 cusecs.)

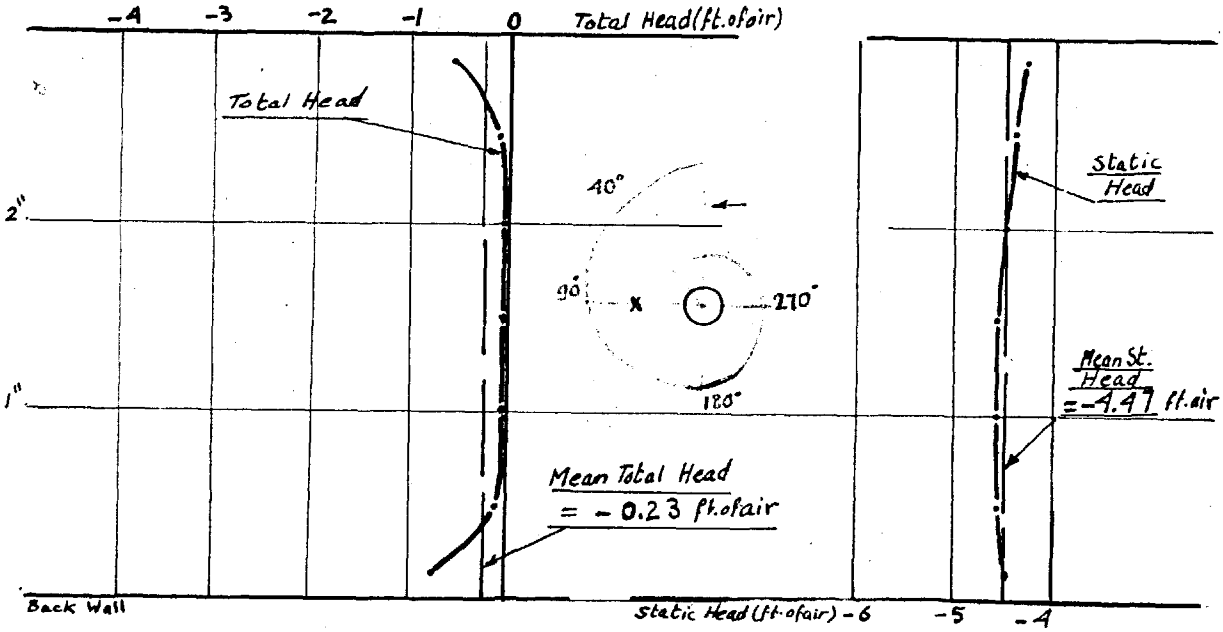

Figure (48) - Total & Static Head Distributions
At θ = 90°, R = 10 inches (Flow = 3.53 cusecs.)

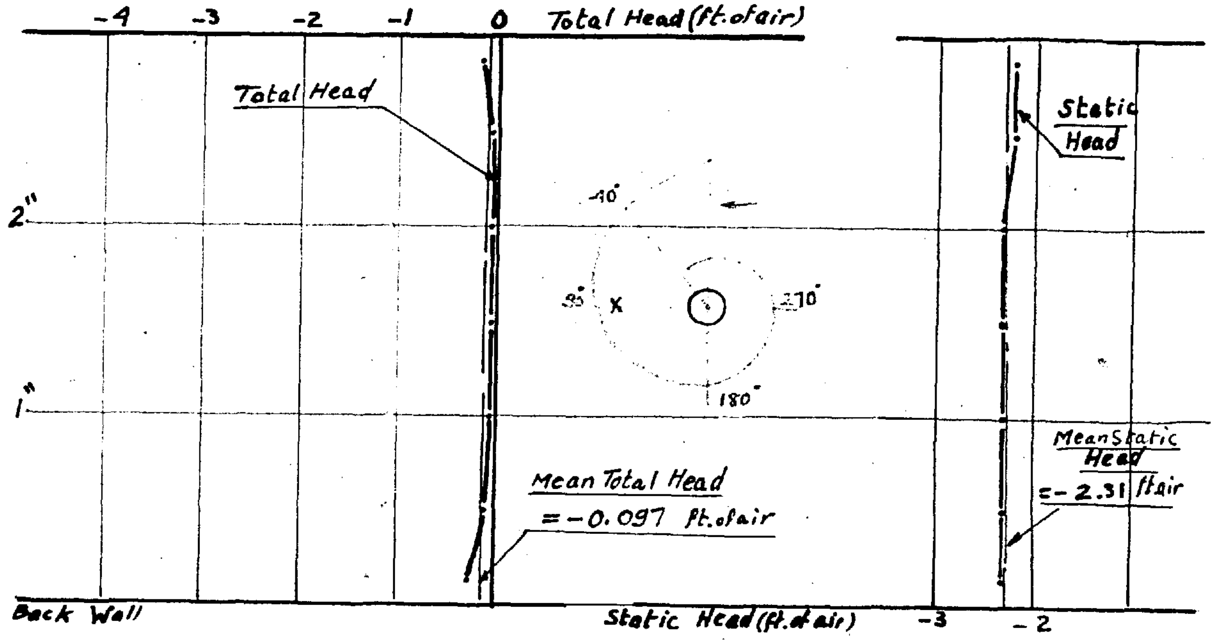

Figure (49) - Total & Static Head Distributions
At θ = 90°, R = 14 inches (Flow = 3.53 cusecs.)

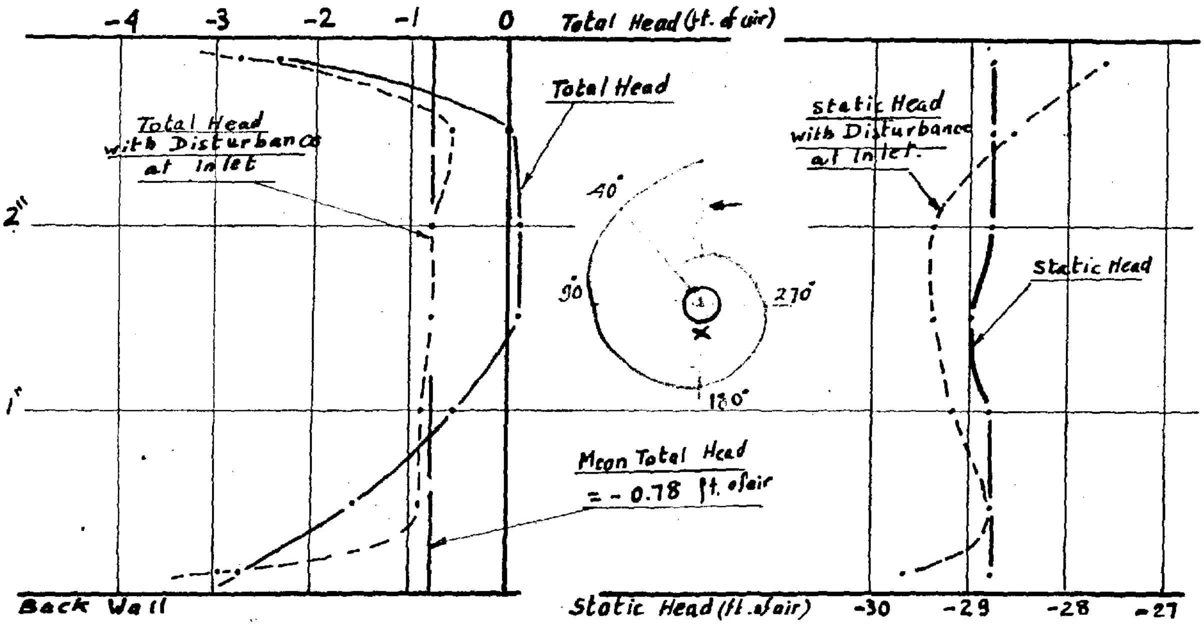

Figure (50). Total & Static Head Distributions

At θ = 180°, R = 4 inches (Flow = 3.53 cusecs.)

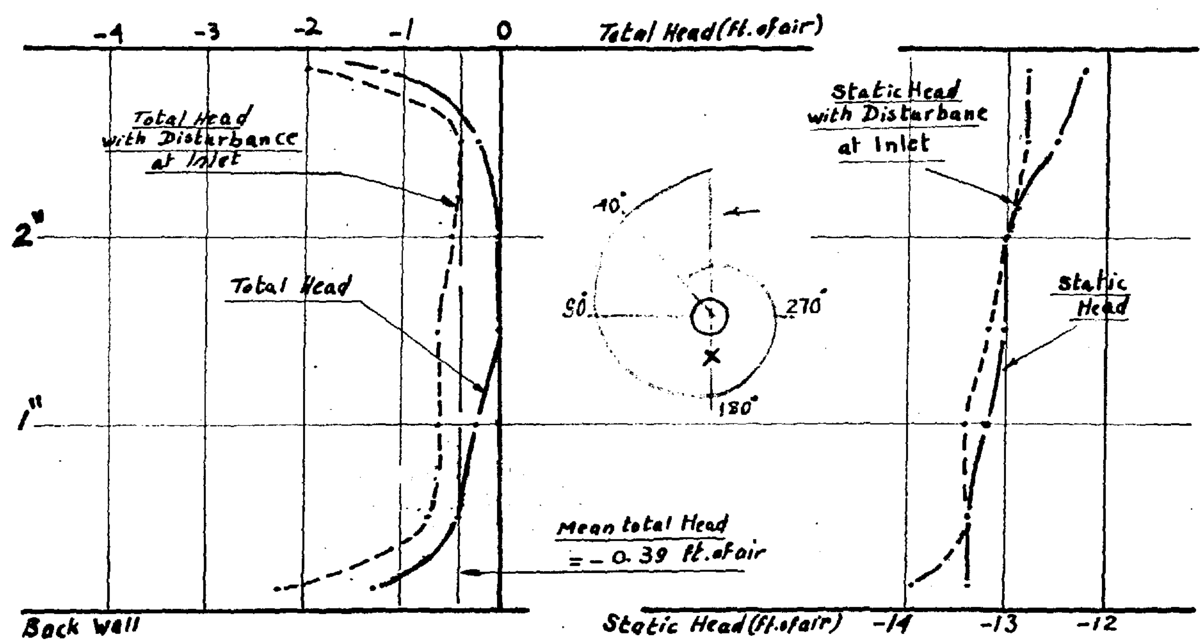

Figure (51) - Total & Static Head Distributions

At θ = 180°, R = 6 inches (Flow = 3.53 cusecs.)

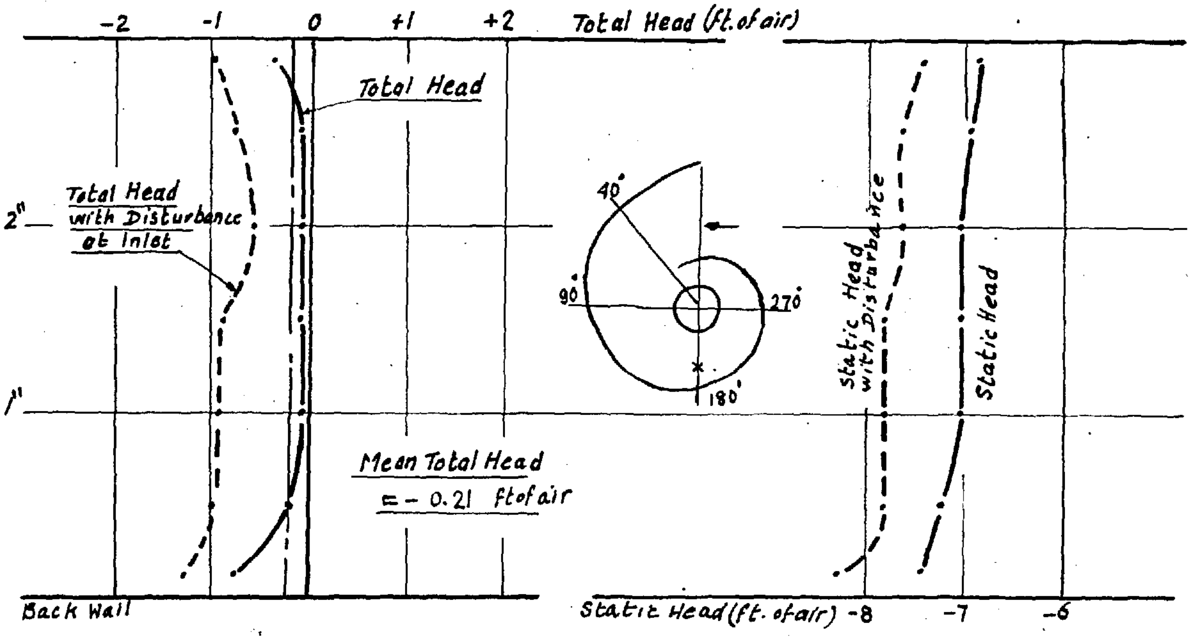

Figure (52) - Total & Static Head Distributions
At $\theta = 180°$, R = 8 inches (Flow = 3.53 cusecs.)

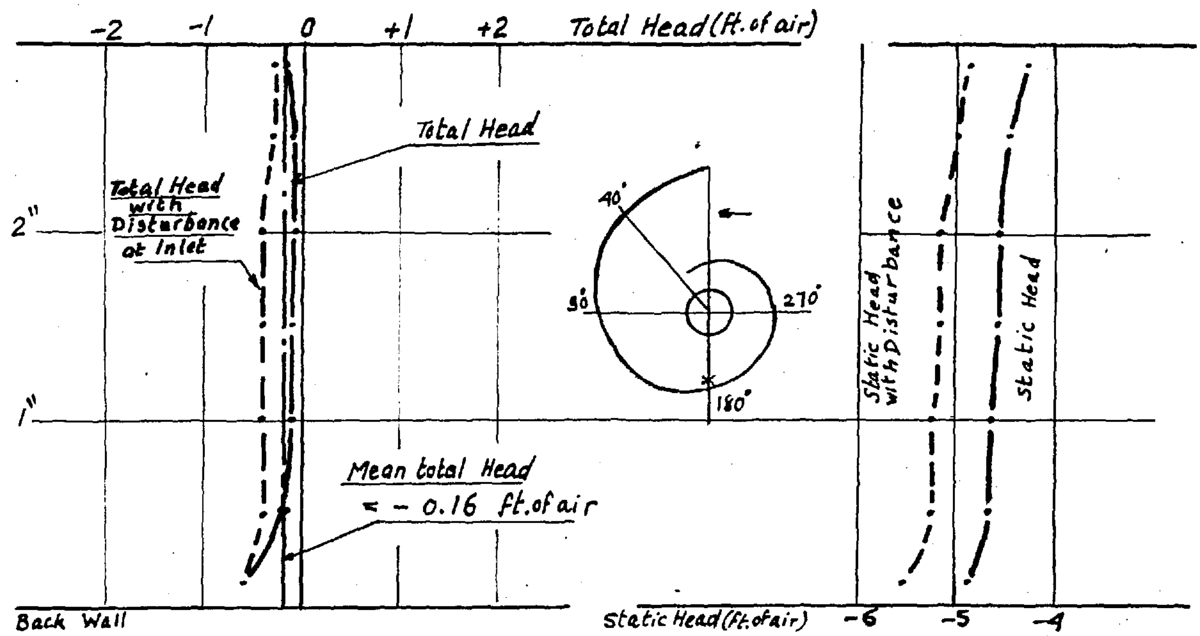

Figure (53) - Total & Static Head Distributions
At $\theta = 180°$, R = 10 inches (Flow = 3.53 cusecs.)

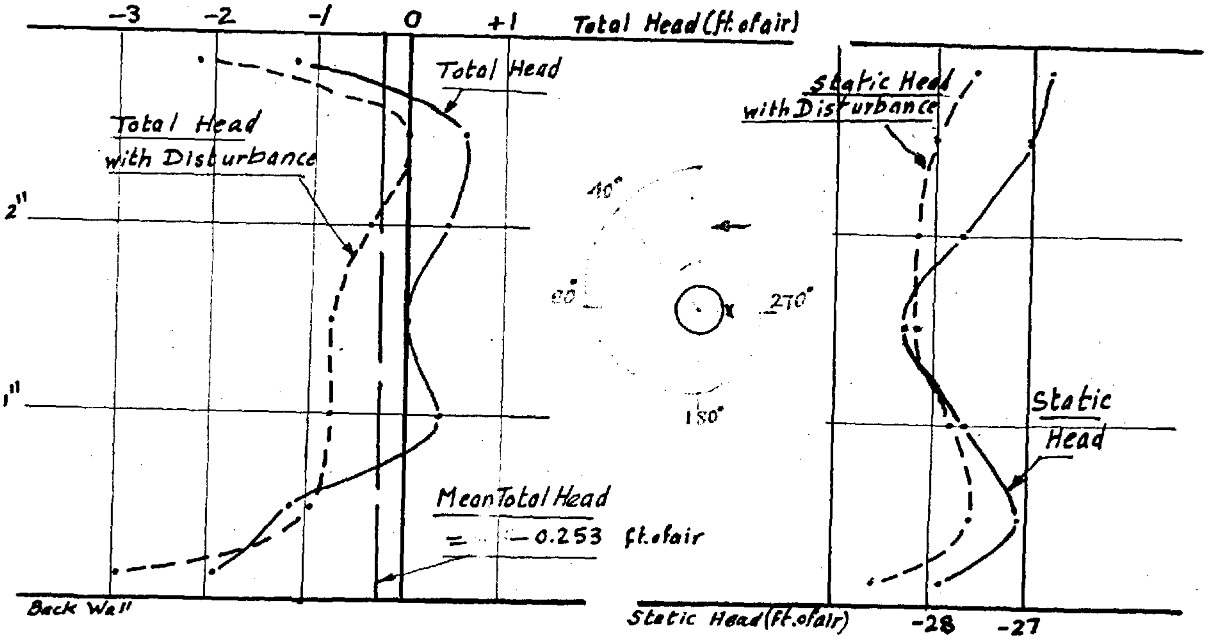

Figure (54). Total & Static Head Distributions
At θ = 270°, R = 4 inches (Flow = 3.53 cusecs.)

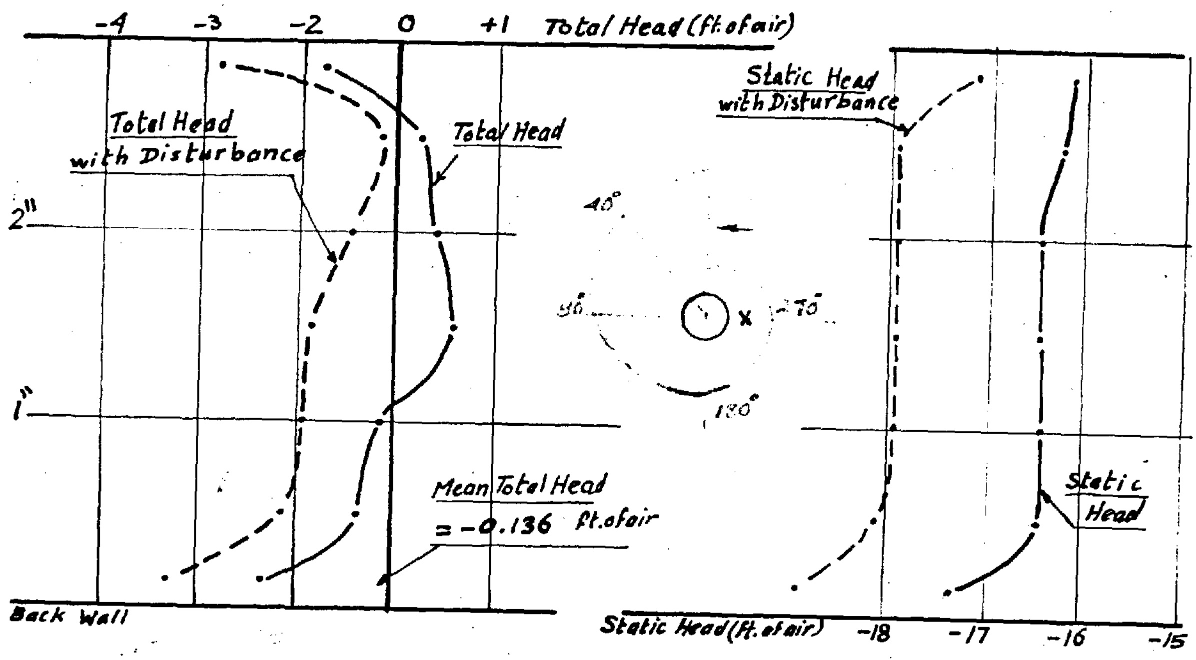

Figure (55). Total & Static Head Distributions
At θ = 270°, R = 5 inches (Flow = 3.53 cusecs.)

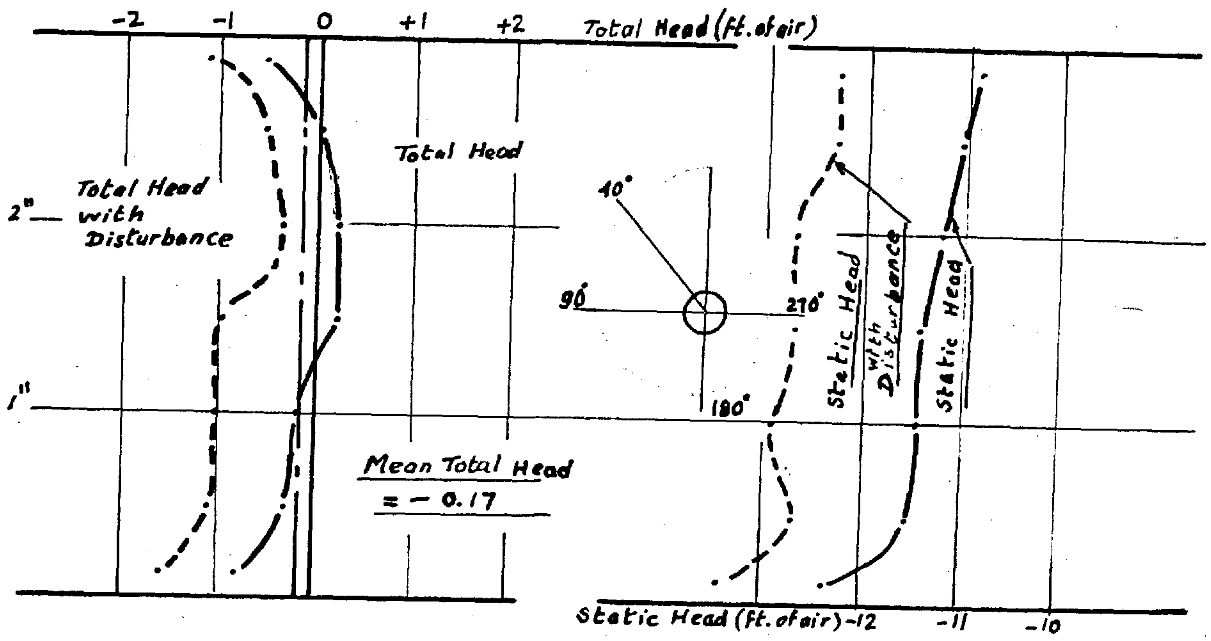

Figure (56) _ Total & Static Head Distributions
At $\theta = 270^\circ$, $R = 6$ inches (Flow = 3.53 cusecs.)

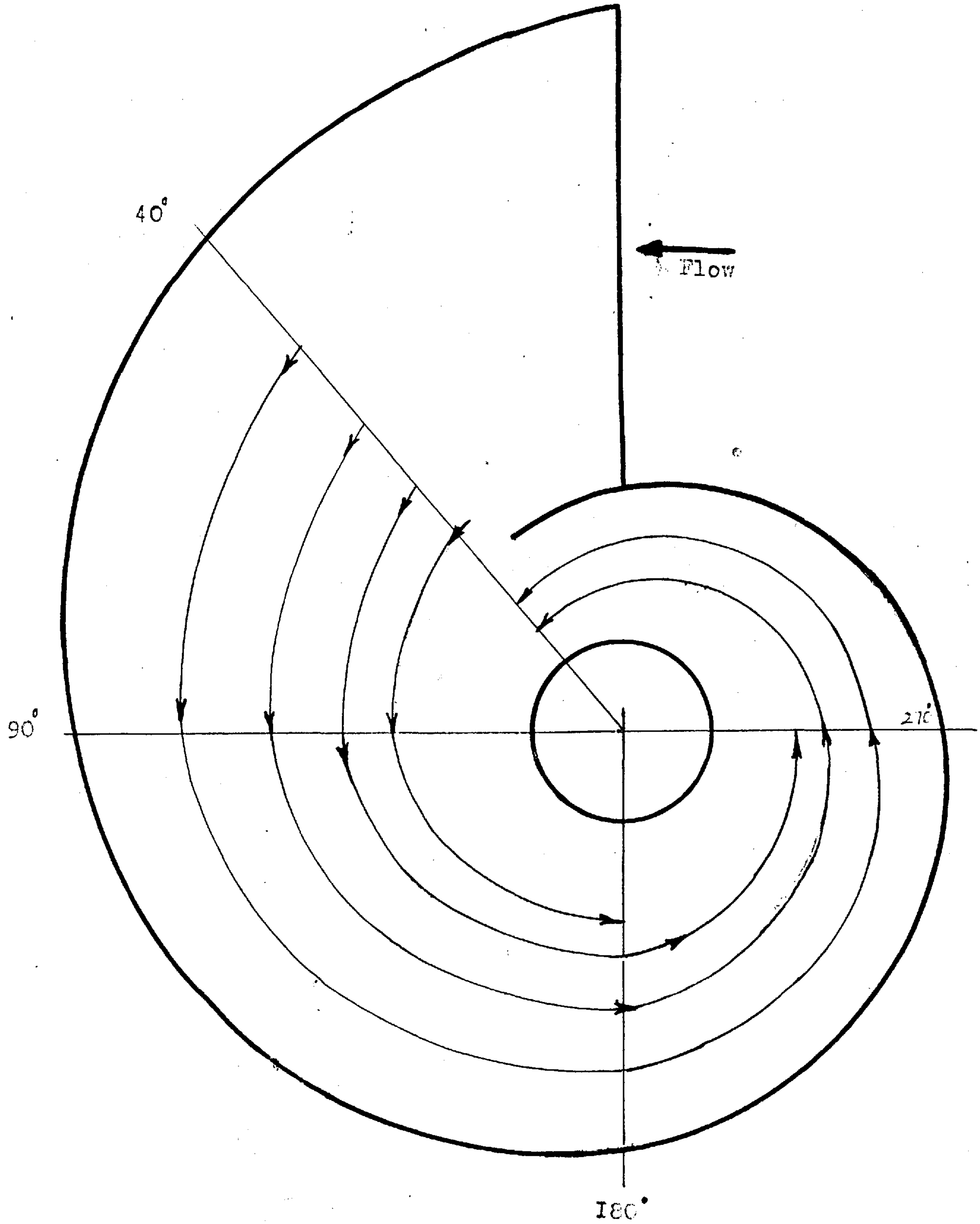

Figure (57) CALCULATED MEAN STREAM LINES
(Flow = 3.53 cusecs.)

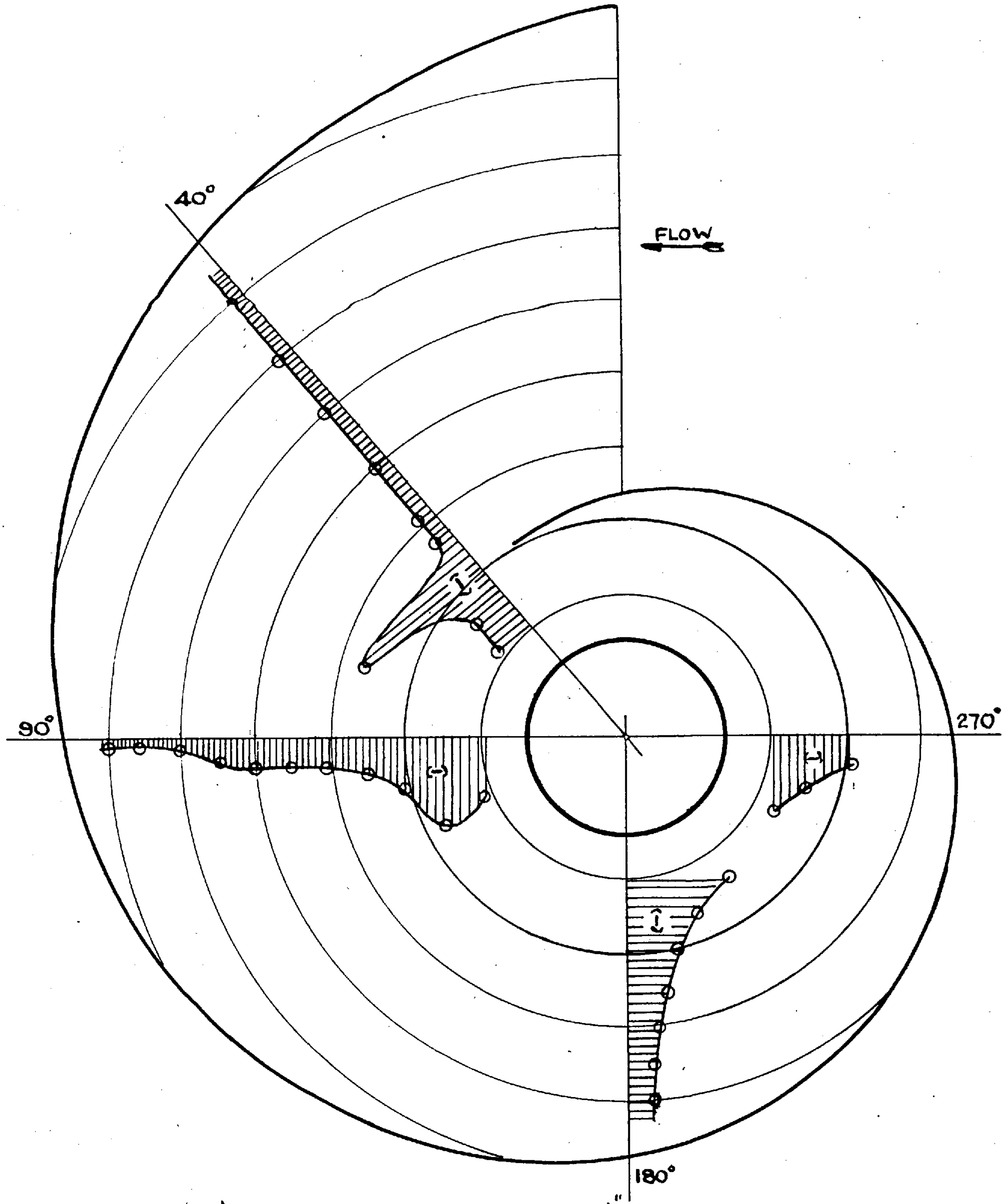

FIGURE (58) _ TOTAL HEAD DISTRIBUTIONS 1/8" FROM BACKWALL

FLOW = 3·53 cusecs

SCALE OF CASING 1:4 SCALE OF HEAD:-

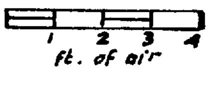

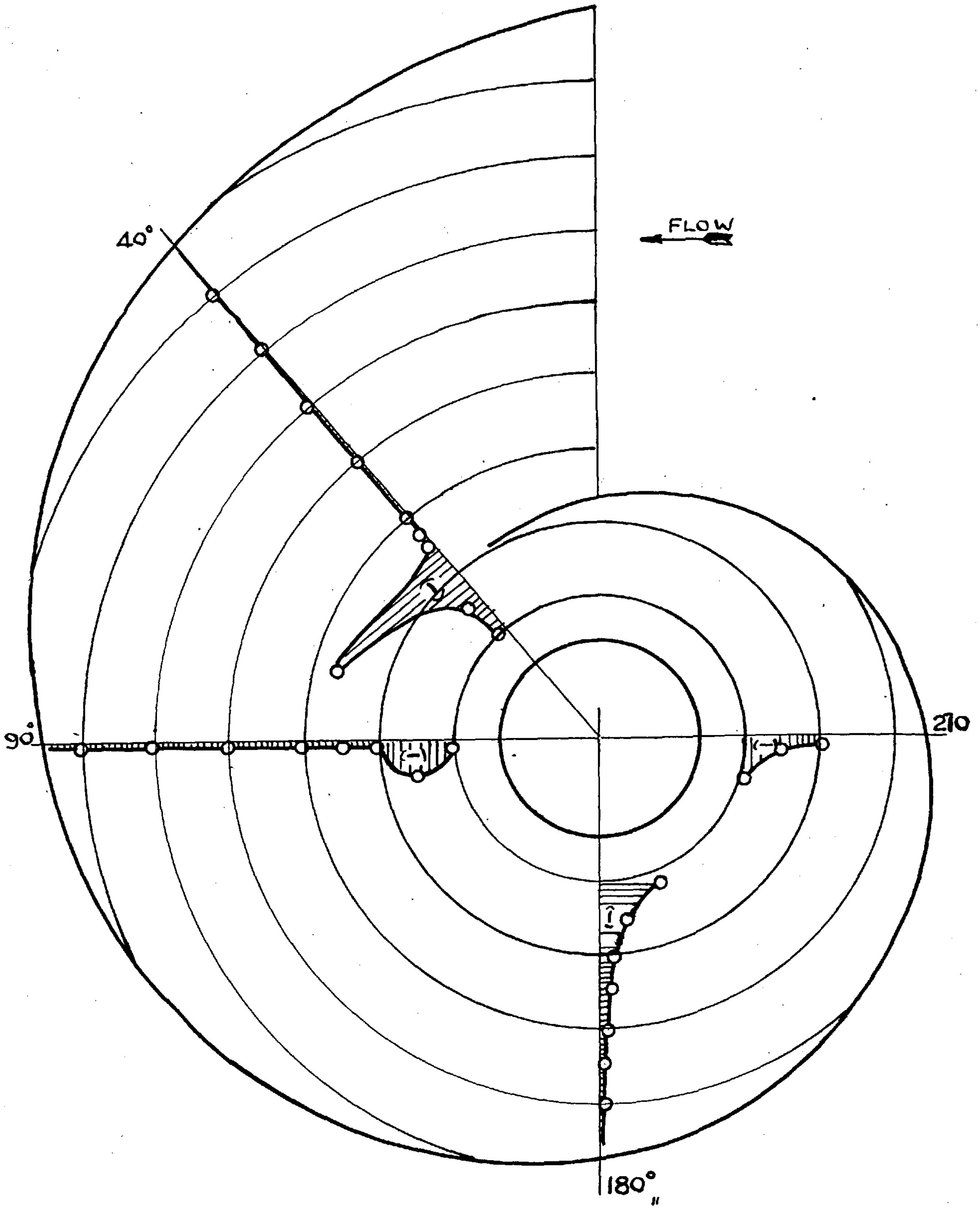

FIGURE (59) - TOTAL HEAD DISTRIBUTIONS ½" FROM BACK WALL

FLOW = 3·53 cusecs.

SCALE OF CASING 1:4

SCALE OF HEAD: 1 2 3 4 ft. of air

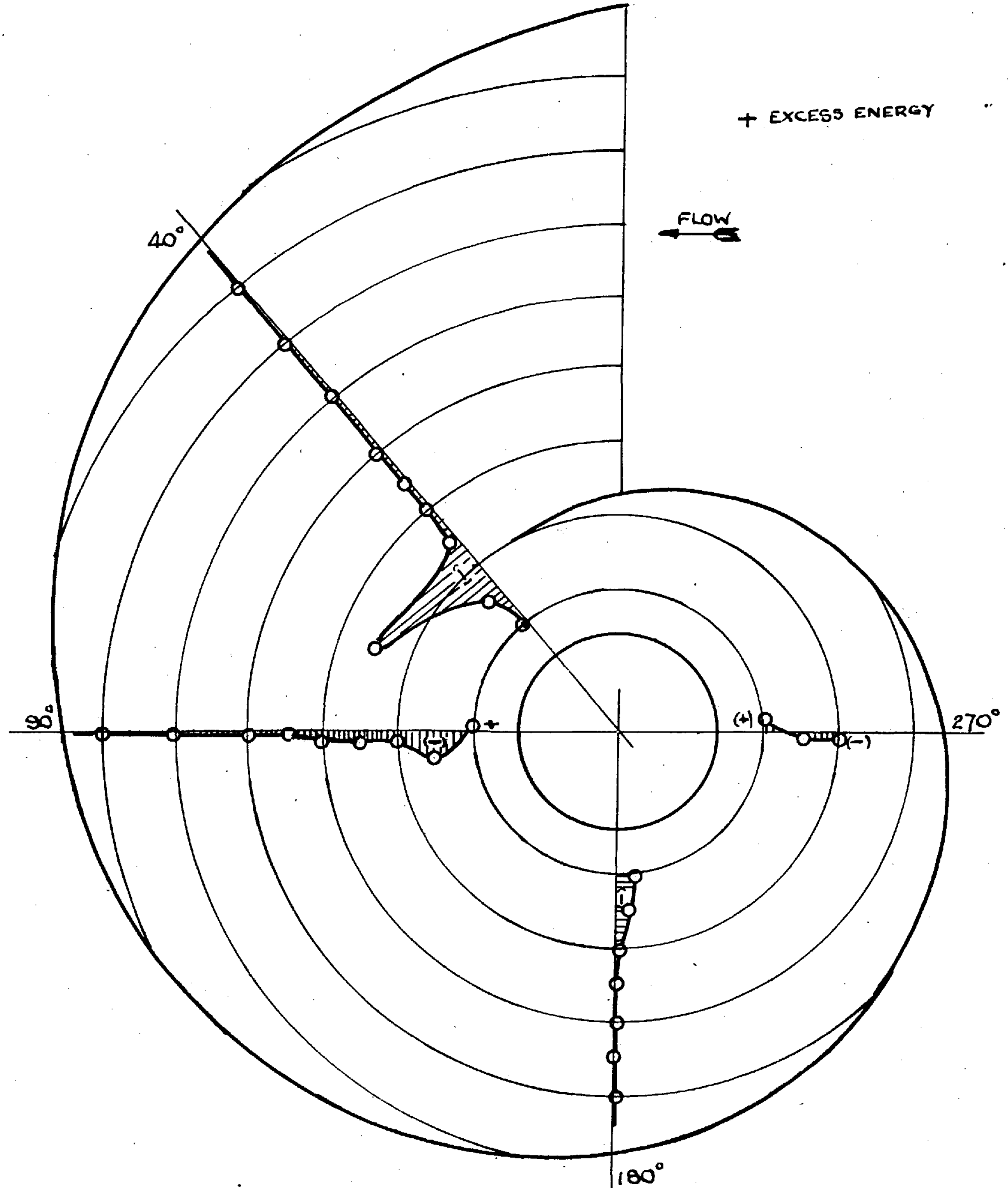

FIGURE (60) - TOTAL HEAD DISTRIBUTIONS 1" FROM BACKWALL

FLOW = 3·53 cusecs

SCALE OF CASING 1:4

SCALE OF HEAD: 1 2 3 4 ft. of air

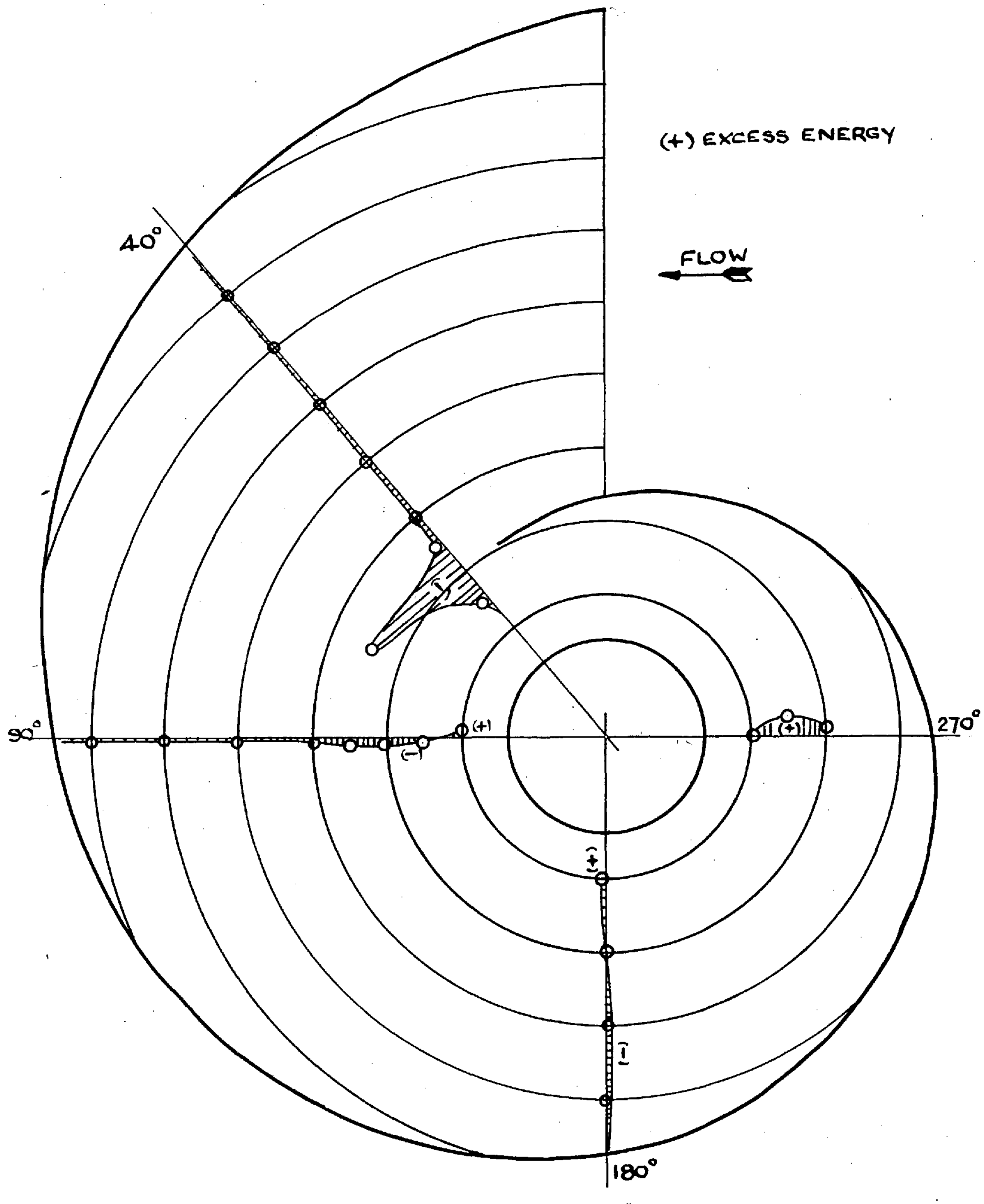

FIGURE (61) _ TOTAL HEAD DISTRIBUTIONS 1½" FROM BACK WALL

FLOW = 3·53 cusecs

SCALE OF CASING 1:4

SCALE OF HEAD: 1 2 3 4 ft. of air

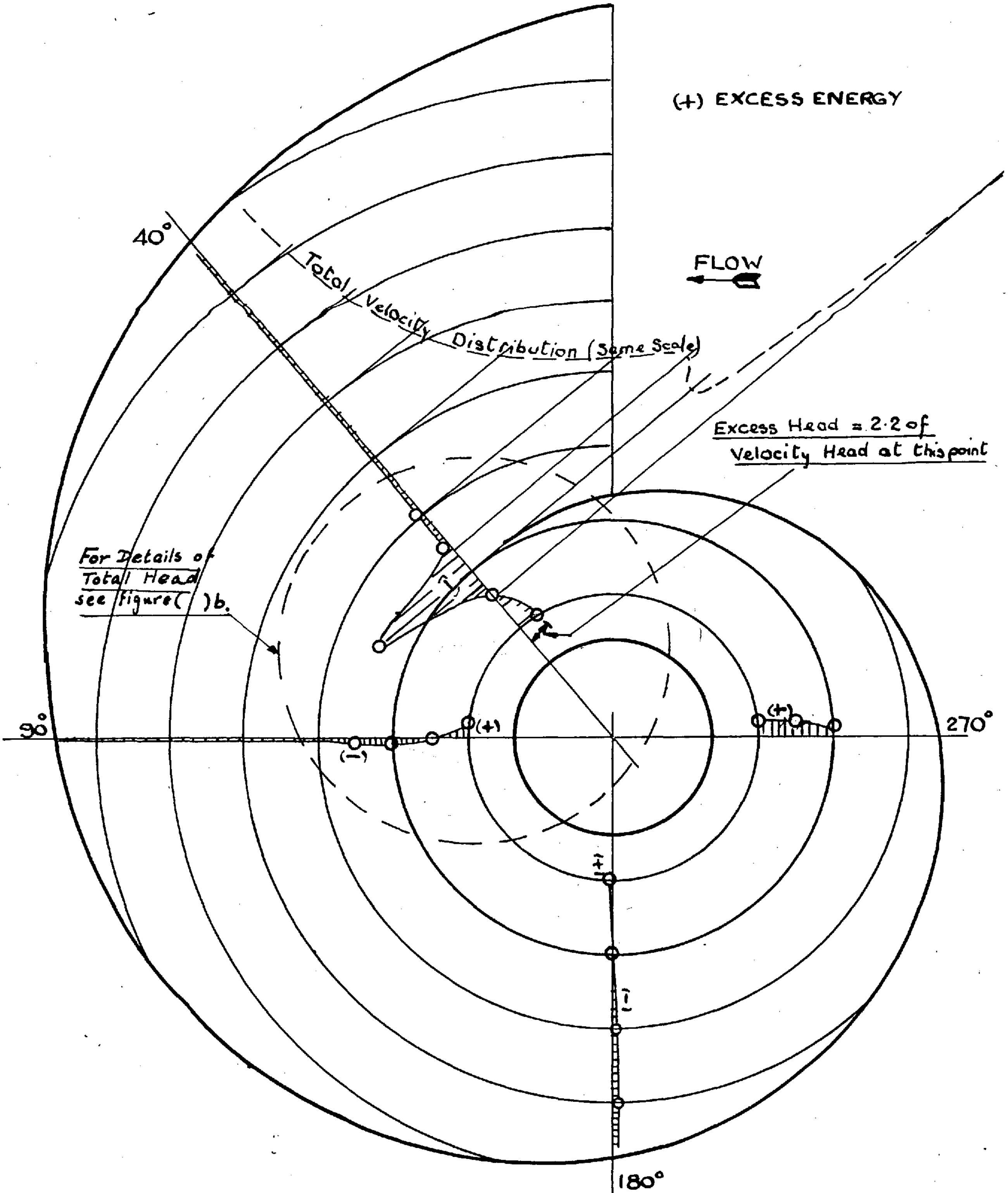

FIGURE (62-a). TOTAL HEAD DISTRIBUTIONS 2" FROM BACK WALL

FLOW = 3·53 cusecs.

SCALE OF CASING 1:4 SCALE OF HEAD: 1 2 3 ft. of air

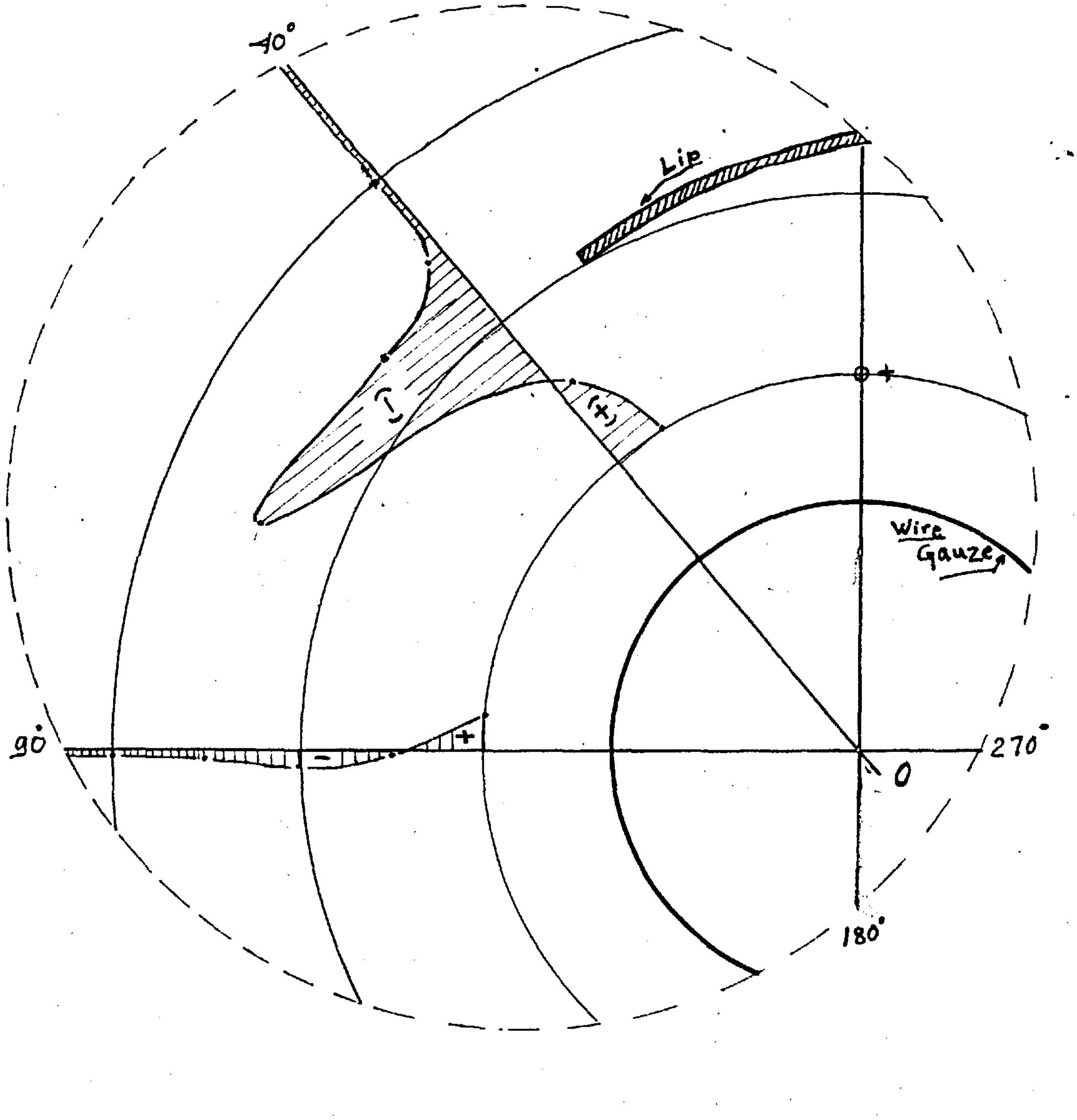

Figure 62 (b) - Details of Total Head

2" from back
(Flow = 3.53 cusecs.)

Scale of casing I:2

Scale of head:
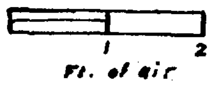

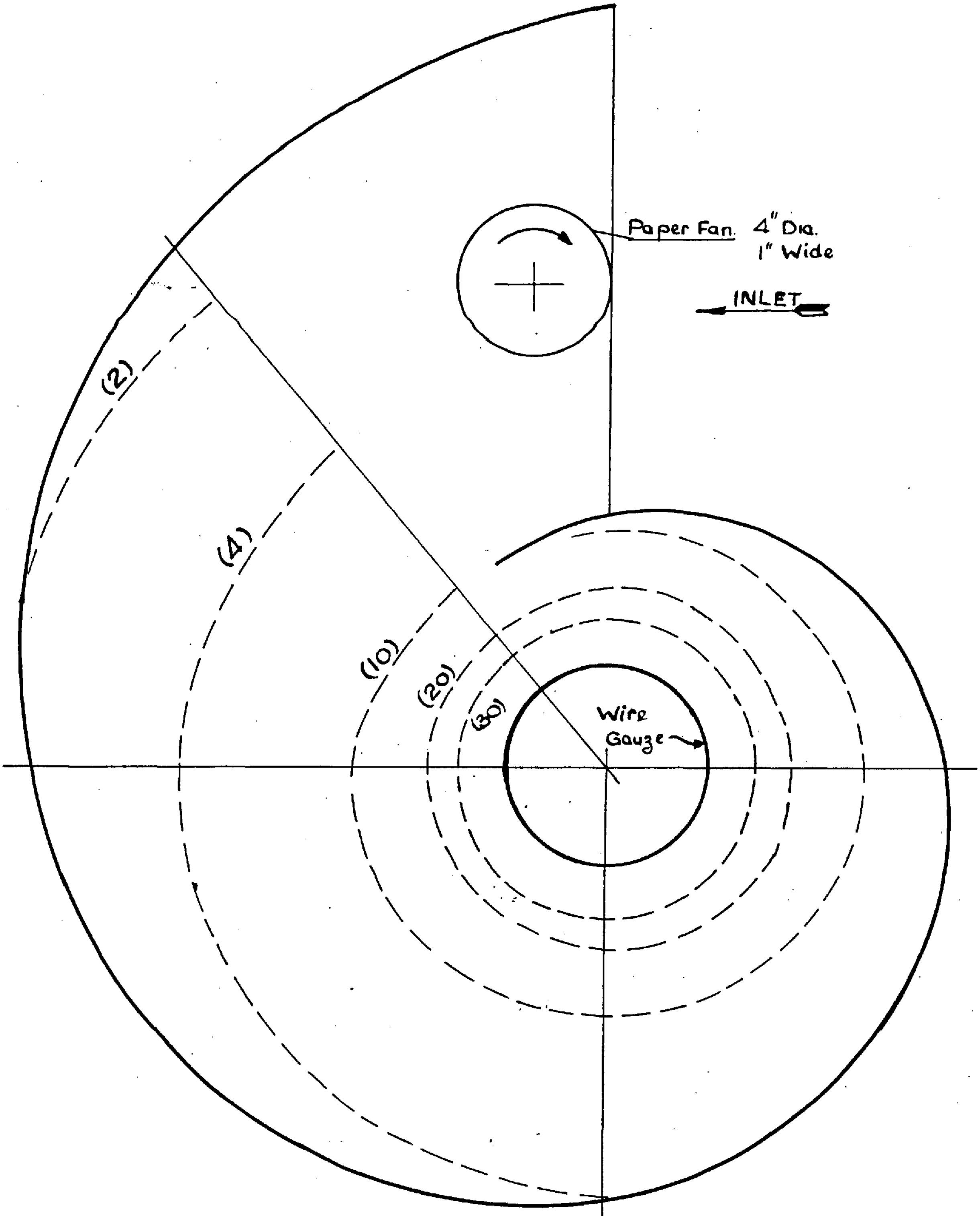

FIGURE (69) - DISTURBANCE AT INLET - CONTOURS OF STATIC HEAD AT MID STREAM (1½")

FLOW = 3·53 cusecs.

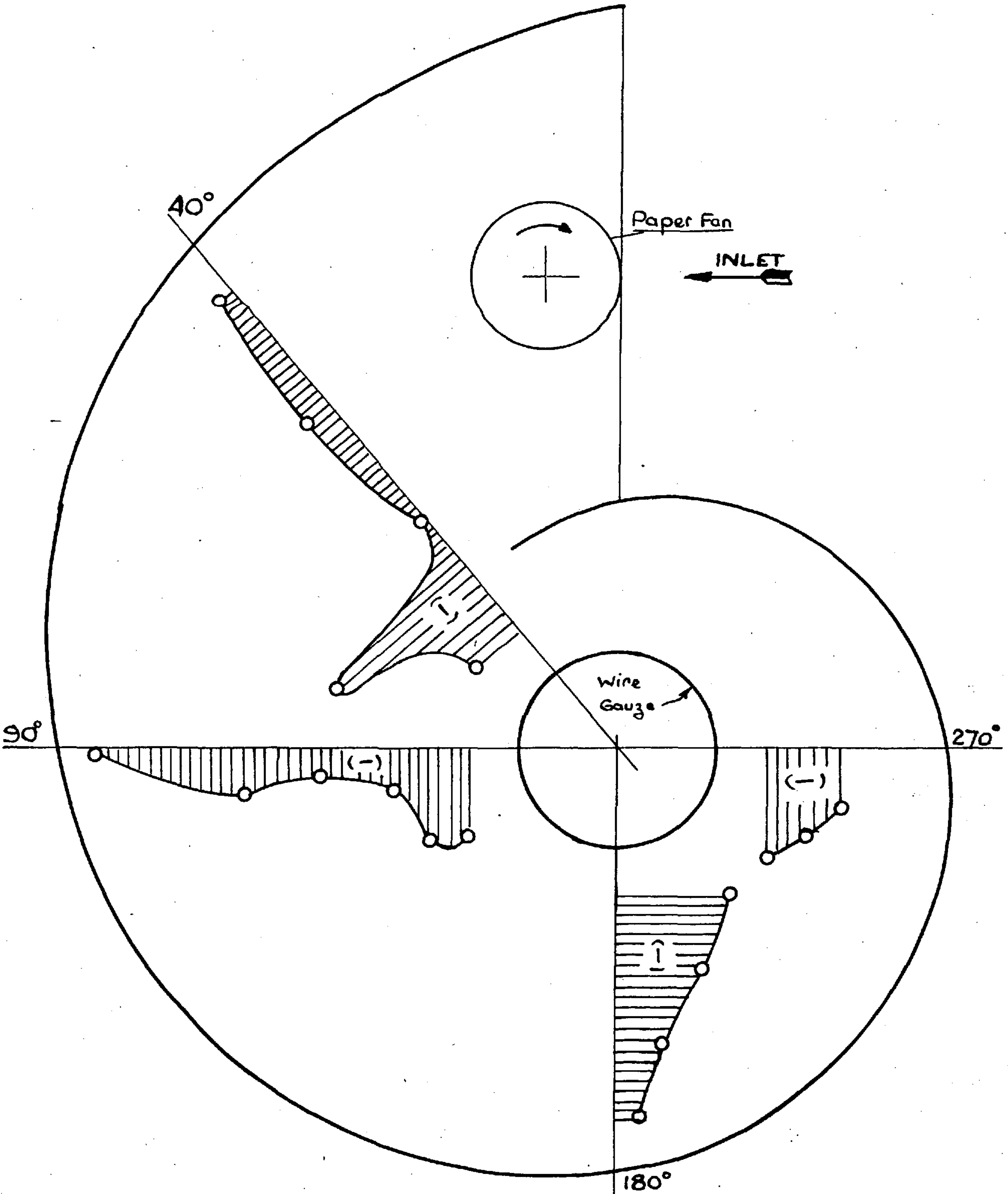

FIGURE (70) DISTURBANCE AT INLET – TOTAL HEAD DISTRIBUTIONS

$\frac{1}{8}$" FROM BACKWALL

FLOW = 3·53 cusecs.

SCALE OF CASING 1:4 SCALE OF HEAD: 1 2 3 4 ft. of air

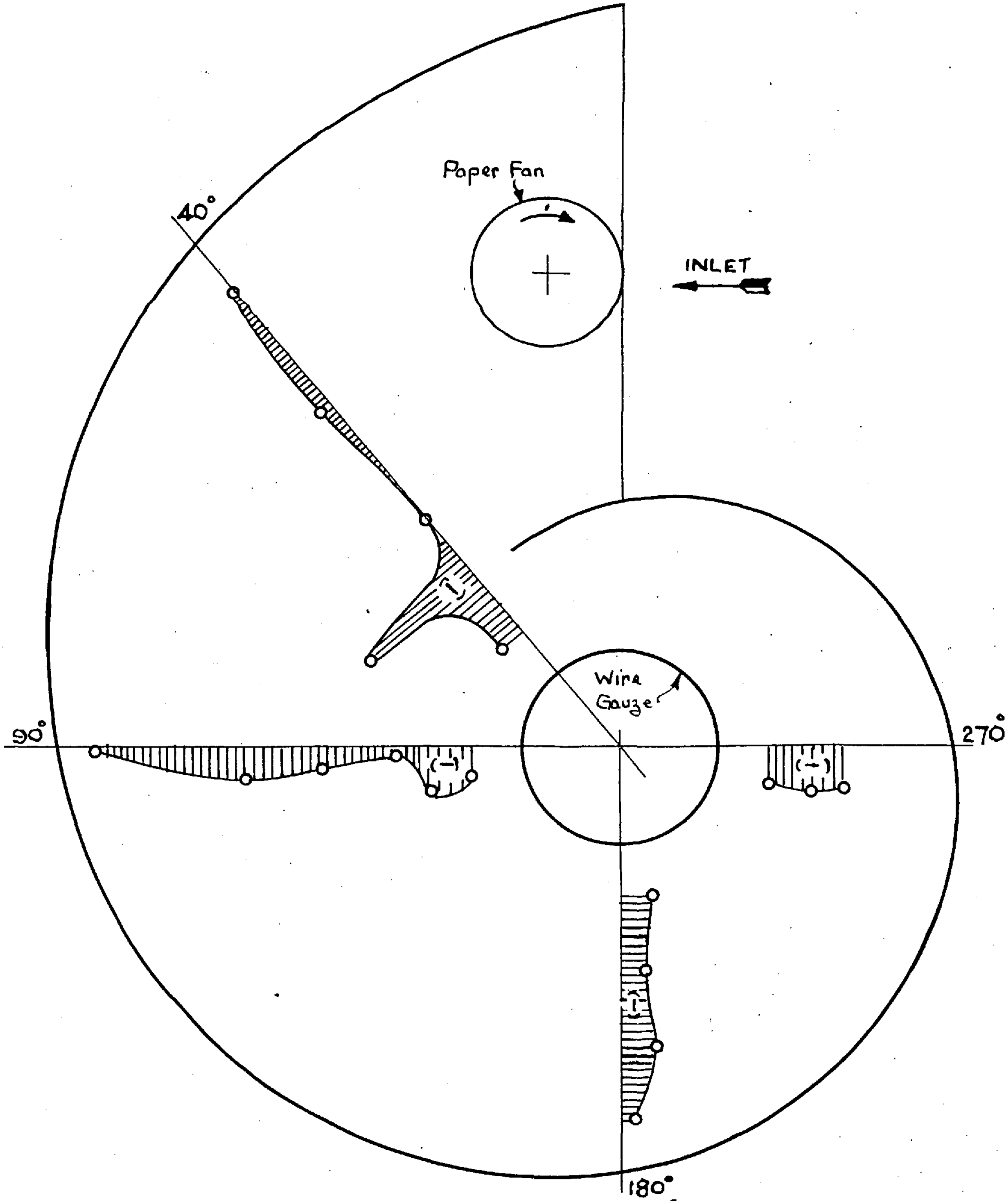

FIGURE (7/) - TOTAL HEAD DISTRIBUTIONS ½" FROM BACK WALL

DISTURBANCE AT INLET FLOW = 3·53 cusecs

SCALE OF CASING 1:4 SCALE OF HEAD: 1 2 3 4 Ft. of air

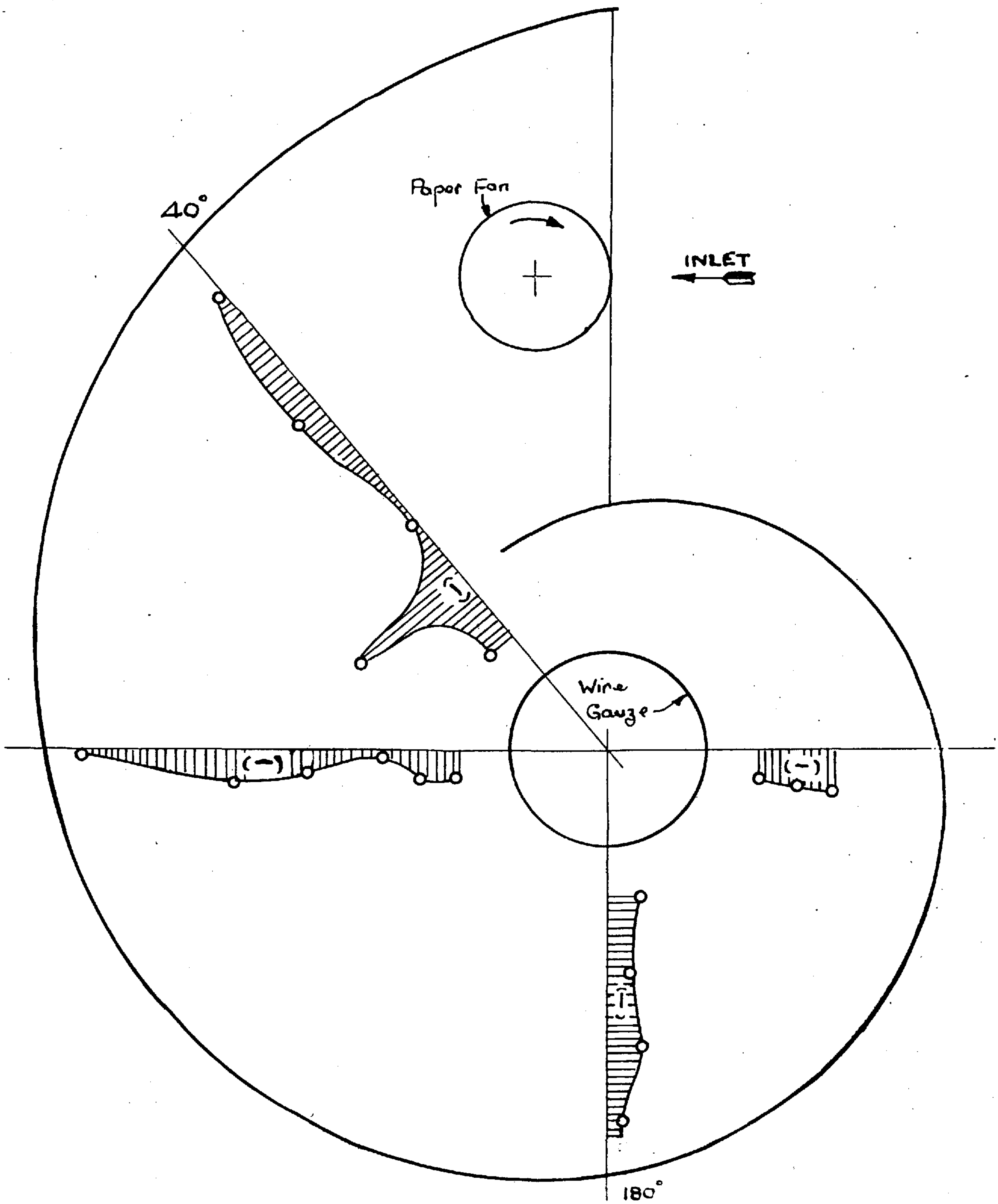

FIGURE(72)_TOTAL HEAD DISTRIBUTIONS 1" FROM BACKWALL

DISTURBANCE AT INLET FLOW = 3·53 cusecs.

SCALE OF CASING 1:4 SCALE OF HEAD:

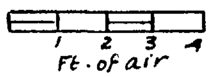

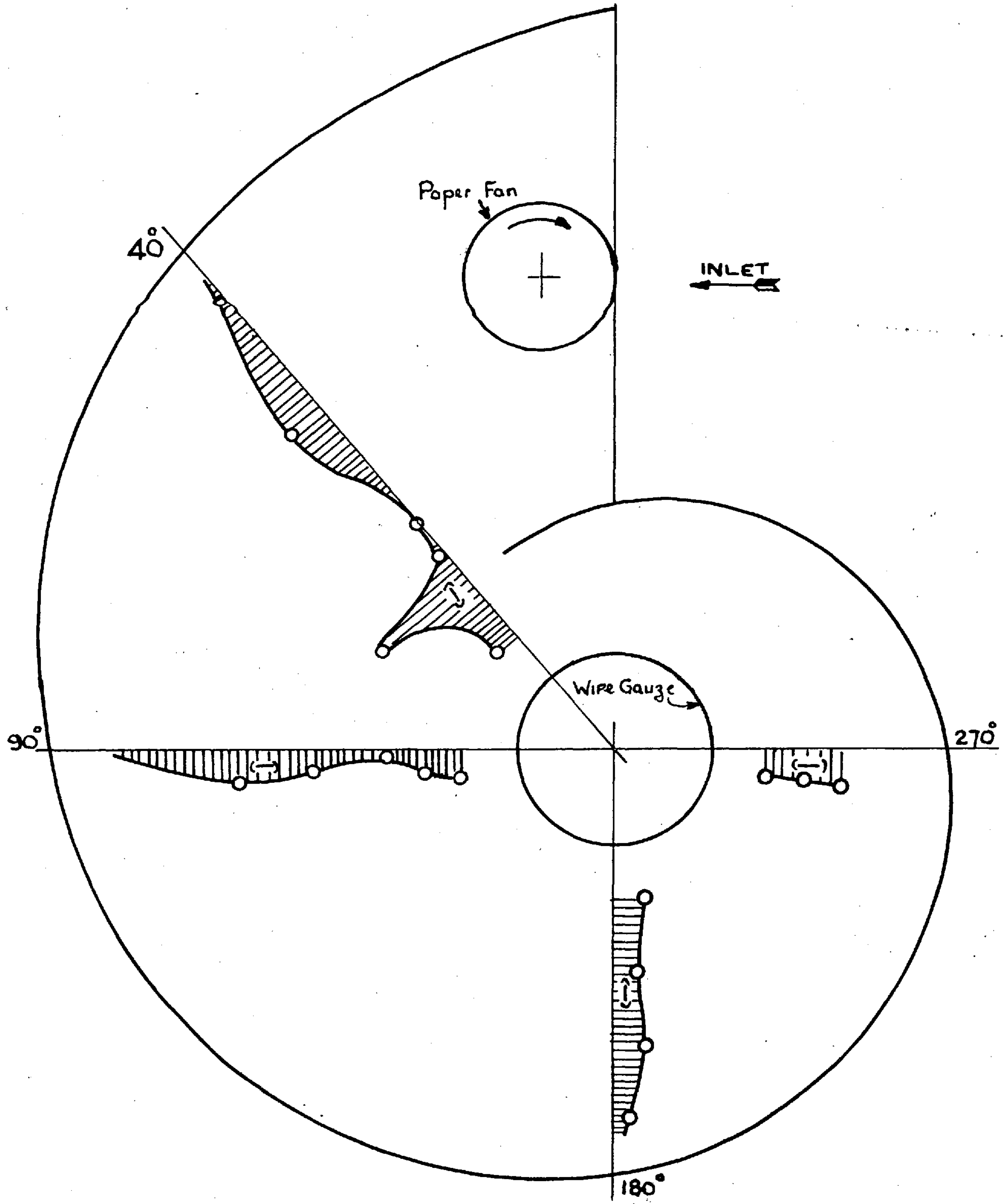

FIGURE (73) TOTAL HEAD DISTRIBUTIONS 1½ FROM BACKWALL

DISTURBANCE AT INLET FLOW = 3·53 cusecs

SCALE OF CASING 1:4 SCALE OF HEAD: 1 2 3 4 Ft. of air

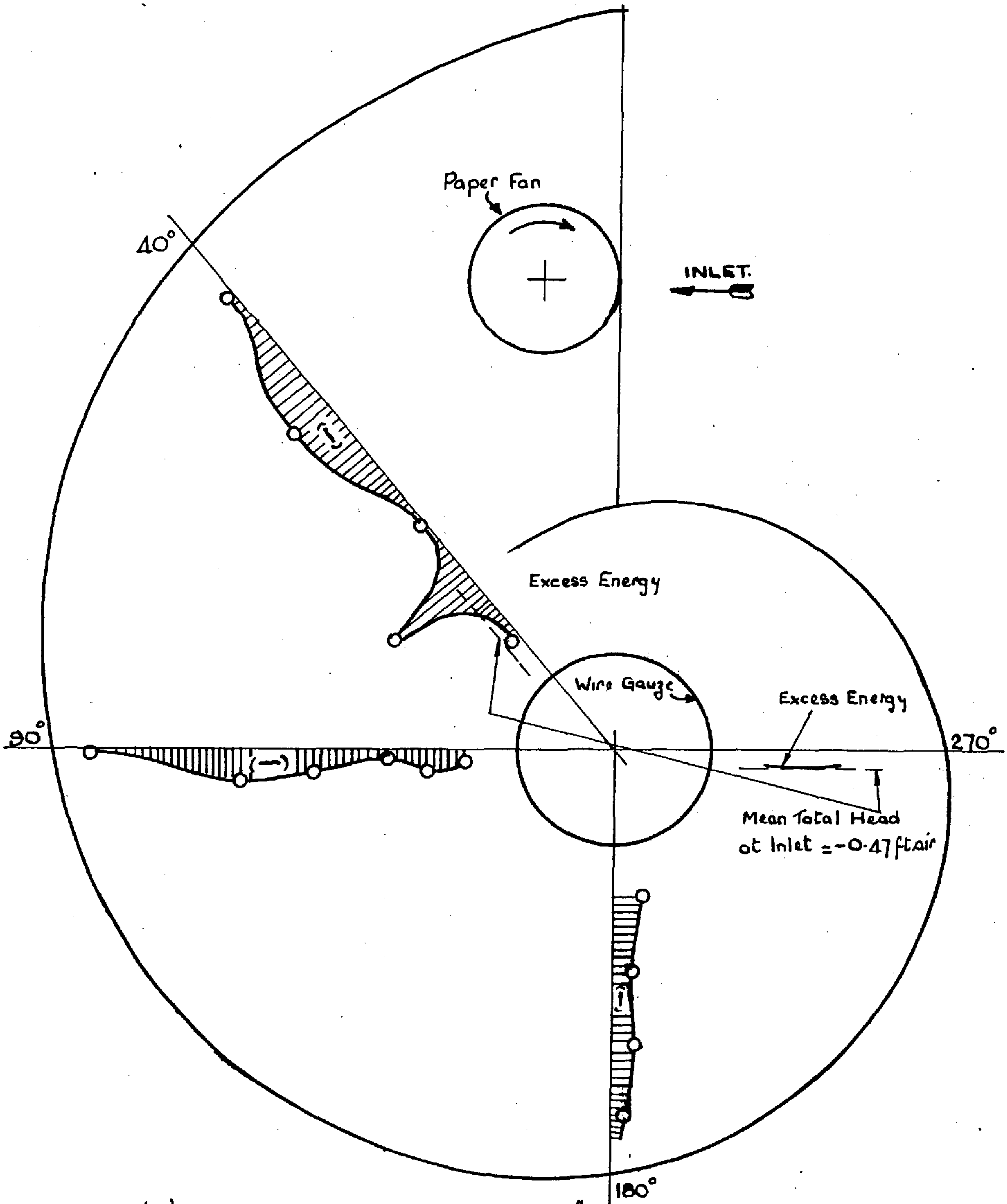

FIGURE (74). TOTAL HEAD DISTRIBUTIONS 2" FROM BACKWALL

DISTURBANCE AT INLET FLOW = 3·53 cusecs.

SCALE OF CASING 1:4 SCALE OF HEAD:

1 2 3 4
ft. of air

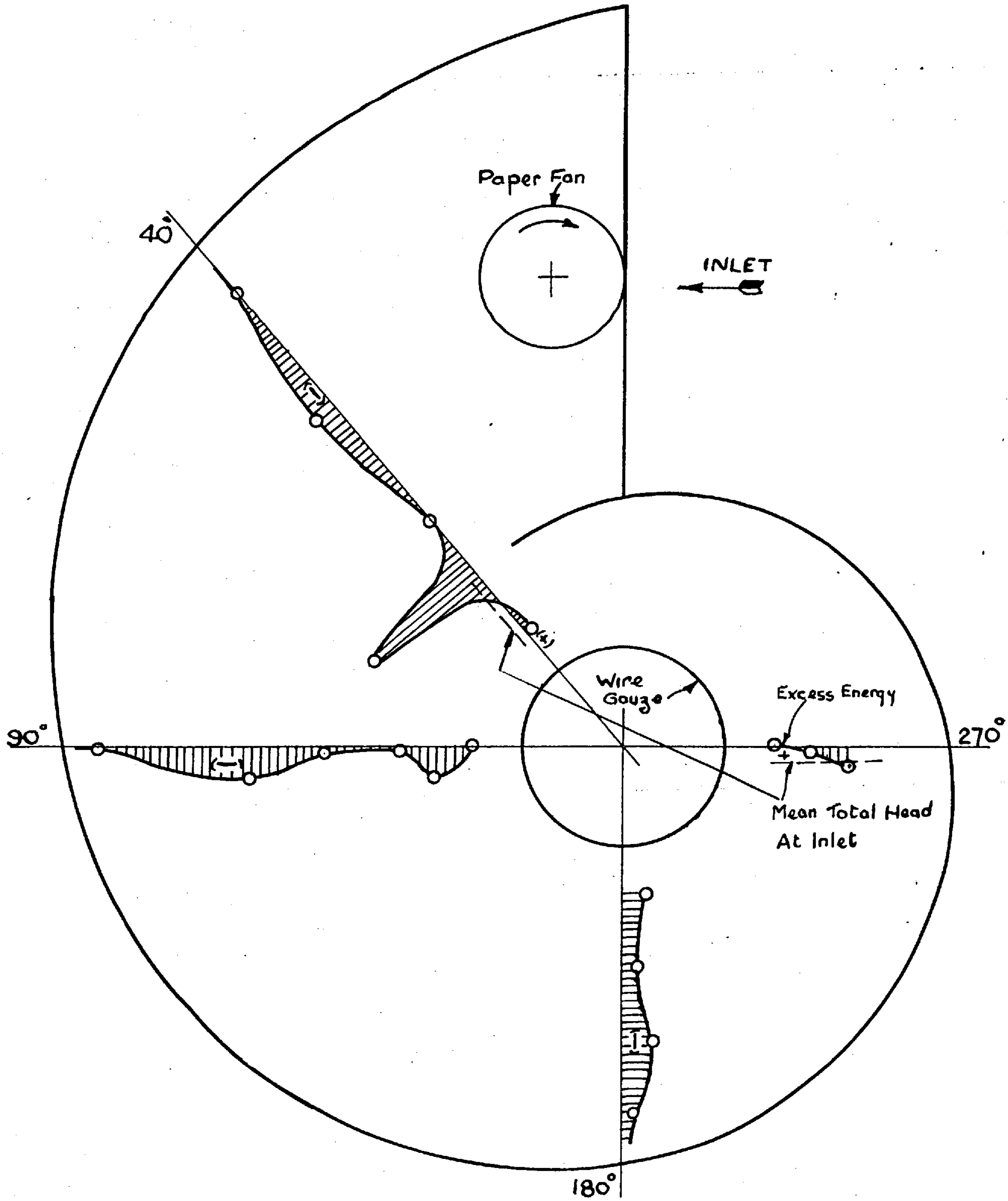

FIGURE (75) - TOTAL HEAD DISTRIBUTION 2½" FROM BACK WALL

DISTURBANCE AT INLET FLOW = 3·53 cusecs

SCALE OF CASING = 1:4 SCALE OF HEAD 1 2 3 4 Ft. of air

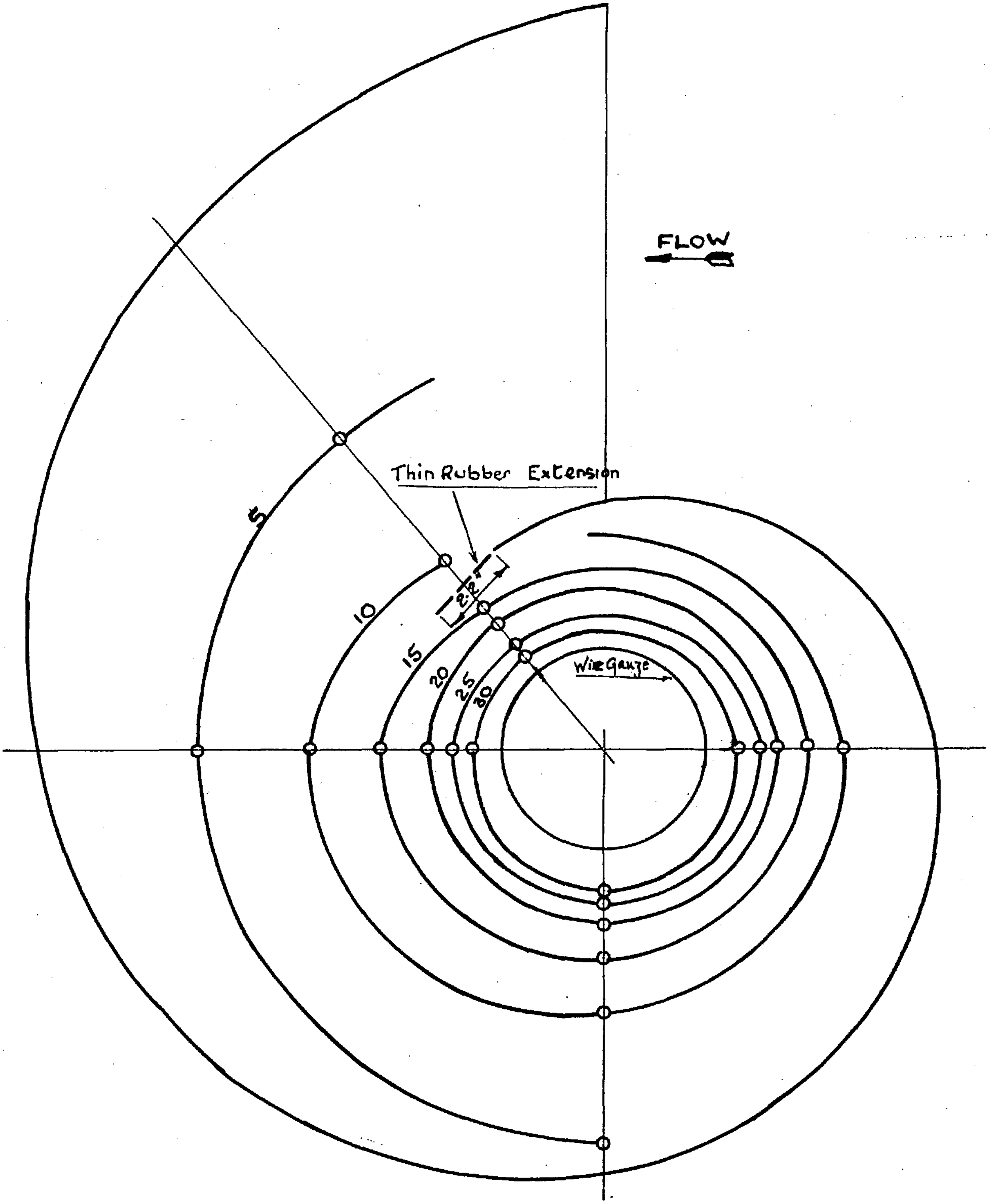

FIGURE(77-a) - CONTOURS OF STATICHEAD AT FRONT WALL

SHORT FLEXIBLE EXTENSION. h_{STATIC} at ($\theta = 120°$, $R = 6"$) = 14.9 ft. of air

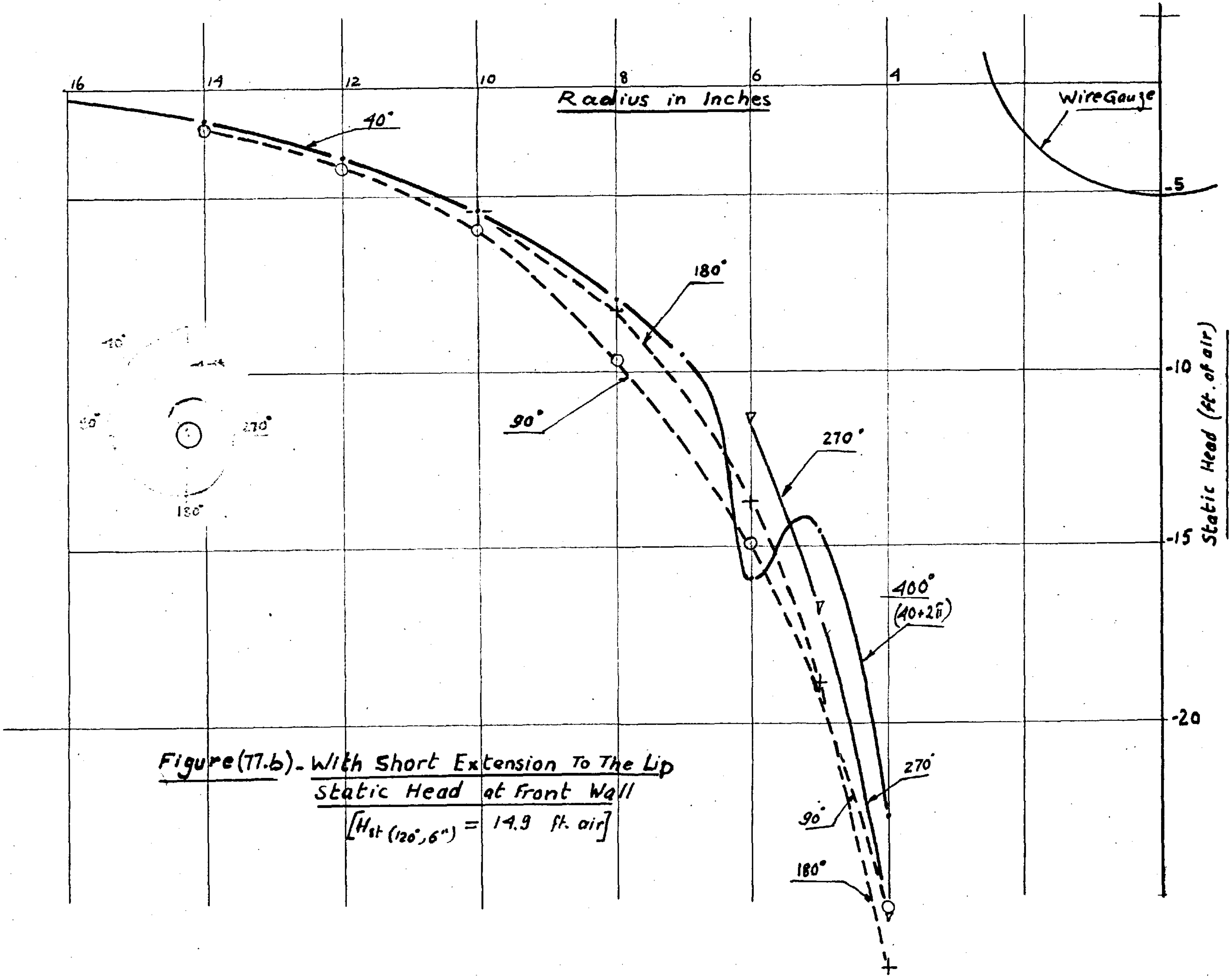

Figure (77.b) - With Short Extension To The Lip
Static Head at Front Wall
[$H_{st\,(120°,\,6'')}$ = 14.9 ft. air]

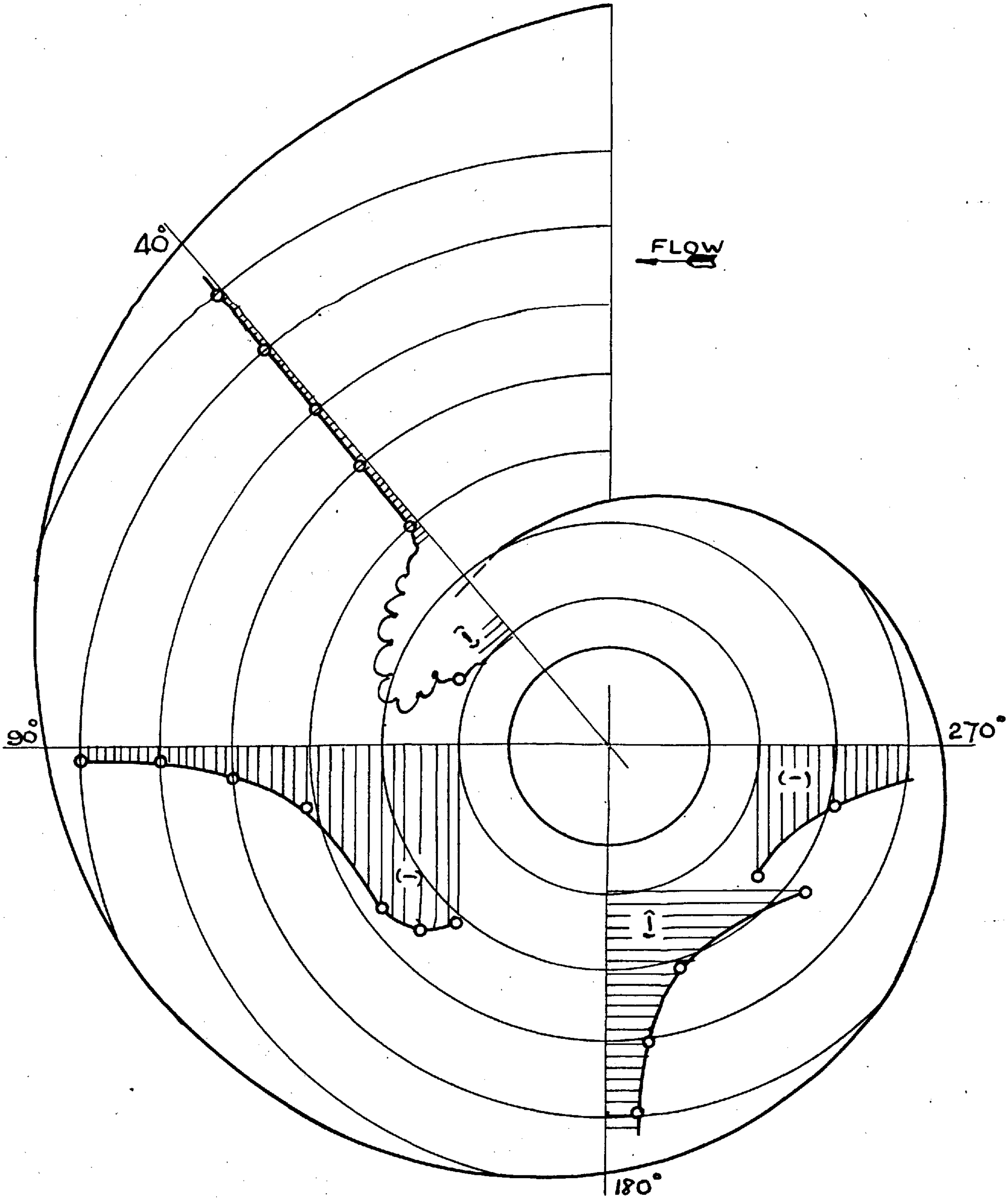

FIGURE (78) TOTAL HEAD DISTRIBUTION $\frac{1}{8}''$ FROM BACK WALL

SHORT FLEXIBLE EXTENSION — h_{STATIC} AT ($\Theta = 120°$, $R = 6''$) = 14.9 ft. of air

SCALE OF CASING 1:4 SCALE OF HEAD: 1 2 3 4 Ft. of air

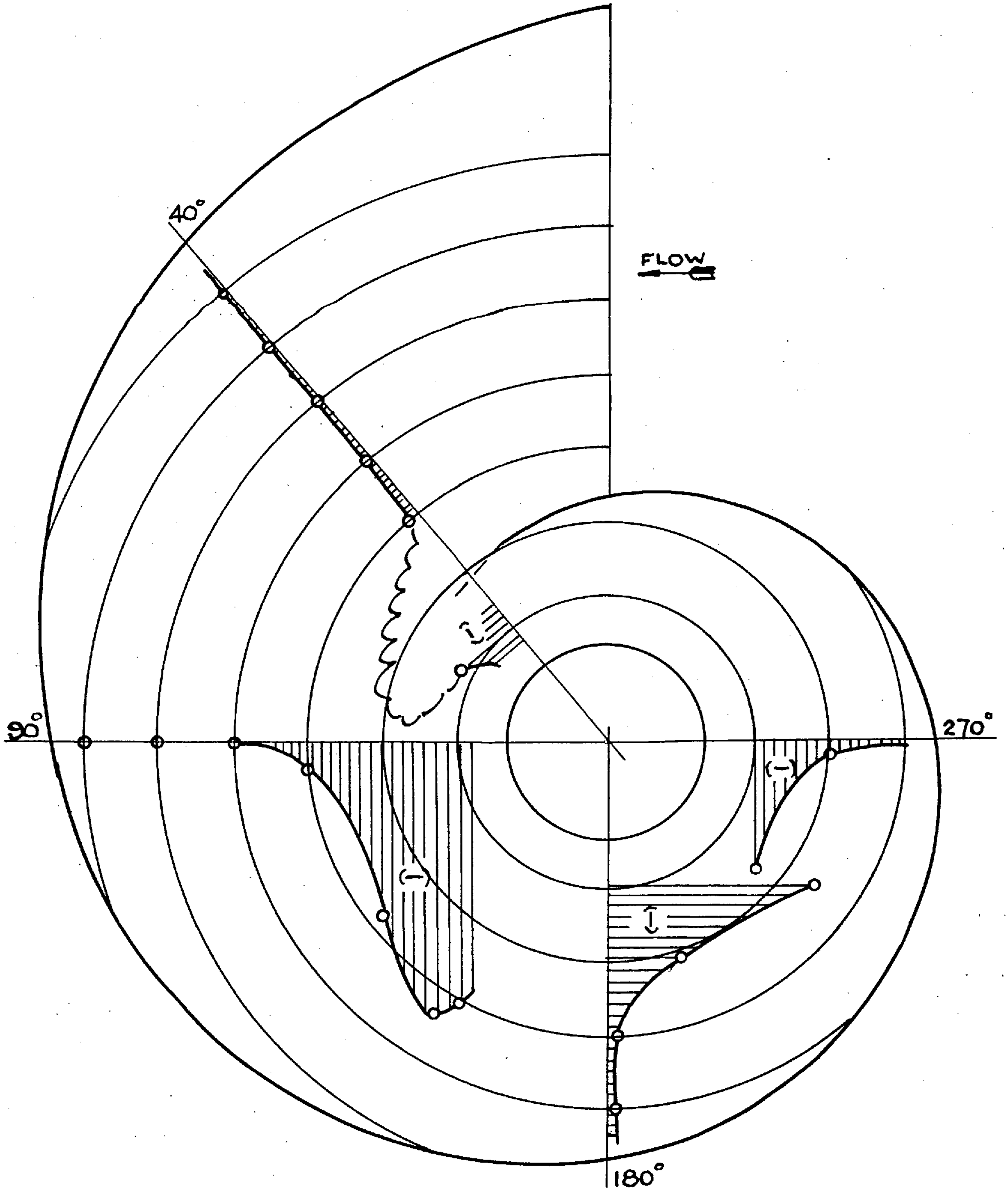

FIGURE (79) TOTAL HEAD DISTRIBUTION 1" FROM BACK WALL

SHORT FLEXIBLE EXTENSION — h_{STATIC} AT ($\theta = 120°$, $R = 6"$) = 14.9 ft. of air.

SCALE OF CASING 1:4 SCALE OF HEAD: 1 2 3 4 Ft. of air

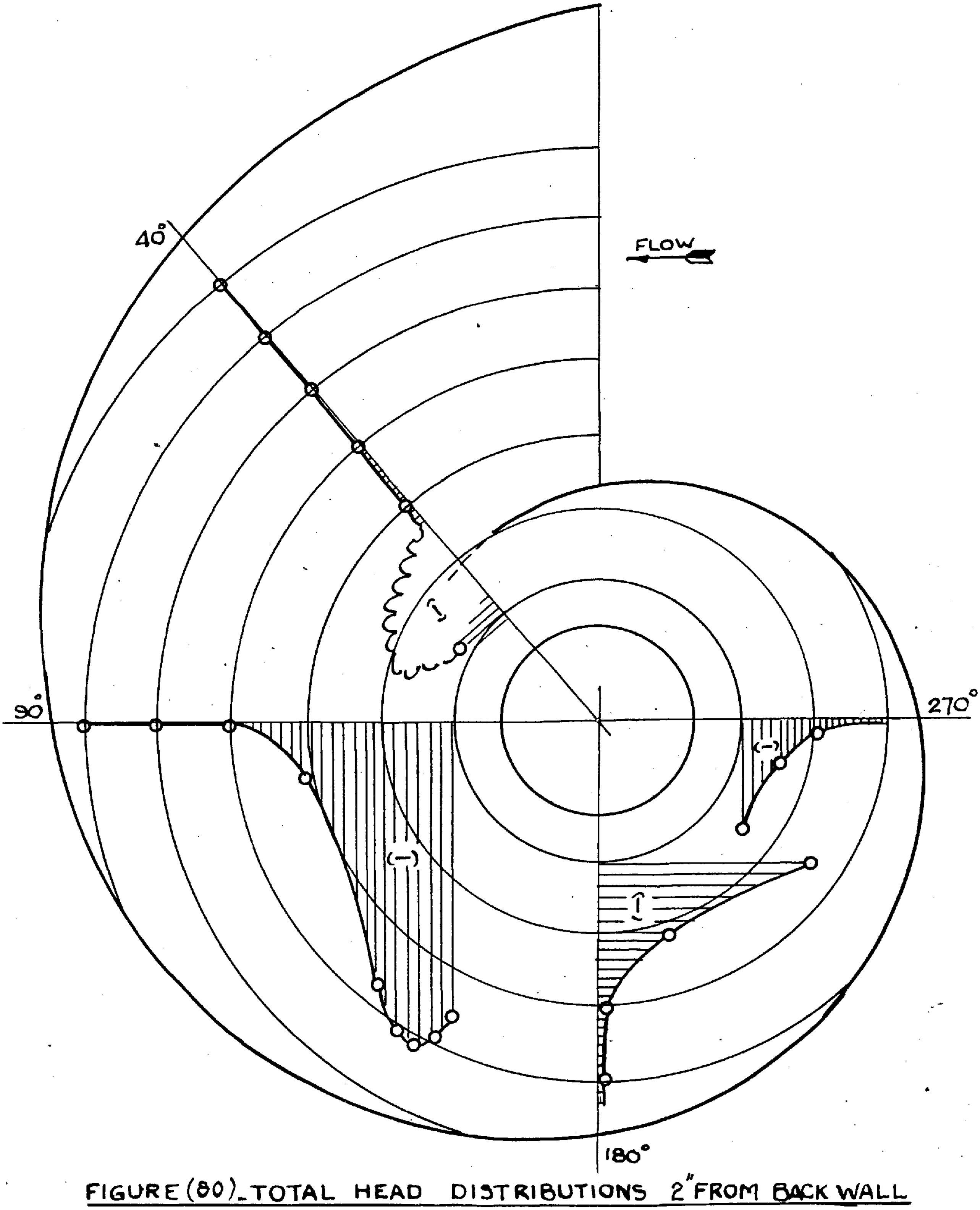

FIGURE (80) _ TOTAL HEAD DISTRIBUTIONS 2" FROM BACK WALL

SHORT FLEXIBLE EXTENSION – h_{STATIC} AT (θ = 120°, R = 6") = 14.9 ft. of air

SCALE OF CASING 1:4 SCALE OF HEAD: 1 2 3 4 Ft. of Air

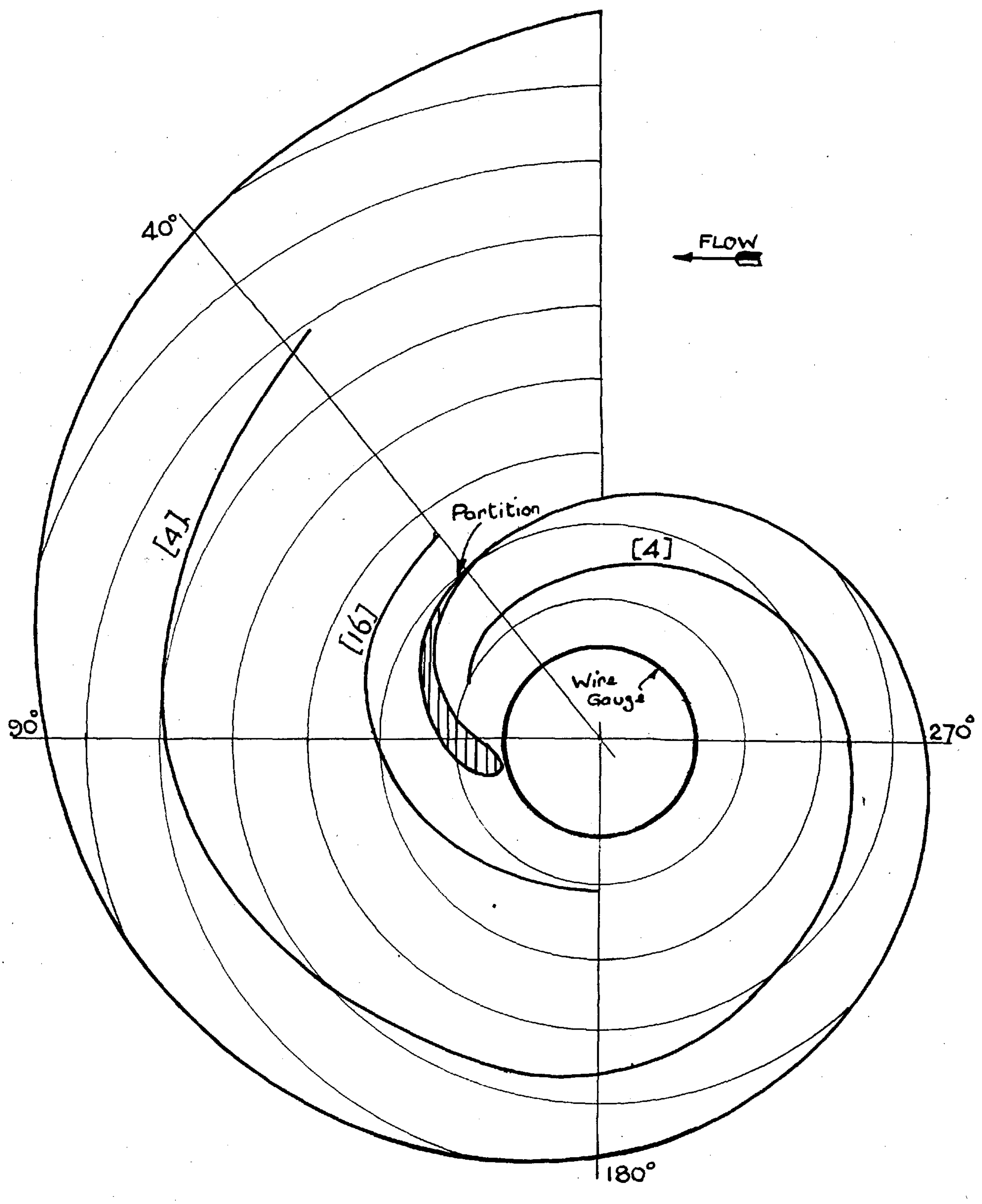

FIGURE (82.a) - CONTOURS OF STATIC HEAD (ft. of air) AT FRONT WALL

WITH PARTITION

SCALE OF CASING 1:4

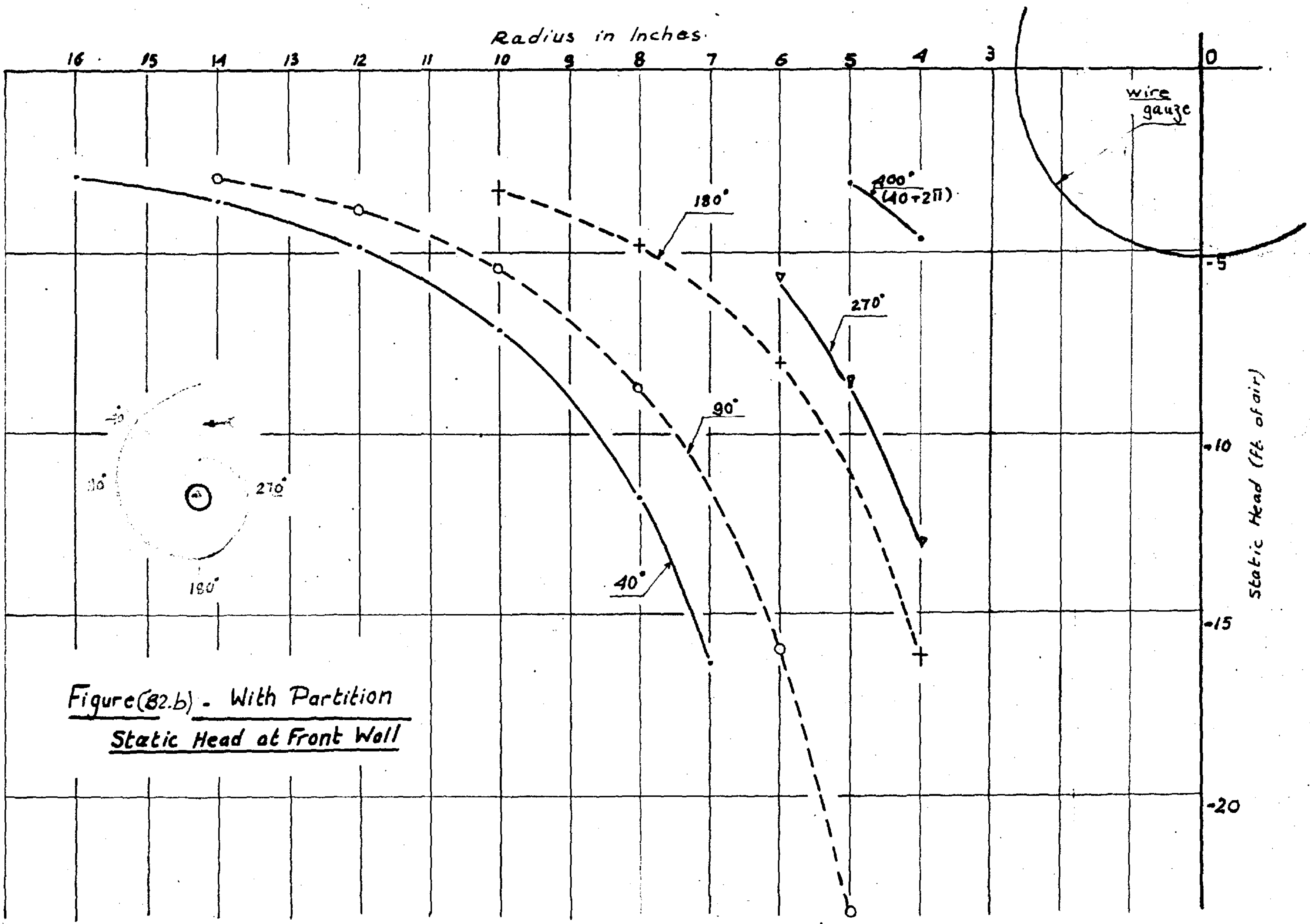

Figure (82.b) - With Partition
Static Head at Front Wall

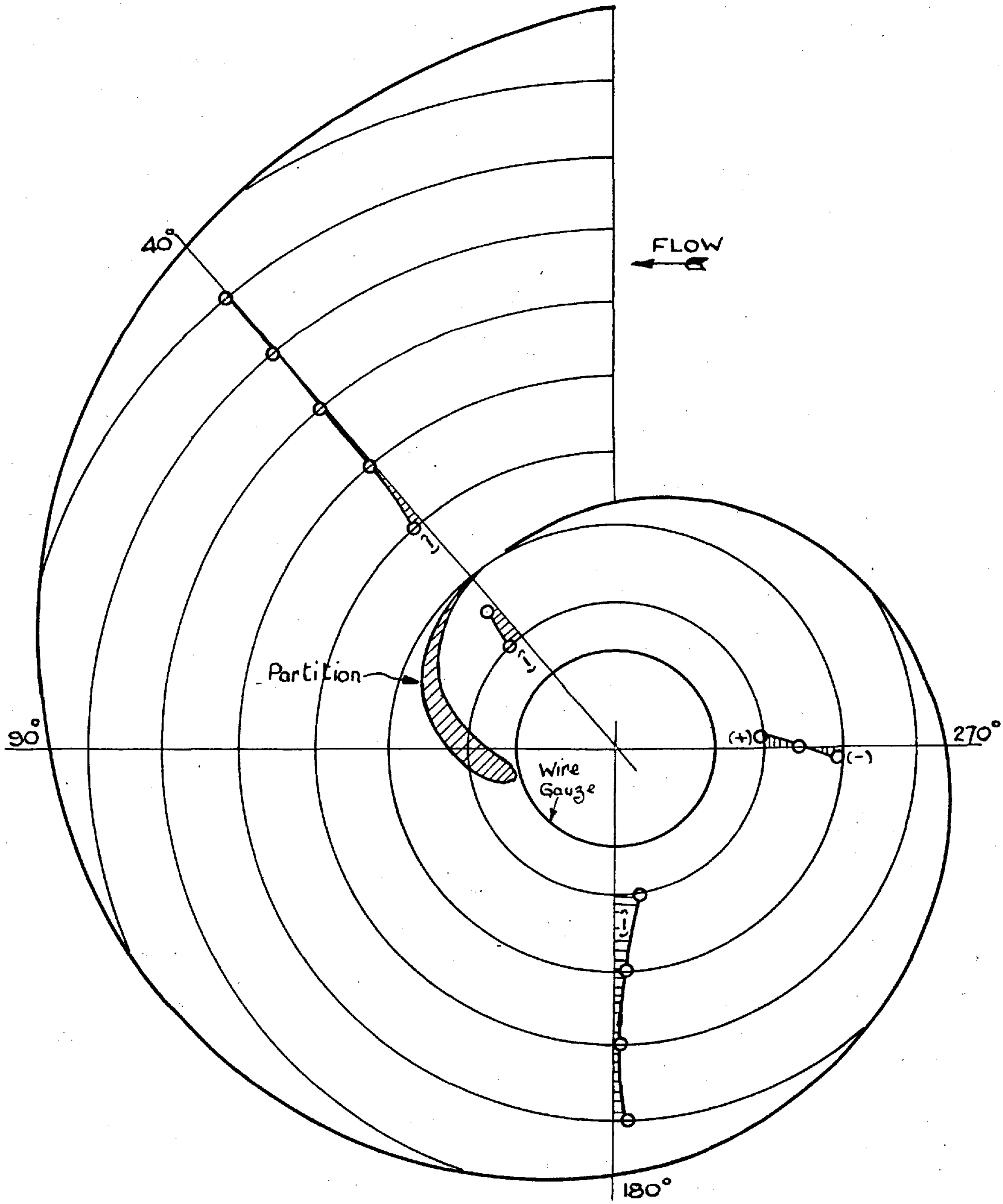

FIGURE (83) TOTAL HEAD DISTRIBUTIONS 2" FROM BACK WALL WITH PARTITION

SCALE OF CASING 1:4 SCALE OF HEAD: 1 2 Ft. of Air

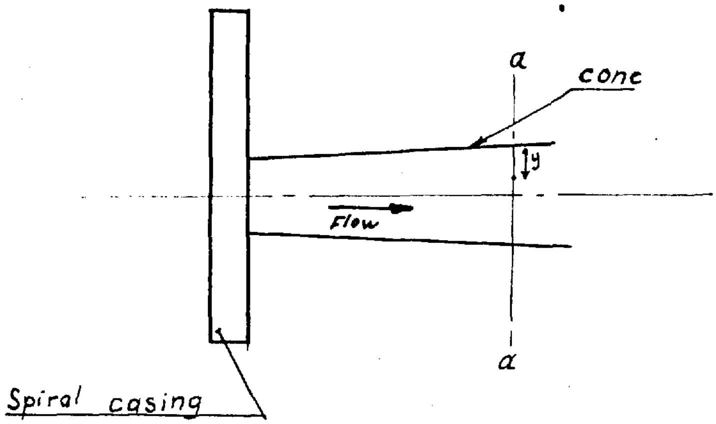

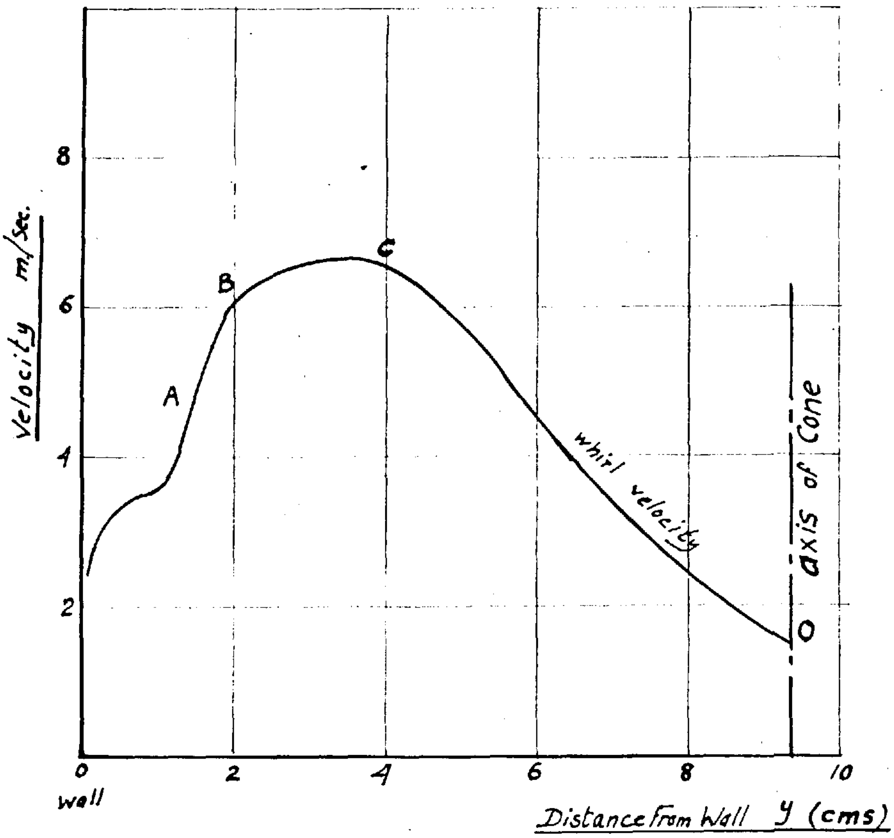

Figure (84). Whirl Velocity in section a-a of the cone

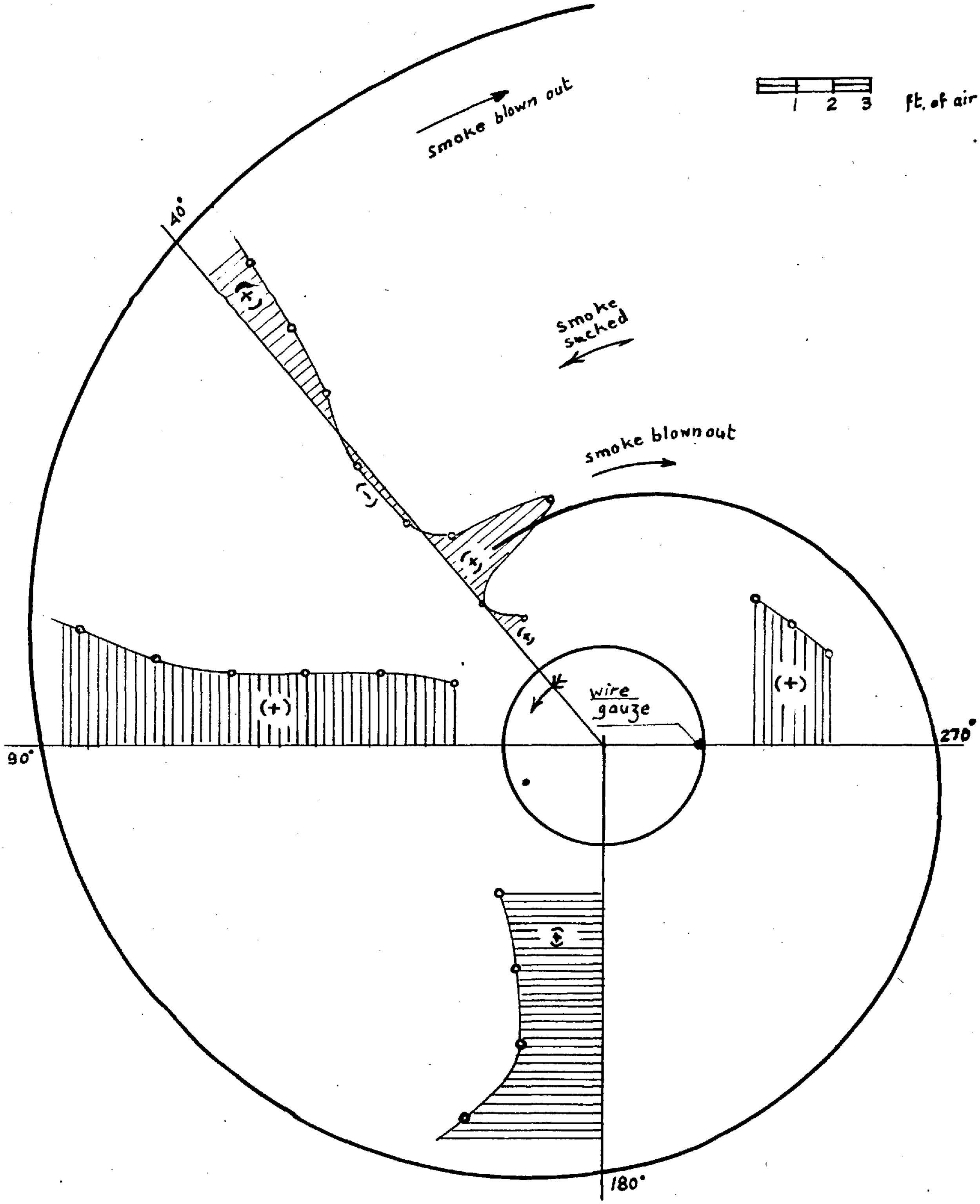

Figure(87) - Static Head at front wall
Wire gauze rotating at 4300 R.P.M. (Fan Stationary)

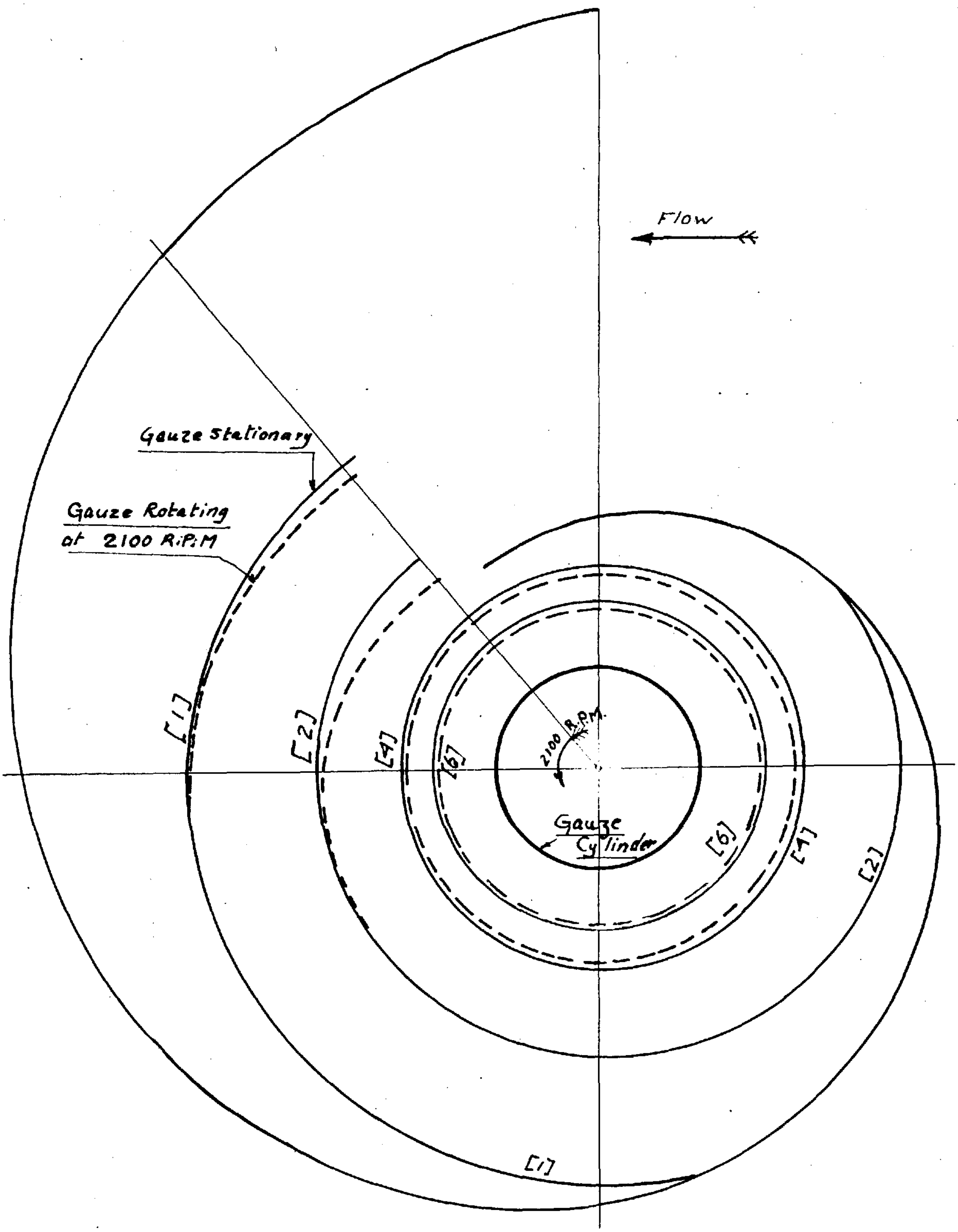

Figure (88) - Rotating Gauze Cylinder

Effect of rotating gauze on Static Head at Front Wall (ft. of air)

Static Head at ($\Theta = 120°$, $r = 6"$) = -2.4 ft. of air

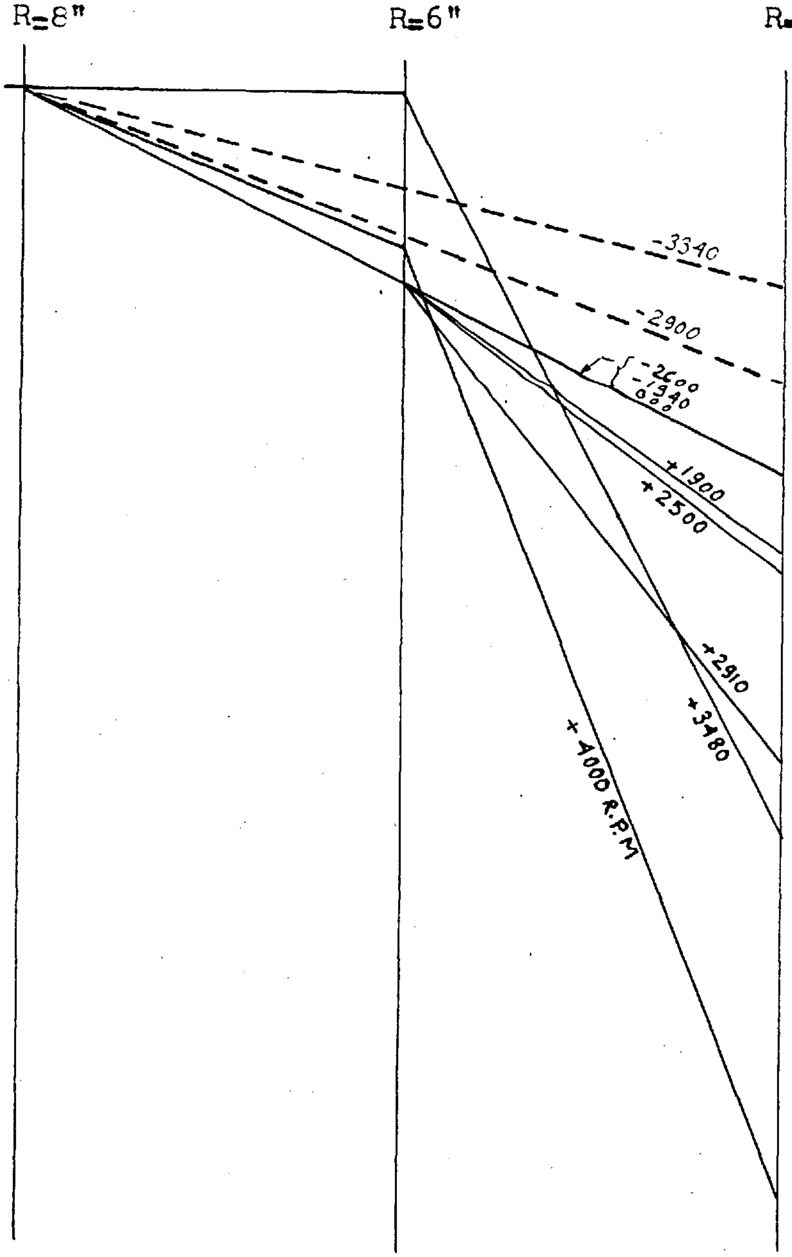

Gauze Speed R.P.M	$\frac{V_G}{V_A}$	Change in Head
-3340	-2.64	+3.45%
-2900	-2.30	+1.72%
-2600	-2.05	0.00
-1940	-1.54	0.00
0000	0.00	0.00
+1900	+1.50	-1.38%
+2500	+1.98	-1.73%
+2910	+2.30	-5.17%
+3480	+2.76	-6.55%
+4000	-3.16	-13.1%

<u>Figure(89) - Diagram showing the change in static head at R= 4" at top wall, due to rotation of wire gauze.</u>

Radial Section making 90 with inlet.
Static Head at R = 8 inches is kept constant at -1.4ft. of air
Static Head at R = 4 inches, when gauze is stationary,
= -5.65 ft. of air

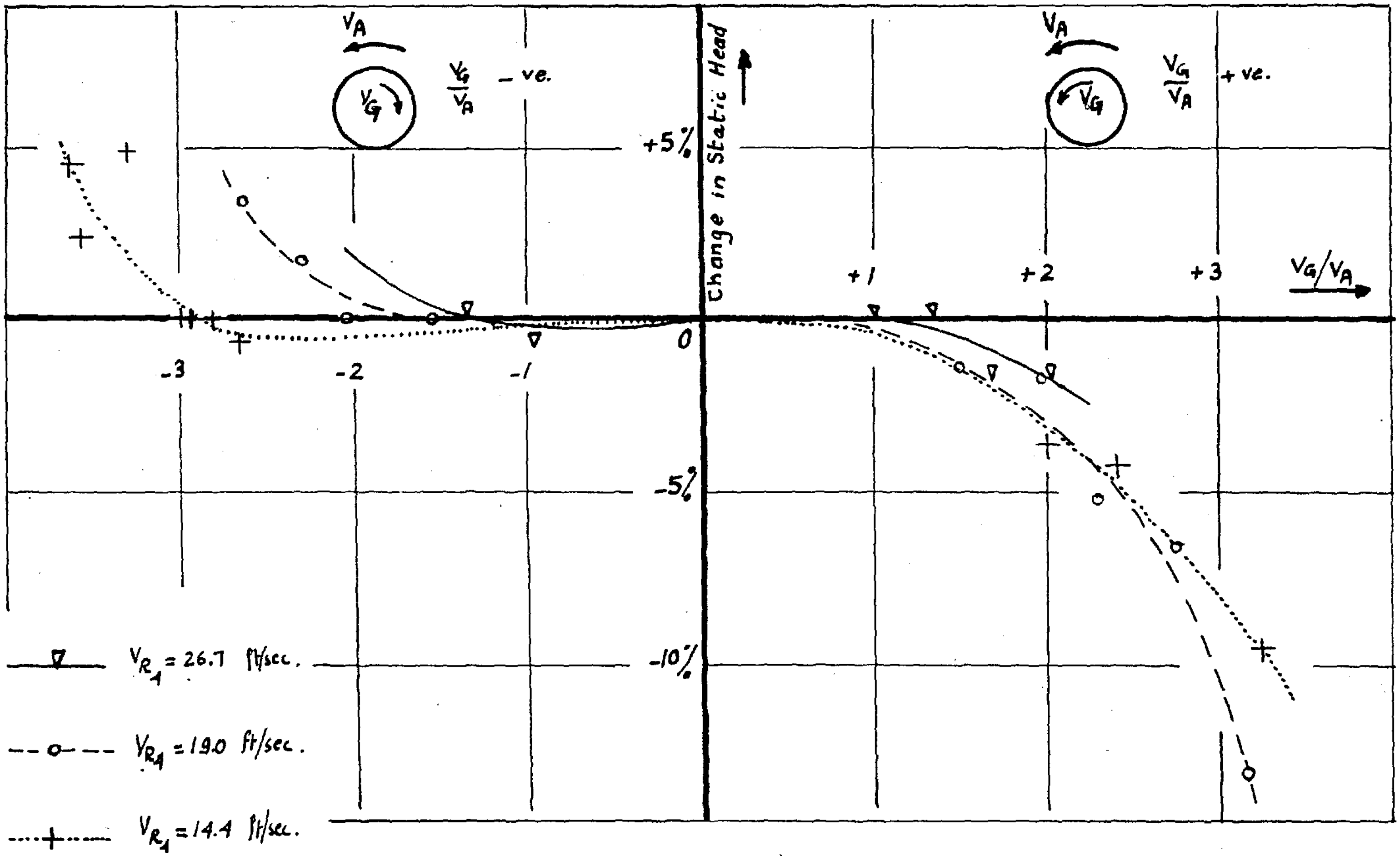

Figure (90) . Change in Static Head at R=4 inches against V_G/V_A For different rates of flow.

Section 90° with inlet

V_G = Velocity of wire gauze , V_A = Velocity of air at the gauze , V_{R_4} = Velocity of Flow at R=4 (indication of the flow)

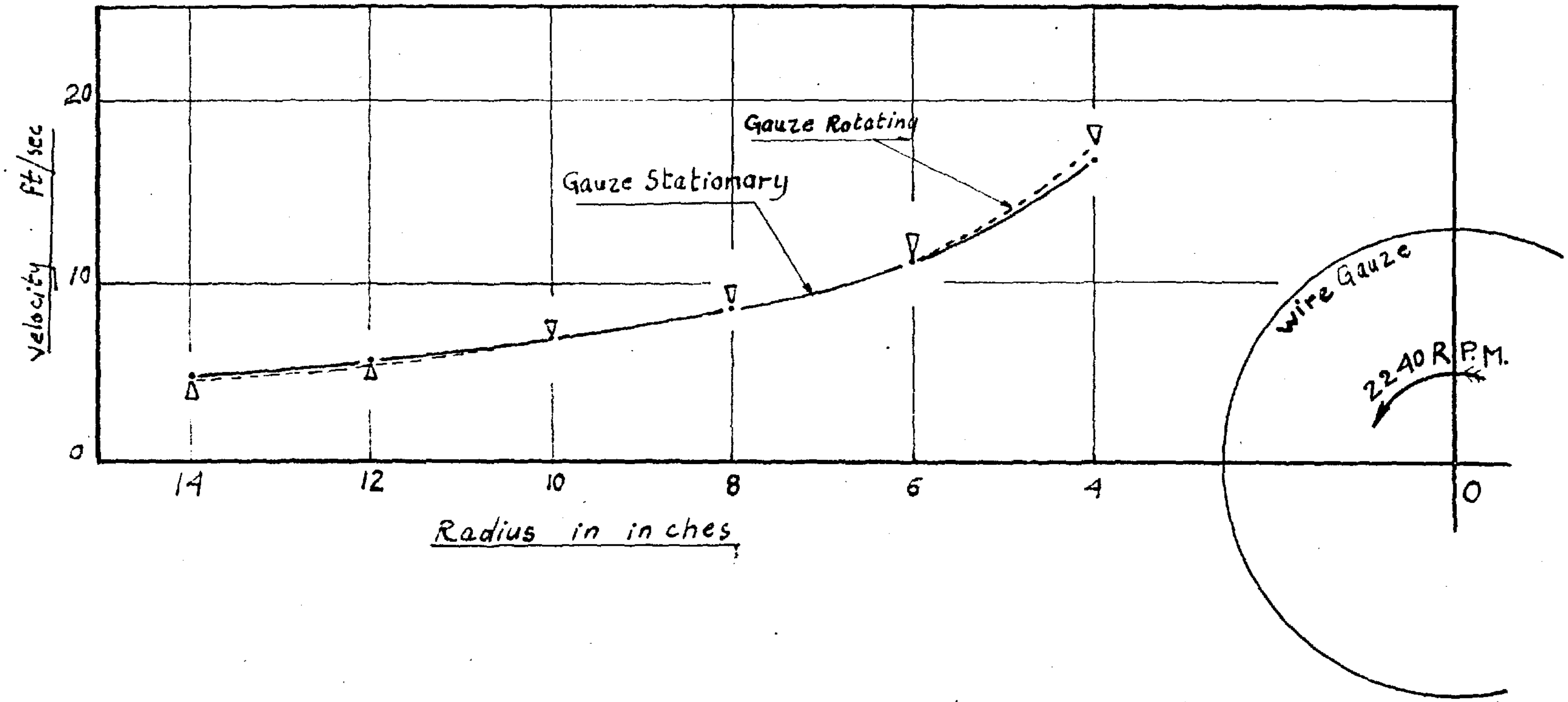

Figure (91) - Effect of **Rotating Gauze** on Velocity Distribution in the middle stream at Radial Section 90° with inlet

———·———·——— Gauze Stationary
____∇____∇____ Gauze Rotating at +2140 R.P.M

} Static Head at ($\theta = 120, R = 6''$) fixed at -1.65 ft. of air

$\left[\frac{V_G}{V_A} = \frac{49}{25.4} = 1.93 \right]$

APPENDIX (I)

Direction of Flow, Total Head (ft. of air), Static Head (ft. of air) & Total Velocity (ft./sec.)

(I) Radial Section making 40° with inlet:

R inch		Distance from back wall in inches $\frac{1}{8}$	$\frac{1}{2}$	I	I$\frac{1}{2}$	2	2$\frac{1}{2}$	2$\frac{7}{8}$
I6	Direc.	I02°	98°	97°	97°	97°	99°	I08°
	Total	-00.39	-00.08	-00.06	-00.06	-00.06	-00.09	-00.39
	Static	- I.7I	- I.7I	- I.7I	- I.7I	- I.7I	- I.7I	- I.7I
	Vel.	9.2I	I0.23	I0.29	I0.29	I0.29	I0.I6	9.2I
I2	Direc.	I03°	99°	98°	98°	98°	98°	I02°
	Total	-00.39	-00.06	-00.06	-00.06	-00.06	-00.06	-00.I9
	Static	- 2.92	- 2.98	- 2.98	- 2.98	- 2.92	- 2.92	- 2.92
	Vel.	I2.70	I3.65	I3.65	I3.65	I3.52	I3.52	I3.20
8	Direc.	I02°	96°	96$\frac{1}{2}$°	97°	97°	98°	99°
	Total	-00.39	-00.06	-00.06	-00.06	-00.06	-00.06	-00.78
	Static	- 6.42	- 6.42	- 6.42	- 6.42	- 6.42	- 6.32	- 6.22
	Vel.	I9.62	20.I5	20.I5	20.I5	20.I5	20.00	I8.67
7	Direc.	I02°	98°	98°	96°	96°	96$\frac{1}{2}$°	97°
	Total	-00.39	-00.I0	-00.I9	-00.I9	-00.I9	-00.I4	-00.04
	Static	- 8.I7	- 8.I7	- 8.I7	- 8.I7	- 8.I7	- 7.97	- 7.97
	Vel.	22.30	22.70	22.60	22.60	22.60	22.40	22.50
6	Direc.	I05°	94°	94°	93°	94°	97°	I0I°
	Total	- 4.08	- 4.08	- 3.50	- 3.30	- 3.30	- 3.30	- 2.33
	Static	-I0.70	-I0.70	-I0.70	-I0.70	-I0.70	-I0.50	-I0.3I
	Vel.	20.55	20.55	2I.45	2I.75	2I.75	2I.45	22.60
5	Direc.	I0I°	95°	92°	93°	92°	94°	97°
	Total	-00.97	-00.39	-00.39	-00.I9	+00.I9	+00.39	+00.I9
	Static	-I6.92	-I5.95	-I6.I4	-I6.33	-I6.33	-I6.I4	-I5.95
	Vel.	3I.9	3I.55	3I.75	3I.90	32.50	32.50	3I.90
4	Direc.	I06°	95°	94°	94°	93°	93°	I00°
	Total	- I.07	-00.I9	-00.I0	-00.00	+00.58	+00.78	-00.00
	Static	-28.00	-26.00	-26.06	-26.06	-26.06	-26.06	-26.06
	Vel.	4I.50	40.70	40.75	40.80	4I.30	4I.40	40.80

APPENDIX (I) Cont.

(2) Radial Section making 90° with inlet:

R inch		Distance from back wall in inches $\frac{1}{8}$	$\frac{1}{2}$	I	I$\frac{1}{2}$	2	2$\frac{1}{2}$	2$\frac{7}{8}$
I4	Direc.	I06°	99°	97°	98°	I02°	I02°	I06°
	Total	-00.25	-00.I4	-00.06	-00.06	-00.06	-00.I0	-00.I9
	Static	- 2.33	- 2.33	-2.33	- 2.33	- 2.33	- 2.24	- 2.24
	Vel.	II.55	II.87	I2.08	I2.08	I2.08	II.70	II.44
I0	Direc.	I09°	98°	97°	95°	95°	98°	I09°
	Total	-00.78	-00.I4	-00.06	-00.06	-00.06	-00.I0	-00.58
	Static	- 4.47	- 4.57	- 4.57	- 4.57	- 4.47	- 4.38	- 4.28
	Vel.	I5.40	I6.88	I7.02	I7.02	I6.83	I6.57	I5.40
7	Direc.	I07°	97°	97°	96°	94°	94°	I07°
	Total	-00.97	-00.I9	-00.29	-00.I9	-00.I4	-00.I4	-00.97
	Static	- 9.53	- 9.I5	- 9.I5	- 8.95	- 8.85	-8.66	- 8.56
	Vel.	23.40	23.95	23.80	23.70	23.65	23.40	22.05
6	Direc.	I05°	97°	96°	94°	94°	96°	I05°
	Total	- I.36	-00.I9	-00.I9	-00.I9	-00.I9	-00.39	- I.36
	Static	-I3.22	-I2.05	-I2.I5	-I2.I5	-II.96	-II.67	-II.58
	Vel.	27.60	27.60	27.70	27.70	27.50	26.90	25.60
5	Direc.	I07°	96°	95°	94°	93°	94°	I07°
	Total	-02.33	-00.97	-00.78	-00.I9	00.00	00.00	-0I.75
	Static	-I8.86	-I7.70	-I7.70	-I7.70	-I7.50	-I7.3I	-I6.52
	Vel.	32.60	32.80	32.95	33.50	33.50	33.30	30.80
4	Direc.	I05°	96°	95°	95°	92°	94°	95
	Total	- I.56	-00.I9	+00.I9	+00.I9	+00.39	+00.78	-00.58
	Static	-30.54	-28.20	-28.20	-28.20	-28.02	-27.23	-25.70
	Vel.	43.I0	42.40	42.70	42.70	42.70	42.40	40.I5

APPENDIX (I) Cont.

R inch		Distance from back wall in inches $\frac{1}{8}$	$\frac{1}{2}$	I	I$\frac{1}{2}$	2	2$\frac{1}{2}$	2$\frac{7}{8}$
(3) Radial Section making I80° with inlet:								
IO	Direc.	I08°	99°	98°	97°	96°	I00°	I02°
	Total	-00.58	-00.I6	-00.08	-00.08	-00.08	-00.08	-00.I6
	Static	- 4.86	- 4.67	- 4.67	- 4.57	- 4.57	- 4.47	- 4.28
	Vel.	I6.57	I7.25	I7.I8	I7.00	I7.00	I6.80	I6.27
8	Direc.	I20$\frac{1}{2}$°	99°	96°	95°	95$\frac{1}{2}$°	99°	I07°
	Total	-00.78	-00.I9	-00.08	-00.08	-00.08	-00.08	-00.39
	Static	- 7.40	- 7.20	- 7.00	- 7.00	- 7.00	- 6.9I	- 6.8I
	Vel.	20.60	2I.20	2I.I0	2I.I0	2I.I0	20.90	20.30
6	Direc.	II7°	I02$\frac{1}{2}$°	94°	93°	93°	I00°	II4$\frac{1}{2}$°
	Total	-0I.26	-00.39	-00.I9	00.00	00.00	-00.I9	-0I.I7
	Static	-I3.4I	-I3.4I	-I3.22	-I3.02	-I3.02	-I2.54	-I2.25
	Vel.	27.95	28.95	28.95	28.95	28.95	28.I5	26.65
4	Direc.	II8$\frac{1}{2}$°	I06°	9I°	9I°	9I°	97°	II3°
	Total	- 2.72	- I.56	-00.58	+00.I0	+00.I0	00.00	- 2.33
	Static	-28.80	-28.80	-28.80	-29.00	-28.80	-28.80	-28.80
	Vel.	40.95	4I.75	42.50	43.20	43.I0	42.90	4I.20

APPENDIX (I) Cont.

(4) Radial Section making 270° with inlet:								
R inch		Distance from back wall in inches $\frac{1}{8}$	$\frac{1}{2}$	I	I$\frac{1}{2}$	2	2$\frac{1}{2}$	2$\frac{7}{8}$
6	Direc.	II2°	I00°	96°	94°	97°	I02°	III°
	Total	-00.78	-00.29	-00.I9	+00.I9	+00.I9	-00.00	-00.58
	Static	-I2.35	-II.48	-II.38	-II.38	-II.28	-II.00	-I0.80
	Vel.	27.30	26.80	26.80	27.30	27.00	26.60	25.60
5	Direc.	II5°	99°	95°	94°	93°	99$\frac{1}{2}$°	I08°
	Total	- I.36	-00.39	-00.I9	+00.58	+00.39	+00.I9	-00.78
	Static	-I7.3I	-I6.42	-I6.42	-I6.42	-I6.42	-I6.23	-I6.I3
	Vel.	32.00	32.I0	32.30	33.I0	32.90	32.50	33.00
4	Direc.	II9°	II0°	94°	94°	94°	I00°	II7°
	Total	- I.95	- I.I7	+00.39	00.00	+00.39	+00.58	- I.I7
	Static	-27.90	-27.I3	-27.70	-28.30	-27.70	-27.02	-26.83
	Vel.	40.80	40.80	42.50	42.60	42.50	42.I0	40.60

APPENDIX (2)

Calculation of Velocities:

The alchol sloping tube manometer used for measuring the velocity heads, was calibrated against a Chattock manometer. It was found that:

I mm. on the manometer = 0.0767 mms. of water.

i.e. I mm. on the manometer $= 0.0767 \frac{0.292}{89}$ ft.water

$$= \frac{0.0767 \times 292}{1000 \times 89} \times \frac{62.4}{0.0807} \text{ ft.air}$$

$$= 0.1945 \text{ ft. of air.}$$

Velocity $= \sqrt{2gh}$

∴ Velocity in feet per second =

$$\sqrt{2g \times 0.1945 \times \text{manometer reading}}$$

$$= 3.535 \sqrt{\text{manometer reading in mms.}}$$

APPENDIX (3)

Calculation of Flow:

From the experimental mean tangential velocity curve, figure (32), the tangential flow between r = 6 inches and r = 17.5 inches is 3.500 cusecs.

The mean radial velocity at r = 6 inches is 2.54 ft./ sec.

∴ Radial flow between lip and r = 6 inches is:

= 0.025 1.27 = 0.032 cusecs.

∴ Total flow entering the casing = 3.532 cusecs.

REFERENCES

I. Carter, Andrews and Shaw,
" Some Fluid Dynamic Research Technique."
The Inst. of Mech. Eng.- Proc.(I950) Vol.I63 p. 260.

2. Dodge and Thompson,
" Fluid Mechanics.",
McGraw-Hill (I937).

3. Firth A.,
" Flow in a Spiral Case.",
Thesis for M.Sc. (Eng.) London (I949).

4. Goldstein S. (Editor),
" Modern Developments in Fluid Dynamics.",
Oxford University Press (I938).

5. Heenan and Gilbert,
" The Design and Testing of Centrifugal Fans.",
Proc. Inst. Civil Eng., Vol. CXXIII (I895)p. 272.

6. Lamb Sir Horace,
" Hydrodynamics.",
Dover Publications, New York (I932).

7. Milne - Thompson,
" Theoretical Hydrodynamics.",
MacMillan (I938).

8. Ower E.,
" The Measurement of Air Flow.",
Chapman & Hall (I949).

9. Winter I.A.,
" Application of Hydraulic Laboratory Researches.",
Trans. Am. Soc. M.E. Vol.53(I93I) HYD. p. 35.